600 Woodland Terrace
Alexandria, VA 22302
703.683.1808 Fax: 703.683.1815
www.armarocks.org

# LASER AND PHOTOGRAMMETRIC METHODS FOR ROCK FACE CHARACTERIZATION

Fulvio Tonon and Joseph T. Kottenstette

Report on a workshop held June 17-18, 2006 in Golden, Colorado

In Conjunction with GoldenRocks 2006
The 41st U.S. Rock Mechanics Symposium
Colorado School of Mines
June 17 - 21, 2006

May, 2007

## Table of contents

## Executive Summary

This report presents the findings of a Workshop on "Laser and Photogrammetric Methods for Rock Face Characterization" held at "GoldenRocks 2006", the 41st U.S. Rock Mechanics Symposium, Colorado School of Mines, June 17 - 18, 2006. The workshop was organized by the American Rock Mechanics Association (ARMA) and sponsored by the Bureau of Reclamation, Research and Development Office, Science and Technology Program, and Split Engineering; FHWA provided logistic and surveying services support. Forty geo-engineering practitioners attended in the workshop, representing four continents.

The workshop was convened to address the topic of remote characterization of rock faces (both outcrops and tunnels). These techniques generally include the following steps:

1. Collecting information on a rock face (e.g., using high-resolution digital cameras or laser scanners (LIght Detection And Ranging, LIDAR));
2. Producing an (oriented) point cloud, and a digital 3D surface and rendering of the face, called Digital Terrain Model (DTM). DTM may be draped with a picture of the face; and
3. Analyzing the DTM to characterize the rock mass (e.g., take dip direction and dip measurements, joint spacing, etc.).

Participants learned the issues involved in laser and digital photogrammetric techniques, the possibilities offered by the new technologies, end-user's difficulties and pit-falls, and got acquainted with various systems developed for rock mass characterization. Practical demonstrations were carried out at an outcrop in the Golden area (Morrison field exercise), and participants subsequently analyzed the data to characterize the rock mass.

Advantages of these remote techniques include:

- The ability to quickly analyze large portions of rock masses (including inaccessible areas), and acquire large data sets;
- The possibility to zoom in and out of a face, which leads to a better understanding of large features;
- Quantification of fracture scale-dependency and invariants;
- Decreased dependence on climatic conditions and decreased impact on construction activities;
- Permanent documentation of the rock face condition and excavation stages for reporting and contractual-legal issues;
- Relative ease of use.

The workshop discussion on the current state-of-the-art suggested that:

- These modern techniques must NOT substitute for qualified characterization of rock masses by an expert engineering geologist or geological engineer. Rather, they are a major aid in rock mass characterization to be used with great care by well-trained engineering geologists or geological engineers;

- Conventional rock mass tools should still be used as a validation tool; automatic trace delineation algorithms are still rock mass specific and should be used with extreme care;
- Rock bridge delineation algorithms are still to be developed;
- Fracture statistics to correctly interpret 3D imaging is still being developed; caution should be exercised in extrapolating 2D methods to 3D imaging, and additional research is needed in this crucial area;
- GPS to accurately determine absolute camera or laser position must be a Real-Time Kinematic (RTK) GPS;
- Roughness is amplified by precision errors.
- Currently, the following quantities required for ISRM quantitative description of fractures cannot (completely) be extracted: roughness (JRC), wall strength (JCS), weathering, humidity/seepage, and filling.

The workshop discussion indicated the following areas of research and development: classification of petrology and mineralogy; detection of rock blocks forming on a face; statistical 3D characterization of rock blocks forming inside a rock mass; fracture statistics for three-dimensional imaging.

Two presenters (AdamTech and 3G) provided their DTM point data and fracture data on the Morrison field exercise; both of these systems used digital photogrammetry. Unfortunately, no LIDAR system provided their data. The comparison of AdamTech and 3G data indicates that:

- Both systems provided high quality DTM results, with deviations of a maximum of 3 cm from the actual rock surface;
- Pictures/scans should be taken from many different angles to ensure that no surface is parallel to all pictures/scans;
- Guidelines on point density are still unavailable, and should be problem-specific;
- Both systems allowed the four most frequent fracture sets to be identified, and yielded the same mean orientations;
- Both systems identified the same fracture set as the most represented, and determined its mean orientation to within 2°;
- For the most represented fracture set, mean joint spacing differed by 60%, and larger discrepancy affected the standard deviation (this was attributed to the waviness of traces and faces);
- Trace lengths showed a very good match, with their means within a 10% difference, and their standard deviations within a 20% difference;
- Heights of roughness profiles differed by a maximum of 1 cm, except for one location, where they differed by 4 cm.

The obtained results indicate that digital photogrammetry yields reliable and reproducible results when applied to rock mass characterization. Digital photogrammetry is thus a mature enough technology that can be used with confidence in the profession provided care is taken to follow the guidelines provided by the presenters in this report.

# Laser and Photogrammetric Methods for Rock Face Characterization: A Workshop

Tonon, F.

*University of Texas, Austin, TX, USA*

Kottenstette, J.T.

*U.S. Bureau of Reclamation, Denver, CO, USA*

Copyright 2006, ARMA, American Rock Mechanics Association

This paper was prepared for presentation at the workshop: "Laser and Photogrammetric Methods for Rock Face Characterization" organized by F. Tonon and J. Kottenstette, held in Golden, Colorado, June 17-18, 2006.

This paper was selected for presentation by F. Tonon and J.T. Kottenstette following review of information contained in an abstract submitted earlier by the author(s). Contents of the paper, as presented, have not been reviewed by F. Tonon and J. Kottenstette, and are subject to correction by the author(s). The material, as presented, does not necessarily reflect any position of USRMS, ARMA, their officers, or members. Electronic reproduction, distribution, or storage of any part of this paper for commercial purposes without the written consent of ARMA is prohibited. Permission to reproduce in print is restricted to an abstract of not more than 300 words; illustrations may not be copied. The abstract must contain conspicuous acknowledgement of where and by whom the paper was presented.

## INTRODUCTION

In the last decade, there have been tremendous advances in the techniques and technologies for the characterization of rock faces (both above- and under-ground). They generally include:

1. Collecting information on a rock face (e.g., using high-resolution cameras or laser scanners);
2. Producing a digital-3D surface and rendering of the face, called Digital Terrain Model (DTM); and
3. Analyzing the DTM to characterize the rock mass (e.g., take dip direction and dip measurements, joint spacing, etc.).

On the occasion of the 40th US Rock Mechanics Symposium held in Anchorage, Alaska, the two authors realized that times were ripe for a workshop on the topic. In the following year, the idea took shape, and a workshop on "Laser and Photogrammetric Methods for Rock Face Characterization" was held on June 17 and 18, 2006 at the Colorado School of Mines in Golden, Colorado, in conjunction with GoldenRocks 2006, the 41st U.S. Rock Mechanics Symposium, June 17 - 21, 2006.

The workshop program (attached at the end of this paper) included a morning of presentations from world-renowned researchers and system developers, an afternoon field exercise at an outcrop near Morrison, Colorado, and a final morning in which participants used the data collected at the Morrison site to perform rock mass characterization.

The invited presenters were as follows:

- Markus Pötsch and Wulf Schubert: Graduate Student and Professor, respectively, Graz University of Technology (Austria); Andreas Gaich: 3G Software & Measurement GmbH (Austria).
- Jason Birch: Managing Director, ADAM Technology (Australia).
- John Kemeny: Professor, University of Arizona (USA).
- George Poropat: Research Group Leader, CSIRO (Australia).
- John Dolan: Business Unit Manager, ISITE (USA).

The success of the workshop is due to the excellent work of the presenters. Indeed, the workshop attracted well over 40 attendees. However, the number of attendees was limited to 40 in order to make the field exercise manageable. As shown in Figure 1, attendees were from four continents.

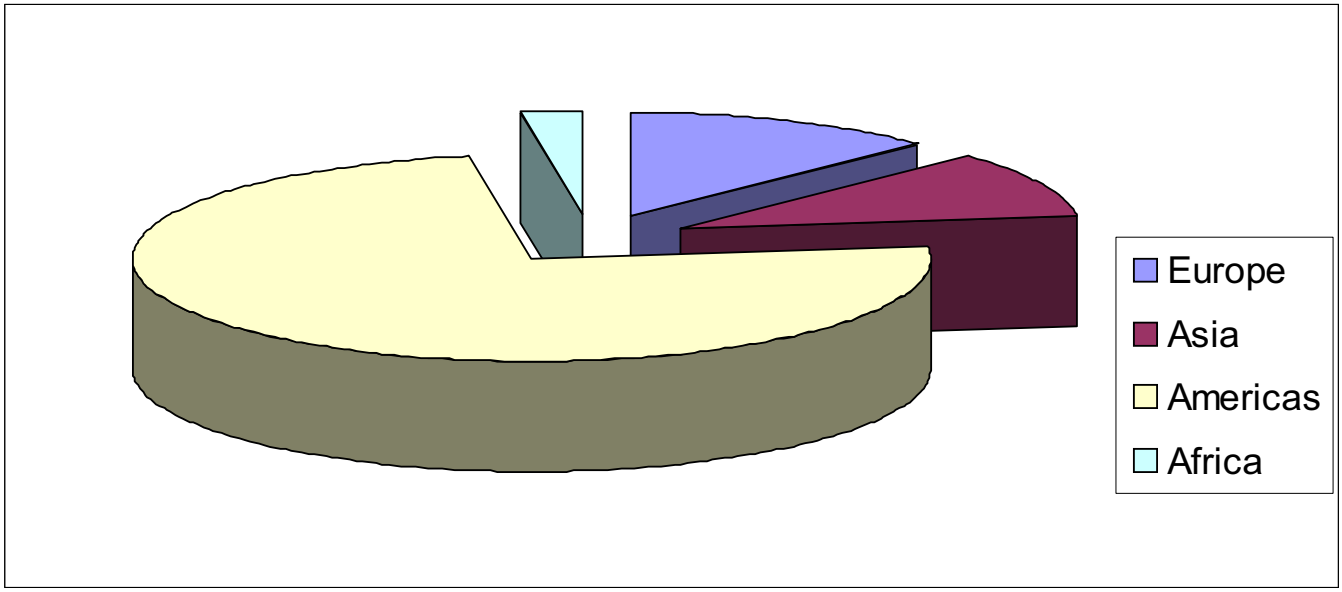


**Figure 1.** Participants breakdown.

This report contains the papers presented in the morning of June 17th, 2006. Due to an unexpected personal emergency, John Dolan could not present his paper nor participate in the field exercise. All papers in this report were reviewed by the authors. Except for Poropat's paper, all papers have been revised. The papers by Jason Birch (AdamTech), and Markus Pötsch, Andreas Gaich, and Wulf Schubert (3G) have been augmented with the results obtained during the Morrison field exercise in the afternoon of June 18th.

Following the presented papers, a summary paper compares rock mass characterization results for the Morrison site. The authors obtained these results by using data provided by AdamTech and 3G. The other presenters were not able to provide the authors with the requested data.

Finally, two supporting papers round-off the report by presenting additional systems and contributing detailed case histories that give the state-of-practice. These papers too were reviewed by the authors and are expanded versions of similar papers presented in a session of GoldenRocks 2006, the 41st U.S. Rock Mechanics Symposium.

This paper summarizes the discussions that took place during the workshop and is organized as follows. At the outset, the paper stresses the advantages of laser and photogrammetric methods for rock face characterization. Next, current technological limits and limitations are reported followed by indications on future developments and research needs. The paper ends up with some general references and the workshop schedule.

Details on the workshop discussion can be found in the recordings of the discussion, which form an integral part of this report.

## ADVANTAGES OF LASER AND PHOTOGRAMMETRIC METHODS FOR ROCK FACE CHARACTERIZATION

Advantages of using these technologies are several:

1. The ability to analyze large portions of rock masses, including inaccessible areas.
2. The ability to collect large data sets yields a more realistic picture of the fracture orientations; new fracture sets are oftentimes discovered that would be missed by manual investigations.
3. New insights into the rock mass structure are gained by selecting fractures or fracture sets on a stereonet and seeing their location on the 3D model.
4. The ability of zooming in and out of the face allows one to identify features, such as major shears or fractures, which are otherwise not apparent when working close to the rock face.
5. Fracture scale-dependency and invariants may be quantified by using triangles of different sizes to generate the DTM.
6. These methods are typically five times faster than manual data collection, without taking

into account the much larger number of data points. Speed in data collection leads to a series of related advantages, such as:

- Methods are less dependent on climatic conditions;
- Minimal impact on construction activities. For example, a yearly mining production saving of $ 200,000/300,000 (2006 value) may be achieved at just one face because data acquisition does not impact schedule.

7. Permanent documentation of the rock face condition for reporting and contractual-legal issues.
8. Permanent documentation of excavation stages with the added bonus of precisely determining excavation volumes. When each stage is documented, valuable information can be extracted, such as fracture persistence and fracture clustering, that allows for a reliable three-dimensional characterization of the rock mass.
9. No need for a photogrammetry expert; for example, in traditional photogrammetry, picking corresponding points in a pair of photographs required a well-trained photogrammetry expert. This expert is now is substituted for by the software bundle adjustment capability.
10. Digital photogrammetry is relatively range invariant. Indeed, if the object distance changes, one may change the focal length with the aim of keeping the image on the camera sensor the same length.

## LIMITS AND LIMITATIONS OF LASER AND PHOTOGRAMMETRIC METHODS FOR ROCK FACE CHARACTERIZATION

Current technological limits are as follows:

- Photogrammetric limits:
  3 km distance from ground (e.g., Nikon D2x with a 300 mm lens and 1.7x adapter, giving a focal length of 510 mm. The pixel size on the ground was just 3.25 cm), 6 km from air (this needs atmospheric correction, beyond this distance, atmospheric distortion makes images too blurred to be useful);
- Laser scanning limits:
  a. 800 m, typical.
  b. Dark layers do not reflect light, and thus no data is collected by laser.
  c. If features have no relief, laser will detect them. Photogrammetry is better in this respect because one can see the fracture traces, and from that determine orientation, spacing, etc

The workshop discussion on the current state-of-the-art suggested that:

1. These modern techniques must NOT substitute for qualified characterization of rock masses by an expert engineering geologist or geological engineer. They are a major aid in rock mass characterization to be used with great care by well-trained engineering geologists or geological engineers.
2. Conventional rock mass tools should still be used to validate the results obtained with these modern techniques.
3. Automatic trace delineation algorithms are still rock mass-specific and should be used with extreme care. Manual delineation by an expert engineering geologist or geological engineer is necessary.
4. Rock-bridge delineation algorithms are still to be developed. Detection and delineation of rock bridges is necessary, for example, to account for effects of non-persistent fractures on rock mass stability (e.g., in tunnels and slopes), and to develop fracture mechanics models of rock masses useful to determine time-dependent rock mass behavior under “static fatigue”.
5. Fracture statistics to correctly interpret 3D imaging is still being developed. The vast amount of literature on fracture statistics was primarily developed based on traditional investigation methods, which were either linear (e.g., scanlines), circular, or, for quite sophisticated exercises, bi-dimensional (face windows). Caution should be exercised in extrapolating these methods to 3D imaging and additional research is needed in this crucial area.
6. In some systems, surveying only needs to be as accurate as the required *absolute* positioning accuracy of the data. For example, if all is needed are the joint orientations to a few degrees, and the joint spacings to a few centimetres, then

surveying is not necessary at all. One or more scale bars and a compass are enough to achieve high relative accuracies and high directional accuracy, and a consumer-grade GPS suffices to position the DTM in the real world.

7. A few systems require more intensive surveying. In this case, GPS to determine camera or laser position must be a Real-Time Kinematic (RTK) GPS. RTK is a process whereby GPS signal corrections are transmitted in real time from a reference receiver at a known location to one or more remote rover receivers. The use of an RTK-capable GPS system can compensate for atmospheric delay, orbital errors and other variables in GPS geometry, increasing positioning accuracy up to within a centimeter. Using the code phase of GPS signals, as well as the carrier phase, which delivers the most accurate GPS information, RTK provides differential corrections to produce the most precise GPS positioning.
8. Roughness is amplified by precision errors.
9. Currently, the following quantities required for ISRM quantitative description of fractures cannot (completely) be extracted: roughness (JRC), wall strength (JCS), weathering, humidity/seepage, and filling.

This leads to the future developments discussed below.

## FUTURE DEVELOPMENTS OF LASER AND PHOTOGRAMMETRIC METHODS FOR ROCK FACE CHARACTERIZATION

The workshop discussion on the future developments indicated the following areas of research and development:

1. Classification of petrology and mineralogy. The first author suggests that the information provided by color photographs could be augmented with additional information, such as spectral analyses typically carried out in astronomy, for which very sophisticated algorithms have been developed, and are generally publicly available:
    - Mössbauer spectroscopy. In its most common form, Mössbauer Absorption Spectroscopy, a solid sample is exposed to a beam of gamma radiation, and a detector measures the intensity of the beam that is transmitted through the sample, which will change depending on how many gamma rays are absorbed by the sample. The atoms in the source emitting the gamma rays are the same as the atoms in the sample absorbing them. It is thanks to the Mössbauer effect that a significant fraction of the gamma rays emitted by the atoms in the source do not lose any energy due to recoil and thus have almost the right energy to be absorbed by the target atoms. The gamma-ray energy is varied by accelerating the gamma-ray source through a range of velocities with a linear motor. The relative motion between the source and sample results in an energy shift due to the Doppler effect. In the resulting spectra, gamma-ray intensity is plotted as a function of the source velocity. At velocities corresponding to the resonant energy levels of the sample, some of the gamma-rays are absorbed, resulting in a drop in the measured intensity and a corresponding dip in the spectrum. The number, positions, and intensities of the dips (also called peaks) provide information about the chemical environment of the absorbing nuclei and can be used to characterize the sample.
    - Thermal emission (different types of compounds will take on different temperatures when exposed to the same amount of sunlight), and
    - Visible-, near-IR, and mid-IR reflectance techniques. Figure 2 shows an example of data gathered by ASTER (Advanced Spaceborne Thermal Emission and Reflection Radiometer), which is an imaging instrument flying on Terra, a satellite launched in December 1999 as part of NASA's Earth Observing System (EOS) (http://asterweb.jpl.nasa.gov/).

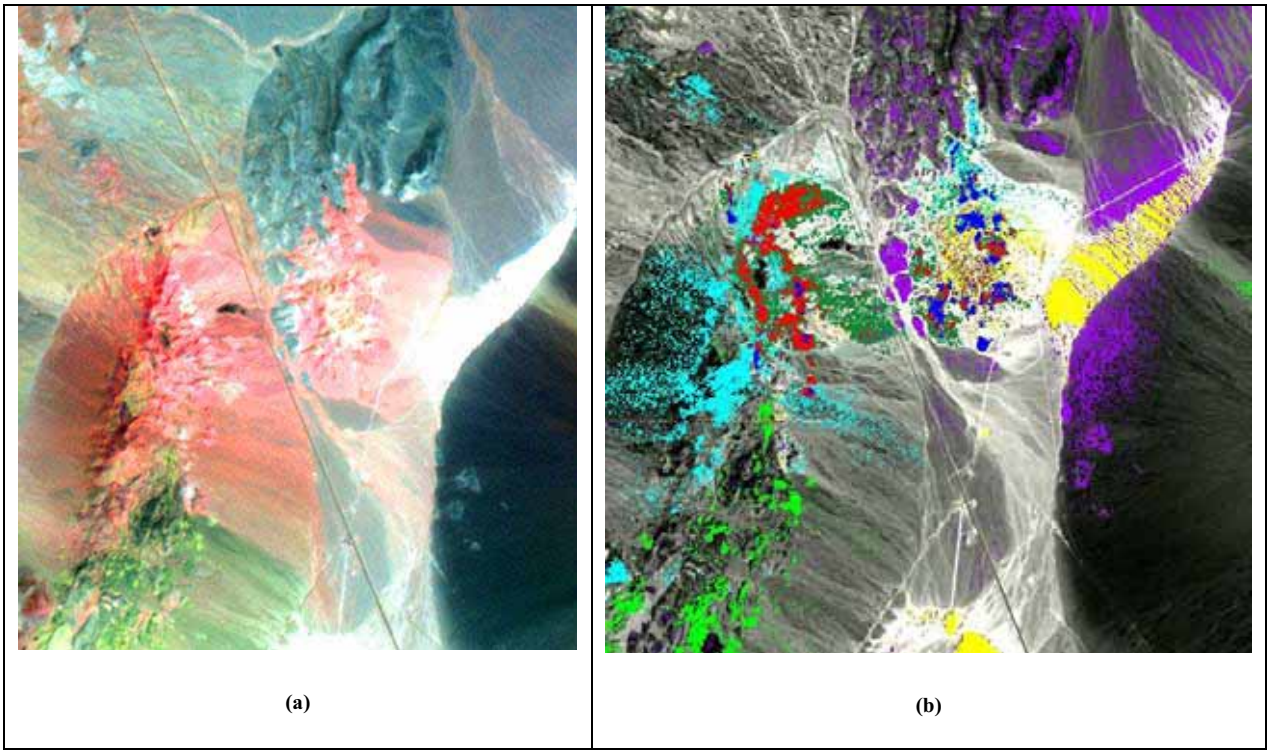

(a) (b)

**Figure 2.** (a) Cuprite Mining District, Nevada, displayed using ASTER SWIR bands 4-6-8 as a RGB composite. Area covered is 15 x 20 km. (b) Spectral Angle Mapper classification of Cuprite SWIR data. blue=kaolinite; red=alunite; light green=calcite; dark green=alunite+kaolinite; cyan=montmorillonite; purple=unaltered; yellow=silica or dickite.

Figure 2a shows a general picture of the hydrothermal alteration for the Cuprite Mining District, Nevada. Bands 4, 6 and 8 in RGB were combined and processed to increase the color saturation. In Figure 2a, red-pink areas mark mostly opalized rocks with kaolinite and/or alunite; the white area is Stonewall Playa; green areas are limestones, and blue-gray areas are unaltered volcanics. Data from the short wave infrared (SWIR) region were processed to surface reflectance to produce Figure 2b, where details of the mineralogy are finely appreciated.

2. Detection of rock blocks forming on a face. This topic is actively being pursued by various researchers, and preliminary results are presented in the papers that follow.
3. Statistical 3D characterization of rock blocks forming inside a rock mass. This topic is currently being investigated by George Poropat and co-workers at CSIRO with application to slope stability analyses.
4. Fracture statistics for three-dimensional imaging.

## GENERAL REFERENCES

### *1.1. Laser scanners*

- Survey of lasers: www.poboline.com
- Hardware and software reviews: http://www.commission5.isprs.org/wg3/

Paper: Geoff Jacobs, Understanding laser scanning terminology. Professional Surveyor Magazine, February 2005.

### *1.2. Photogrammetry*

- International Society for Photogrammetry and Remote Sensing: http://www.isprs.org/
- http://ldipinter.sunsite.dk/
- http://www.univie.ac.at/Luftbildarchiv/wgv/intro.htm

Books:

- Michel Kasser and Yves Egels, Digital photogrammetry. London ; New York : Taylor & Francis, 2002.

- Wilfried Linder, Digital photogrammetry : theory and applications, Springer Vlg 2003.
- Glenn Rand, David Litschel, Robert Davis, Digital photographic capture. Burlington, MA: Focal Press, 2005.


## WORKSHOP PROGRAM

Workshop participants learned the issues involved in laser and digital photogrammetric techniques, the possibilities offered by the new technologies, the difficulties and pit-falls the end-user must be aware of in the different stages (data collection, rendering, and rock mass analysis), how to address these problems, and various systems developed for this purpose. Practical demonstrations were carried out at an outcrop in the Golden area, and participants subsequently analyzed the data to characterize the rock mass.

There were three major sessions organized around a Saturday/half-day Sunday workshop:

**1.** *A morning session* on theory with presentations addressing:

- Issues involved in developing techniques;
- The possibilities offered by specific techniques;
- The difficulties and pit-falls the end-user must be aware of (data collection, rendering, and rock mass analysis), how to address them, and various systems developed to this aim) including:
  - Why is camera calibration so important and how does it affect the results?
  - What is the best measure of the quality of one's results?
  - What is the advantage of mixing cameras of different focal lengths?
  - What are the critical components of a system (calibration tools, automatic point cloud generation, detailed bundle adjustment and error checking, post processing tools and connection to high quality cad systems)?

**2.** *An afternoon demonstration/data collection session* at an outcrop. Presenters demonstrated how to effectively collect data using their systems. In order to allow for a uniform and fair comparison, all presenters were required to follow common specifications.

**3.** *A morning session on data analysis* including rock mass characterization. Workshop participants used the actual software developed by the presenters to create Digital Terrain Models (DTMs), and then use the DTM to characterize the rock mass (e.g., trace length, discontinuity orientation, contouring, number of discontinuity sets, presence of major structural features, such as major faults or shears).

## ACKNOWLEDGMENTS


The workshop was sponsored by: US Bureau of Reclamation, Split Engineering, and the American Rock Mechanics Association (ARMA). FHWA provided logistic support as well as surveying services for the field exercise.

**WORKSHOP PROGRAM:**

**Saturday, June 17th**: Location: Colorado School of Mines.

| | | |
|---|---|---|
| 7.30 8.30 | Registration | |
| 8.00 8.30 | Welcome, Introduction and Logistics | **Fulvio Tonon**:: Assistant Professor, University of Texas, Austin (workshop co-chair)<br>**Joe Kottenstette**:: US Bureau of Reclamation (workshop co-chair) |
| 8.30 9.15 | Basics, principles and application of 3D imaging systems with conventional and high-resolution cameras | **Markus Pötsch** and **Wulf Schubert**:: Graduate Student and Professor, Graz University of Technology (Austria)<br>**Andreas Gaich**:: 3G Software & Measurement GmbH (Austria) |
| 9.15 10.00 | Using 3DM Analyst Mine Mapping Suite for rock face characterisation | **Jason Birch**:: Managing Director, ADAM Technology (Australia) |
| 10.00 10.15 | Break | |
| 10.15 11.00 | LIDAR for Rock Mass Characterization: Hardware, Software, Accuracy and Best-Practices | **John Kemeny**:: Professor, University of Arizona (USA) |
| 11.00 11.45 | Remote 3D Mapping of Rock Mass Structure | **George Poropat**:: Research Group Leader, CSIRO (Australia) |
| 11.45 12.30 | Rapidly Acquiring and Analyzing Rock Mechanics Data Using Laser Scanning Technology | **John Dolan**:: Business Unit Manager, ISITE (USA) |
| 12.30 1.00 | Discussion | |
| 1.00 2.00 | Lunch (provided for full participants) | |
| 2.00 2.30 | Transfer to site | |
| 2.30 6.00 | Field exercise | |

**Sunday June 18th**: Location: Colorado School of Mines Computer Lab.

| | | |
|---|---|---|
| 8.00 8.30 | Welcome Back and Logistics | **Fulvio Tonon**:: Assistant Professor, University of Texas, Austin (workshop co-chair)<br>**Joe Kottenstette**:: US Bureau of Reclamation (workshop co-chair) |
| 8.30 9.15 | Outcrop Data Analysis and Rock Mass Characterization | **Markus Pötsch** and **Wulf Schubert**:: Graduate Student and Professor, Graz University of Technology (Austria)<br>**Andreas Gaich**:: 3G Software & Measurement GmbH (Austria) |
| 9.15 10.00 | Outcrop Data Analysis and Rock Mass Characterization | **Jason Birch**:: Managing Director, ADAM Technology (Australia) |
| 10.00 10.15 | Break | |
| 10.15 11.00 | Outcrop Data Analysis and Rock Mass Characterization | **John Kemeny**:: Professor, University of Arizona (USA) |
| 11.00 11.45 | Outcrop Data Analysis and Rock Mass Characterization | **George Poropat**:: Research Group Leader, CSIRO (Australia) |
| 11.45 12.30 | Outcrop Data Analysis and Rock Mass Characterization | **John Dolan**:: Business Unit Manager, ISITE (USA) |
| 12.30 1.00 | Discussion | |
| 1.00 2.00 | Lunch (provided to full participants)- -Adjourn | |

**Note**: Due to an unexpected personal emergency, John Dolan could not present his paper nor participate in the field exercise.

# Using 3DM Analyst Mine Mapping Suite for Rock Face Characterisation

Birch, J. S.
*ADAM Technology, Perth, Western Australia*

Copyright 2006, ARMA, American Rock Mechanics Association

This paper was prepared for presentation at the workshop: "Laser and Photogrammetric Methods for Rock Face Characterization" organized by F. Tonon and J. Kottenstette, held in Golden, Colorado, June 17-18, 2006.

This paper was selected for presentation by F. Tonon and J.T. Kottenstette following review of information contained in an abstract submitted earlier by the author(s). Contents of the paper, as presented, have not been reviewed by F. Tonon and J. Kottenstette, and are subject to correction by the author(s). The material, as presented, does not necessarily reflect any position of USRMS, ARMA, their officers, or members. Electronic reproduction, distribution, or storage of any part of this paper for commercial purposes without the written consent of ARMA is prohibited. Permission to reproduce in print is restricted to an abstract of not more than 300 words; illustrations may not be copied. The abstract must contain conspicuous acknowledgement of where and by whom the paper was presented.

**ABSTRACT:** One of the most popular uses of 3DM Analyst Mine Mapping Suite is the generation of 3D images for geotechnical analysis. This paper will describe the benefits of using digital photogrammetry for this application as well as some of the common problems that are encountered and how to solve them. It will also discuss the importance of camera calibration and how it is performed, the various options for planning a project, and how to predict the accuracy that will be achieved.

## INTRODUCTION

3DM Analyst Mine Mapping Suite is a digital photogrammetric system that is currently being used by mapping, surveying, mining, and engineering companies in Australia, Canada, Indonesia, Japan, Norway, the UK, the US, and Venezuela. It represents the culmination of ten years' research and development in digital photogrammetry and builds on ADAM Technology's 20-year history of designing and manufacturing analytical stereoplotters and the associated mapping software.

Although photogrammetry has a well-established reputation for remote measurement and remains a mainstay of the aerial mapping industry, until recently its use was limited to well-trained professionals with good stereo perception and an intimate knowledge of the underlying theory.

With the advent of high quality yet affordable digital cameras, ADAM has developed a system that retains all of the rigor of a state-of-the-art photogrammetric system but with a degree of performance and automation that make it accessible to anybody who can capture a photographic image.

A measure of our success in achieving that goal can be gleaned from the range of tasks that the software is being used for today: geological and geotechnical analysis, resource modelling, end-of-month pickup, stockpile volumes, truck volumes, aerial mapping, road subsidence monitoring (accurate to 1mm), denture wear measurement (accurate to 5 microns), and the monitoring of stretch, wear, and corrosion on the chains used to anchor offshore oil and gas platforms — almost all of which are being performed by customers who had no prior experience with photogrammetry.

One of the most popular applications is pit wall mapping for geotechnical analysis. Key reasons for this include:

**(i)** The ability to capture large areas of pit wall easily and safely simply by photographing them.

**(ii)** The ability to obtain data from up to 3 km away or from the air when there is no safe access to the area being mapped.

**(iii)** The ability to identify features that would otherwise not be apparent when working too close to the rock face.

**(iv)** The speed with which the data can be generated compared to other techniques.

**(v)** The level of accuracy and detail of the data generated compared to other techniques.

**(vi)** The fact that acquiring the data has little impact on mining activities.

**(vii)** The ability to acquire data in a wide range of climactic conditions.

**(viii)** The fact that the images form a permanent record that can be referred back to in the future for reporting and legal issues.

(ix) The fact that the physical components of the system, namely the computer and the digital camera — which are the only parts that can break down — are relatively cheap, available from many suppliers, and easy to replace.

Using a modern digital camera, a pit wall can be photographed and a detailed Digital Terrain Model (DTM) and 3D image generated in less than ten minutes. Given the distance between any two points in a scene (or between any two camera positions) our software is able to generate correctly-scaled data even without any control points or surveyed camera positions; with at least three known locations — control points and/or camera positions — the data can also be registered in a real-world co-ordinate system, even when it is impossible to place control points in or near the area of interest.

Key features of 3DM Analyst Mine Mapping Suite that make it especially attractive as a digital photogrammetric package include:

(i) The speed of the software — given a pair of 11 megapixel digital images, a user can digitise control points, specify camera stations, determine the absolute orientation, and generate a surface model consisting of 350,000 points in under five minutes on a modern PC. Projects can also be processed in batch mode so users don't need to wait for the data to be generated.

(ii) The level of automation — the software can usually determine the relative orientation of the cameras fully automatically and generate surface models without operator input.

(iii) The ability of the software to detect problems with the data supplied by the user and advise the user on how to rectify those problems.

(iv) The accuracy of the data provided — customers have achieved accuracies of 5 microns from 100 mm away, 0.7 mm from 20 m away, and 0.1 m from 2.8 km away, using standard consumer digital cameras.

(v) The ability of the software to calibrate almost *any* modern digital camera.

(vi) The level of support offered by ADAM Technology to ensure customers maximize their benefit from using the software.

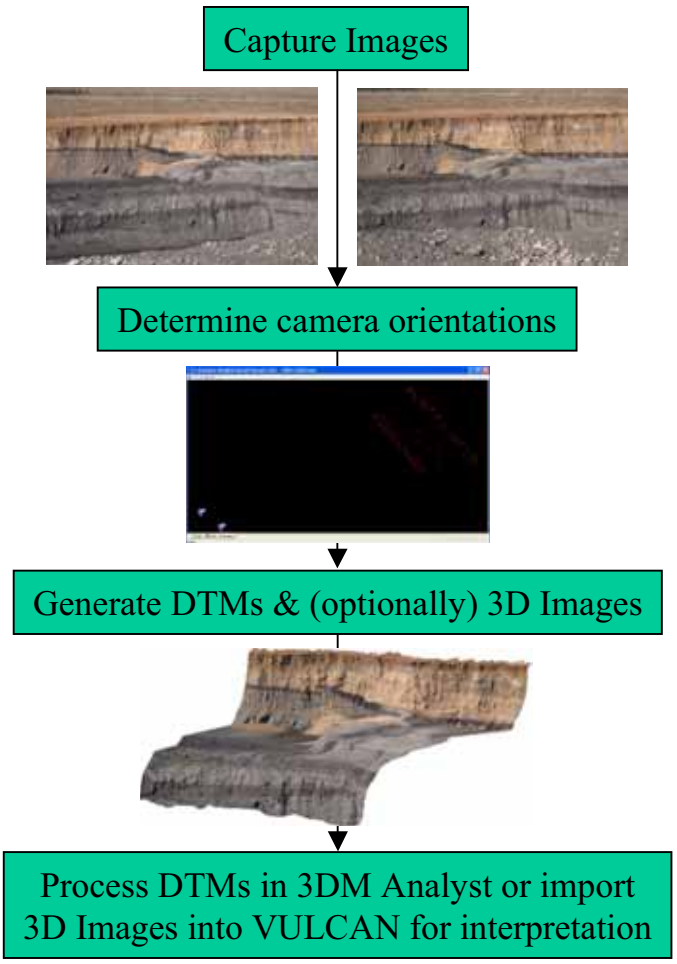


**Figure 1. Geotechnical analysis workflow.**

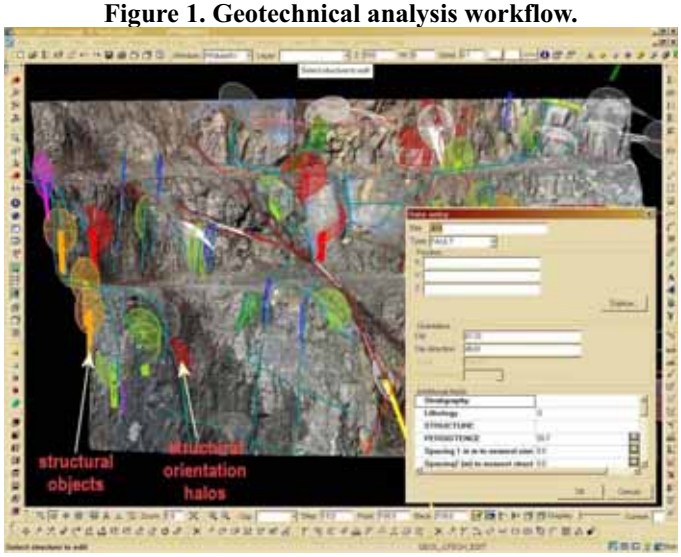


**Figure 2. Geotechnical analysis of a pit wall in VULCAN.**

To illustrate where 3DM Analyst Mine Mapping Suite fits in the food chain, Figure 1 shows the typical workflow for geotechnical analysis, while Figure 2 is a real-life example of a 3D Image generated by 3DM Analyst being analysed in Maptek's VULCAN software.

## PRINCIPLES OF PHOTOGRAMMETRY

Photogrammetry is the science of determining 3D data from two or more 2D images of a scene. It does this by identifying the same point in each image and then projecting a ray into the scene from each point through the *perspective centre* of each camera to find the location where they intersect (Figure 3).

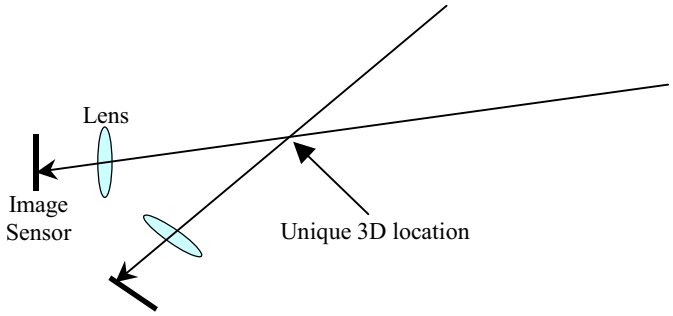


**Figure 3. Light that arrived at a particular pixel in an image could have originated at any point in the scene along the ray depicted. By intersecting two such rays we can determine the unique 3D location where the light for that point must have originated.**

In order to do this, the precise location and orientation of the camera when each image was captured (the *exterior orientation*) must be known.

To determine the exterior orientation, 3DM Analyst Mine Mapping Suite uses an algorithm called a *least squares bundle block adjustment*. This is a sophisticated algorithm that takes as input:

- The image co-ordinates of each point being used for orientations;
- The estimated accuracy of the image co-ordinates of those points ($S_x$,$S_y$);
- The ground co-ordinates of the control points, if any;
- The ground co-ordinates of the camera stations (i.e. camera locations), if any; and
- The estimated accuracy of each co-ordinate of each control point and camera station ($S_x$,$S_y$,$S_z$)

As output it produces:

- The adjusted (i.e. corrected) image co-ordinates of all points;
- The adjusted ground co-ordinates of all points digitized in the images, whether they were previously known (control points) or not (relative-only points); and
- The exterior orientation of each image.

Note that not all points digitised in the images need to have known ground co-ordinates. *Relative-only* points are automatically generated by the software to help establish the relationship between the camera positions with respect to each other, and can also be manually digitised by the user in order to generate a ground co-ordinate for a point of interest with a previously unknown location.

No matter how many images are in a project, only three points with known locations are required (any combination of control points and camera positions) to register the data in a real-world co-ordinate system, and none are required at all if a real world co-ordinate system is not needed. Using more than three points provides redundancy, which is an important part of estimating the accuracy of the generated data as well as insuring against bad observations (which the software can also automatically detect).

Control points and camera stations can also be used even if not all co-ordinates are known — for example, points with a known height or a known easting and northing can be used for control just as easily as points for which full co-ordinate information exists.

There are also no requirements placed on the orientations of the camera beforehand — they can be in any position, in any orientation, and can even be hand-held or in motion if desired. This allows the same software to be used for aerial mapping, pit wall mapping, tunnel mapping, and underwater mapping, without any changes required to the software at all.

Finally, there are no limits placed on the number of images that can be used in the same project, as the software never *needs* more than two images in memory at once, although it will load in more to improve performance if memory is available. The largest projects reported by our customers to date consist of over 200 images — enough to map 800,000 $m^2$ of pit wall to an accuracy of better than 25 mm with a good camera.

### *Accuracy Prediction*

The first question that should be asked when planning any project is “What accuracy is required?”

One of the great strengths of photogrammetry is the degree to which the accuracy of the data can be

tailored to fit by choosing the appropriate lens and working distance. (The accuracy in the direction of view — the *depth* accuracy — also depends on the ratio between the separation of the cameras and the distance to the pit wall.)

The reason for this is that the accuracy of the generated data depends primarily on the pixel size on the ground — a pixel that is 1 cm × 1 cm on the ground will generally be about ten times as accurate as a pixel that is 10 cm × 10 cm on the ground. (The reason it is not always exactly ten times as accurate is because the final accuracy depends on other factors as well, such as the surveying accuracy of the control points and camera locations.)

The good news is that the size of a pixel on the ground is completely determined by (1) the distance from the camera to the surface in question (*distance*), and (2) the focal length of the lens being used (*f*):

$$pixelsize_{ground} = \frac{distance}{f} pixelsize_{sensor} \qquad (1)$$

(All values should be in the same units, e.g. meters.)

For example, a Canon EOS 20D has a pixel size of 6.42 microns. A 28 mm lens from 174 m away will give a ground pixel size of 4 cm × 4 cm. So will a 50 mm lens from 312 m away, a 100 mm lens from 623 m away, a 200 mm lens from 1250 m away, and a 300 mm lens from 1870 m away. (So far, the record for a 3DM Analyst user mapping pit walls for geotechnical analysis is a 3 cm × 3 cm ground pixel size from 2.8 km away using a 300 mm lens with a 1.7 × adapter on a Nikon D2x.) Conversely, given a working distance of 500 m, for example, a user can choose between a pixel size of 11 cm × 11 cm (28 mm lens), 6 cm × 6 cm (50 mm lens), 3 cm × 3 cm (100 mm lens), and so on.

Given the ground pixel size, the actual *accuracy* that can be expected in the plane parallel to the camera's image plane (the *planimetric* accuracy — typically similar to the plane of the pit wall for face mapping) depends on the quality of the calibration, the ability to accurately locate control points in the image, and the accuracy of the control point co-ordinates themselves. The best planimetric accuracy that ADAM Technology has seen so far is a value of 0.05 pixels (0.7 mm in that case) using circular targets located in the image using the software's automatic centroiding function. A more typical value for planning is 0.3 pixels, with 0.5 pixels being a good conservative value.

Given the expected planimetric accuracy, the separation between the cameras (the *base*), and the distance from the cameras to the pit wall (*distance*), the depth accuracy is simply:

$$\delta_{depth} = \frac{distance}{base} \delta_{planimetric} \qquad (2)$$

(Note that this applies to measurements using two images only; observing a point in multiple images captured from different locations allows the depth accuracy to be improved greatly even if the base is small.)

Looking at the formula, it is clear that as the base tends to zero (i.e. the cameras are moved to the same location) the standard error of the depth tends to infinity, as one would expect — when the two camera positions are identical all depth information is lost.

To ensure a good depth accuracy requires a small distance:base ratio, with 1:1 giving the same accuracy in all dimensions. Unfortunately, increasing the base also increases the difference in appearance of the scene from each camera position, making it difficult for the software (or the user!) to recognize common points. Moving the cameras closer together makes it easier for the software to recognize common points, but reduces the depth accuracy.

Fortunately, the "sweet spot" where the software has little difficulty matching common points while depth accuracy remains good is quite large — we normally recommend distance:base ratios of between 2:1 and 10:1, but the software has been shown to handle a ratio of 1:1 if the surface is reasonably flat (like a pit wall). This gives the user a great deal of flexibility in planning their project to meet both the planimetric and depth accuracy requirements.

*Accuracy Evaluation*

The difference between theory and practice, of course, is that in theory there isn't any.

In practice, however, it's a good idea to actually *check* the accuracy that was achieved before using the data — preferably before generating it!

There are several methods of doing this. The most tedious, time-consuming, but accurate method

would be to generate the surface models and from them manually measure the locations of the control points to see how close they are to the surveyed locations. The advantage of this is that it not only measures the accuracy of the orientations but also that of the DTM generation algorithm and the user's ability to digitise features as well, so we recommend doing this once in a while.

A much faster and easier method is to simply read the post-orientation report from the software.

Before performing an orientation, the user specifies how accurate they expect the image co-ordinates to be by specifying the expected size of a single standard deviation (or "sigma")[1]. (For a calibrated camera this should generally be in the range of 0.1 to 0.2 pixels.) They also specify how accurate they expect the control points to be in the same way.

The software will take both of these into account when it performs the bundle adjustment and the first number that the user should check is the overall Sigma reported by the software — a value larger than 1 indicates that the data is not as accurate as they claimed it was going to be (indicating a potential problem), and a value smaller than 1 indicates that it is more accurate than expected (suggesting they may have been overly pessimistic on their image co-ordinate sigmas or control point sigmas, or perhaps they don't have enough redundancy.) A value close to 1 is a good sign.

The next thing to look at is the residuals of the control points (i.e. the differences between the supplied control point co-ordinates and the co-ordinates derived by the software using the bundle adjustment). Provided there is enough redundancy, this should give a good indication of how accurate the orientations are.

Finally, the user should look at the residuals of each individual control point and check that none of them are anomalous — an unusually large figure suggests a problem with the control point that warrants further investigation. (In our experience, the answer often turns out to be bad survey data; the biggest error in a control point's location we have seen so far was *2 km*, but smaller errors are not uncommon.) The software can automatically check control points and report any that are suspicious.

Photogrammetric best practice dictates that the user should also consider withholding the co-ordinates of a set of control points to allow them to be used as *check points*. These should be digitised in the usual manner and the software used to derive their locations, and these locations then checked against the surveyed locations. If all is well, their residuals should be similar to the residuals of the other control points that were used to control the orientations. (If they are much larger then there may be insufficient redundancy and the software is "over-fitting" the orientations to the limited control it has.) A simple way to do this is to simply give them very large sigmas (e.g. 1000 m or more) so they have no bearing on the bundle adjustment solution — this has the advantage of getting the software to calculate the residuals automatically.

It is worth noting that the accuracy of the control points (determined by looking at their residuals) will tend to be higher than the accuracy of other features, particularly those that are measured using the generated surface model.

This is partly because control points tend to be easy to identify; in the best case, circular targets are used and the software can locate the centre of those *very* accurately — often better than 0.1 pixels, much more accurately than a human can identify a point. Even when manually measured, the user will tend to take more care trying to locate the point accurately than when digitising normal features.

The other reason, however, is that data derived from the surface model is also subject both to the matching accuracy of the software when generating the points on the surface (typically about 0.3 pixels), and the sampling error caused by the discretization of the surface itself (the software will only generate points about every 8 pixels by default, although this can be adjusted by the user down to every 4 pixels if desired) in addition to the accuracy of the orientations themselves.

The matching accuracy can also be degraded by noise in the images, which is why ADAM always recommends using ISO 100 for the image sensor sensitivity.

[1] Also known as the Root-Mean-Square ("RMS") of a population, the standard deviation indicates how accurate the data is. Assuming a normal distribution, approximately 68% of the measured values should lie within one standard deviation (1σ) of the true values, and approximately 95% within 2σ. A smaller RMS therefore means measured values are closer to the true values, and hence accuracy is higher.

For this reason, it is still wise to occasionally check control point locations by hand using the DTM as recommended at the beginning of this section.

(Note that operators using the Stereo View are not subject to the accuracy of the DTM; manual observations in this view can often approach the accuracy of the orientations.)

## IMAGE CAPTURING TECHNIQUES

The flexibility of the software with regard to camera orientations that was mentioned previously allows a great deal of latitude in the design of image capturing procedures.

The three most common procedures that we recommend to our customers are convergent images (for individual models), strips (for large projects where the camera cannot be moved very far from the pit wall), and image fans (where the camera *can* be moved further away).

In each case, the primary goal is to find the optimum balance between conflicting aims:

(i) To minimise the time and risk associated with capturing images.

(ii) To maximise the robustness and accuracy of the resulting data.

*Independent, Convergent Models*

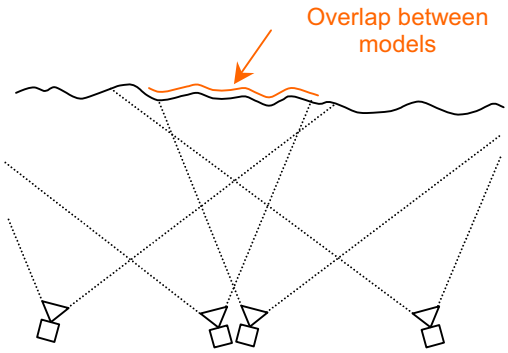


**Figure 4. Independent, convergent models.**

The key characteristic of this method is that close to 100% of each image is used in a single model, and if multiple models are required to cover the pit wall there is very little overlap between them. (In practice it would be wise to plan for a 10–20% overlap between models to ensure there are no gaps in the generated DTMs.)

The downside of this method is that each model needs to be fully controlled, and so the surveying requirements are more onerous. (There *is* some scope for passing control information between models by taking advantage of the overlap between them (see Figure 4), but the accuracy will be worse than if the model was controlled unless the overlap is 30% or more, as shown in the image.)

This method is most desirable when only a single model is required.

Other advantages of this technique are:

(i) There is a great deal of flexibility in the distance between the camera stations. The distance:base ratio can be freely chosen between about 2:1 and about 10:1, with the choice being largely determined by the desired depth accuracy of the model and convenient shooting locations.

(ii) This method can be used with cameras of any focal length operating over any distance.

*Strip of Models*

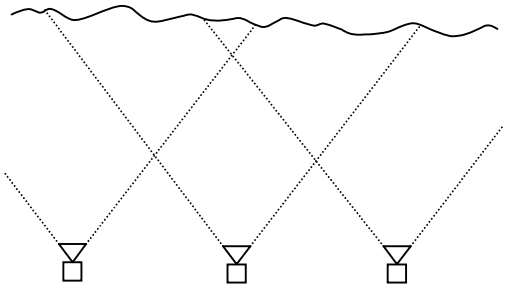

**Figure 5. Strip of models.**

In this method, a series of parallel images with large overlap (typically 60%) are captured.

The key advantage of this technique is that the large degree of overlap between images allows orientation information to be reliably and accurately passed between models, drastically reducing the number of control points required for a given job without sacrificing accuracy.

Apart from being the normal method used with aerial photography, this method is best used when mapping a long stretch of pit wall from a short distance and a short focal length lens (e.g. 28 mm). The Object Distance spreadsheet supplied with 3DM Analyst Mine Mapping Suite can calculate exactly how far apart the camera stations need to be to ensure the entire wall is captured optimally.

During a trial conducted by BMA Coal in 2004 we were able to demonstrate that this technique could be used to control a project consisting of 36 images (mapping 700 m of pit wall) to better than 6 cm using just one control point in addition to the surveyed camera locations, and better than 4 cm using nine control points. BMA Coal now routinely

uses one control point for every five images and reports an accuracy of 2 cm on average.

One drawback to using this technique is that the lens focal length determines the distance:base ratio necessary to ensure adjacent images overlap correctly, reducing camera position flexibility. It also makes it less desirable for longer focal length lenses because the distance:base ratio becomes larger, reducing depth accuracy.

*Image Fans*

Fortunately, in the cases where long focal lengths are desirable — namely, when the distance to the pit wall is large — the best technique overall becomes available: Image fans (Figure 6).

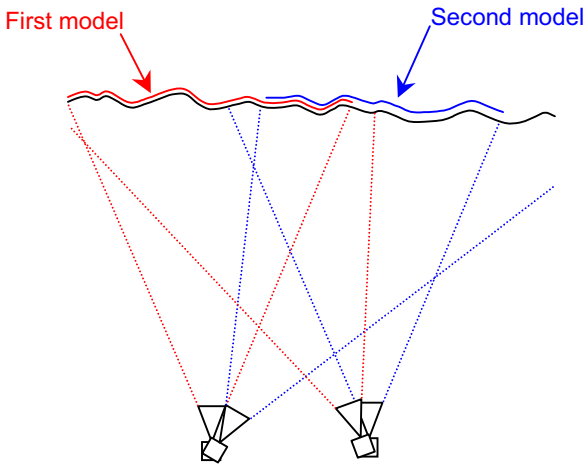


**Figure 6. Image fans.**

Image fans are similar to independent, convergent models, except that a series of images are captured from each camera location. Ideally, the images should be captured with a small overlap (at least 10%) to reduce the chance of gaps in the models, and provide the option of sharing orientation information so each model does not necessarily need to be individually controlled.

A key advantage that image fans have over the independent, convergent models is that because multiple images were captured from each location there are far fewer unknowns to be determined by the bundle adjustment. This improves the strength of the solution, makes the bundle adjustment run faster, and reduces the minimum number of control points required to find a solution down to one for the entire image fan if both camera locations are known (three if the camera locations are unknown).

Another advantage is that 3DM Analyst Mine Mapping Suite supports *image merging*, where any number of images captured from the same location can be merged into a single, high-resolution image to sub-pixel accuracy, similar to the panorama software that ships with some digital cameras, but photogrammetrically correct. These merged images can be used in 3DM Analyst as a substitute for the original images (Figure 7). The practical benefits of

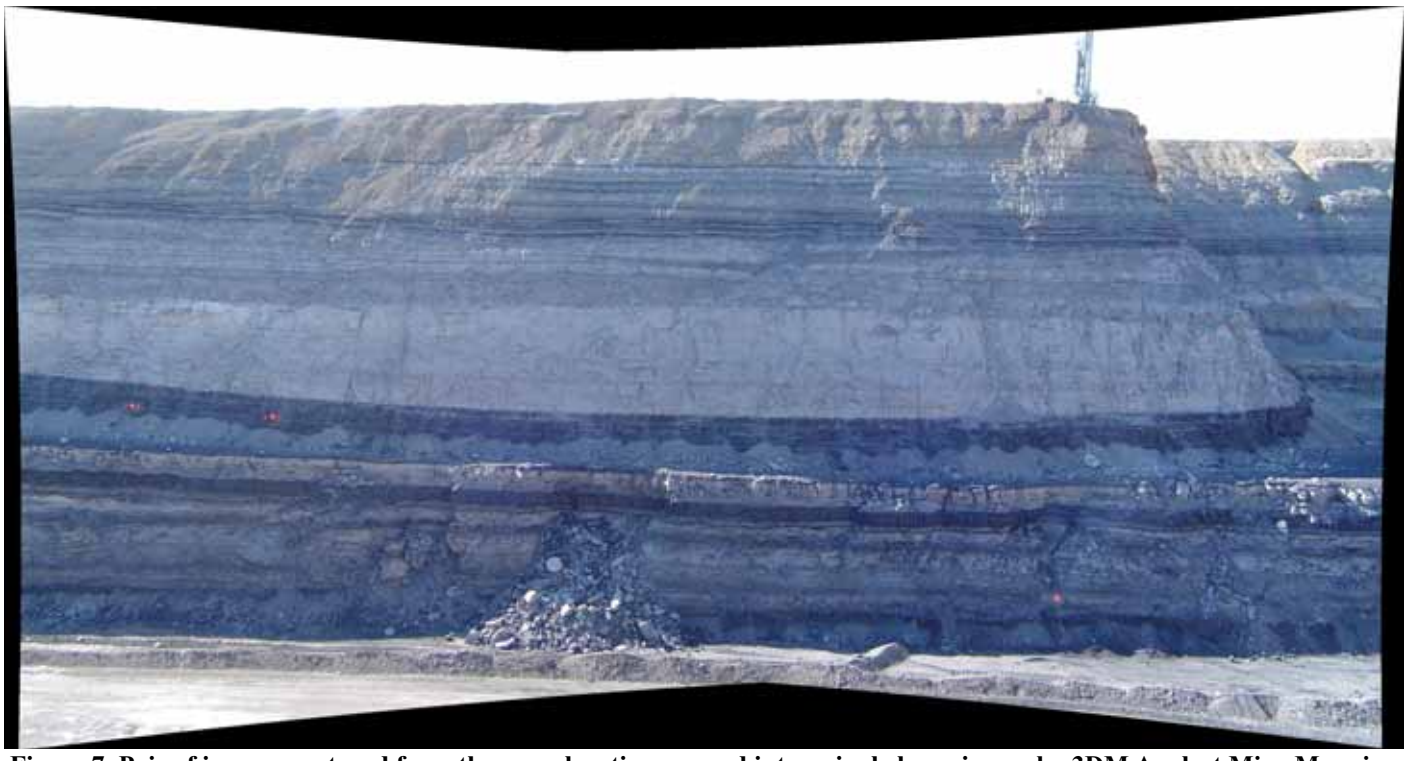

**Figure 7. Pair of images captured from the same location merged into a single large image by 3DM Analyst Mine Mapping Suite. Black areas around the image show how far pixels were moved to remove distortions.**

this are:

(i) A cheaper and lower-resolution camera can be used instead of a much more expensive high-resolution camera to produce the same results, reducing the capital expense of the camera at the cost of slightly increased labour costs (time is spent rotating the camera to capture multiple images and merging them afterwards).

(ii) Images can be captured to build up the fan without regard for precisely where they are pointing. All the operator needs to do is ensure there is about 10% overlap between adjacent images captured from the same location. For example, imagine the user captured the two images depicted by the red and blue lines in Figure 6 from the left camera station and then moved to the right camera location to capture the corresponding images from there. Normally they would need to ensure that the image of the first model area captured from the second location lined up with the image of the first model area captured from the first location (red lines) so that a convergent model could be formed. Using image merging means that they just need to ensure that the images captured from each location cover the entire area of interest, and later a single, merged image will be created.

The only drawback with this technique is that the merged images can become very large if many images are merged together — the comfortable limit for 3DM Analyst on a PC with 2 GB of RAM is about 65 megapixels. (There is another version of the software, 3DM Analyst Professional, which can handle images in excess of 250 megapixels. This version is normally used by mapping companies with scanned large format aerial images.)

To alleviate that, 3DM Analyst Mine Mapping Suite allows the user to tile a merged image to create images that can be processed more comfortably; this is still an advantage over using the original images because the benefits of not having to line images up in the field are retained, and the user is free to choose an image size larger than the native image size of their camera.

Image fans are ideal when longer focal length lenses are used over large distances. Customers have used image fans to capture a 1 km stretch of pit wall with a 4 cm ground pixel size from just two locations on the opposite pit wall, 1 km away.

Apart from the fact that multiple images are captured from each camera location rather than a single, low-resolution image, there really isn't any conceptual difference between image fans and independent, convergent models, so all of the other attributes of the latter apply to this method as well.

*Combinations*

Apart from directly supporting image fans by optionally using a single camera location for multiple images, 3DM Analyst Mine Mapping Suite is completely agnostic when it comes to the method used to capture the images.

One advantage of this is that the user is free to use any combination of techniques they wish in the same project without any limitations. For example, if the pit wall was too high to be photographed in sufficient detail in a single image, the user might opt to use a strip of images but from each camera location capture two or more images vertically to create a mini-fan.

Alternatively, if the middle two camera positions in Figure 4 were co-located, then image fanning could be used to create a single, wider merged image at each location, with the merged images conceptually forming a strip of images.

The user could also use one method for one section of the wall and a different method for another section if that was more appropriate.

*Control*

As mentioned previously, to form an absolute orientation requires at least three known locations — either control points or camera stations.

One of the advantages of surveying camera stations is that the point in question must be safe for the surveyor to access — the image was captured from there, after all. The disadvantage is that the point is further away from the area of interest, which magnifies the surveying error.

Photogrammetric best practice is to bracket the area of interest with control points — the accuracy of the data will be maximized within the region surrounded by control. Going outside this region requires extrapolation, magnifying error.

Sometimes it is not possible to place control near the region being mapped — for example, when mapping a pit wall failure. The most accurate way to map areas like this is to place control a safe distance away on either side (and/or in the

background) and capture overlapping images from one controlled area to the other, crossing over the area to be mapped in the process.

Another alternative is to place control points in the foreground, far enough away from the wall to be safe, but not so close to the camera that the surveying error is magnified beyond the accuracy required at the pit wall.

Former images of an area that were previously controlled can also be incorporated into a project to control it — even if the control points used in the former images have been subsequently removed.

*Effort*

The amount of effort that should be spent in planning and placing and surveying control should be related to the cost of recapturing images if required and the ability to do so.

Some of our customers use our software to make accurate and detailed models of subsea structures on gas and oil platforms. The daily cost of capturing the images required for that task can be $250,000 per day. Clearly, in their case, they *never* want to have to go back and capture the images again.

Aerial photography, too, is expensive, often costing around $25,000 to photograph a single mine. It makes sense to plan carefully, place additional control points, and capture additional images, to reduce the chance of having to do the flight again.

Capturing a pit wall, however, is generally a lot less expensive and time-consuming. Except in cases where it will be impossible to capture the pit wall again, it may make more sense to build in less redundancy and occasionally have to re-do the field work than to survey large numbers of control points and go to great lengths to ensure the photography is perfect.

## GENERATING DATA

Once the camera orientations have been determined, the next step is to identify common points in stereo image pairs in order to project rays into the scene and determine their 3D locations.

In 3DM Analyst this is fairly straightforward — simply clicking on the “GO” button will generate a DTM that can then be viewed in 3D with texture draped over it for analysis, or in stereo with the appropriate viewing hardware.

The time taken to generate the data depends on the size of the images, but between two and five minutes is common. For large projects this can be batch-processed in the DTM Generator, which can process any number of jobs without user intervention, e.g. overnight.

Both 3DM Analyst and DTM Generator can also automatically create 3D Images suitable for use in VULCAN, Surpac, and other software supporting that file format, and 3DM Analyst can also export the DTM in DXF format as points, triangles, or both, or as a textured Alias Wavefront *.obj file.

3DM Analyst can also create contours and cross-sections, and calculate volumes — both to a datum and as a difference between two DTMs. It can also merge DTMs together.

Another useful tool is 3DM Ortho Mosaic — an optional extra package that can be used to create seamless mosaics of orthorectified DTMs projected onto any plane.

*Traditional Mapping*

Because it is a fully-fledged mapping package, 3DM Analyst features a full complement of mapping tools. It allows up to 160,000 user-defined feature styles to be specified in a hierarchy of four levels with 20 feature styles per level (Figure 8).

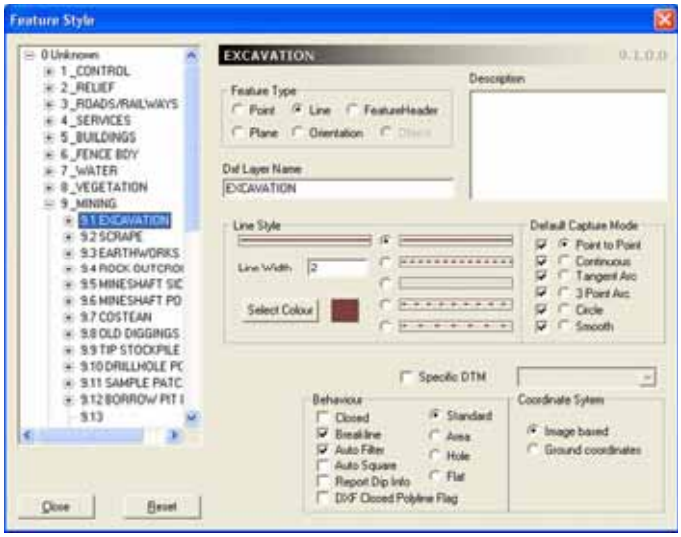

Figure 8. Feature definitions.

Each feature style can be assigned a DXF layer name for importing from and exporting to DXF. The most important feature types are points, lines, and planes, and line features can be captured in point-to-point mode, continuous mode (points are added to the line continuously as the floating mark is moved, recording every movement the operator makes), two different arc modes (for curbs, etc.), circle mode,

and smooth mode (like point-to-point mode except the points are connected by smooth arcs). The user can switch between modes at any time while digitising a line.

Line features can also affect the DTM:

- *Breaklines* allow the user to specify that triangles should not cross a certain feature;
- *Areas* allow the user to specify a subset of the model area where DTM points should be automatically generated;
- *Holes* allow the user to specify where DTM points should *not* be generated, leaving a hole in the DTM; and
- *Flats* allow the user to specify that there should be no points within the area delimited by the line feature but that area itself should remain part of the surface (good for buildings, allowing contours to be generated through buildings as if they weren't there).

Areas, holes, and flats can be nested and the system will honour them all (e.g. the user could specify a hole or a flat line feature around a lake, but an area line feature around an island within the lake).

Lines can also be automatically squared (the software will make nearly parallel lines parallel and nearly perpendicular lines perpendicular if it can do so without moving any point by more than the amount you have specified in the job's accuracy setting — good for digitising buildings) and closed.

Data can be digitised in full colour stereo using either a StereoGraphics' Z-Screen with polarising glasses or LCD shutter glasses, or in anaglyph mode. It can also be digitised in the 3D View directly onto the DTM, or in the Images View in Single Image Digitising mode (where the software automatically locates the corresponding point in the other image, first by using the DTM then fine-tuning it by performing image matching).

For serious mapping the software supports ADAM's full range of handwheels, footdisks, and foot-switches as well.

*Structural Mapping*

For mapping discontinuities the most important feature type is the plane feature type.

3DM Analyst offers a range of options for digitising discontinuities, depending on whether they are visible as traces or faces. Faces can be digitised semi-automatically using the "single point digitising" option, where a single point is placed on the face and the software automatically determines the extent of the face and digitises it, using all points on the DTM within the face to determine the plane's orientation. This allows the user to determine which faces are relevant while keeping the workload to a minimum. Faces can also be digitised manually by placing three or more points on the face, and the software will fit the plane to the points the user has digitised. Finally, they can be digitised fully automatically, by having the software detect all flat surfaces in the scene, which the user can select on a stereonet to add to the project. In each case, the software finds the best fit plane for the points in question and reports back to the user how well the points fit the plane in the form of the RMS of the distances of each point from the plane.

Traces cannot be digitised automatically; instead, the user digitises three or more points along the trace in exactly the same way as the manual face digitising option (). Normal polylines can also be used to digitise plane features — the software can be instructed to create the plane feature automatically as soon as the polyline is saved, or existing polylines can be selected and used to create plane features.

Once digitised, planes can be intersected with the DTM to create a polyline that exactly follows the shape of the DTM. For traces, the best option is to intersect the plane with the DTM directly; for faces,

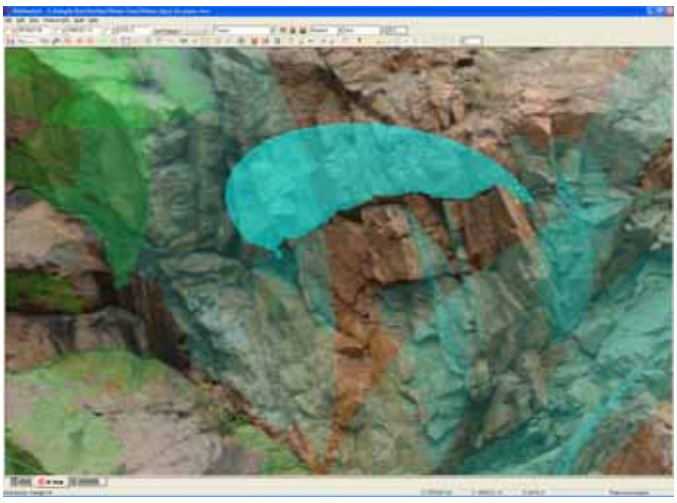

**Figure 9. Digitising a trace. The orientation and location of the disc updates automatically as points are added to the feature. Other features become more transparent when a new feature is started to make it easier to see the surface while digitising. The view can be rotated at any time while digitising to see the structure more clearly.**

a plane perpendicular to the given plane and parallel to the dip direction can be used to create a profile.

The dip, dip direction, location, and size can all be edited as well, and comments added on a feature-by-feature basis (Figure 10). All of these can be exported for use in other software, like Dips, and poles can be plotted on a stereonet for analysis within 3DM Analyst itself.

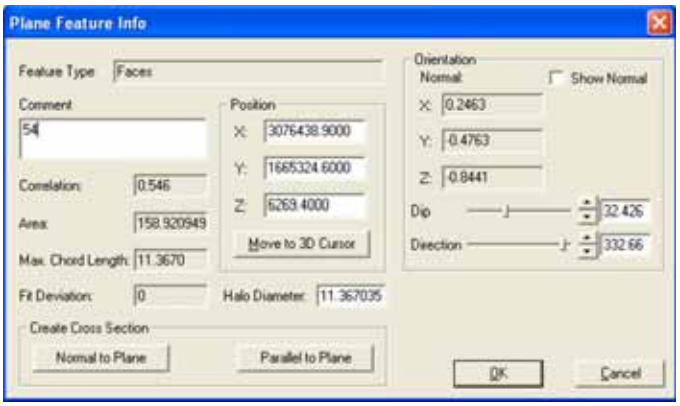


**Figure 10. Information available for plane features.**

## CAMERA CALIBRATION

Photogrammetry has traditionally been used with metric cameras — cameras that are designed to resemble the "ideal" camera as much as possible and require very little calibration. Large format film cameras, for example, often have such small lens distortions that verifying the calibrations are being applied correctly can sometimes be a challenge!

In contrast, a compact digital camera or digital SLR with a short focal length lens can easily have lens distortions in the range of 50 to 100 pixels (Figure 11).

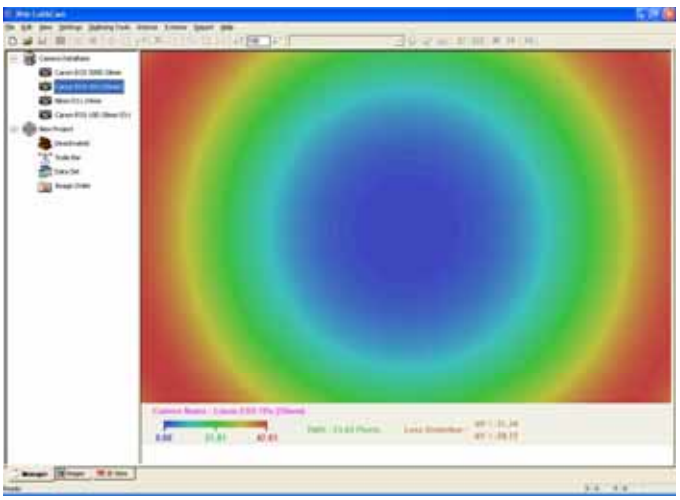

**Figure 11. Colour-coded lens distortions of a 28mm lens.**

Using 3DM Analyst Mine Mapping Suite these cameras can usually be calibrated to an accuracy of between 0.1 and 0.2 pixels using a total of eleven parameters:

(i) Focal length (C): The perpendicular distance from the image sensor to the perspective centre of the lens.

(ii) Principal Point Offset (Xp, Yp): The offset from the centre of the sensor to the point on the sensor where the direct axial ray passing through the perspective centre of the lens intersects the sensor.

(iii) Radial Distortion (K1, K2, K3 & K4): The co-efficients of a polynomial equation describing the distortion radially from the principal point. (Generally only very short focal length lenses need all four terms.)

(iv) Decentring Distortion (P1 & P2): All elements in a lens system should ideally be aligned at the time of manufacture. Any displacement or rotation of a lens element from perfect alignment will cause geometric displacement of images.

(v) Scaling Factors (B1 & B2): Pixel scaling factors that can compensate for any difference in pixel width and height (B1) and non-perpendicularity of the horizontal and vertical axes of the sensor (B2).

Not all lenses require all parameters to correctly characterize their distortions; if this is the case, the affected parameters will be strongly correlated and 3DM Analyst Mine Mapping Suite will identify this during calibration, giving the user the option of disabling one or more of the parameters. We strongly recommend that the user do this — the aim is to use the smallest set of parameters possible because this will maximize the accuracy of those parameters and avoid "over fitting" the data.

### *Camera Restrictions*

3DM Analyst Mine Mapping Suite is capable of calibrating virtually any digital camera.

Whether the calibration is generally useful, however, depends on the ability of the user to reproduce the same optical settings on that camera.

On a zoom lens, for example, by far the biggest factor that affects the validity of the calibration is the zoom setting itself. If the zoom setting cannot be reproduced reliably, then the calibration may not be

valid. For this reason, we generally discourage the use of zoom lenses: the only two zoom settings that can be reliably reproduced are the minimum and maximum zoom settings, which means a zoom lens is only equivalent to two prime lenses. Since a zoom lens of comparable quality to a prime lens will cost a lot more than two primes (and, generally, it isn't possible to obtain a zoom lens of comparable quality anyway) then it is better simply to have a set of calibrated prime lenses available to suit the desired working ranges and ground pixel sizes than to try to reduce the number of lenses required by using a zoom.

Of course, compact digital cameras are generally equipped with zoom lenses, so there may not be much choice in the issue. This is one of the reasons why digital SLRs are preferable to compact digitals. (The other main reason is that digital SLRs will have a higher optical resolution and lower noise at a given pixel count than a compact digital.)

Assuming the zoom is constant, the next largest factor that affects the validity of a calibration is the focus setting of the lens. For most outdoor work the traditional approach has been to focus the lens at infinity and tape it up so it can't move. Whether this is practical or not depends on the range of distances that will be encountered, the aperture size that can be used, and the focal length of the lens.

For example, with a 28 mm lens set to an aperture of f/8 and focused at infinity, everything from about 9 m away should be very sharp.

With a 100 mm lens on f/8 focused at infinity, however, points closer than about 100 m away will start to get blurry.

If a larger aperture is required — for example, to let in more light so a faster shutter speed can be used (e.g. because the camera is being used for aerial photography) or because there isn't much light to begin with (e.g. underwater or in a tunnel) — then the range of distances that remain acceptably sharp can drop dramatically.

One option is to adjust the focus for the job in question and perform an on-line calibration just for that job (see the next section). However, it is still very important that the user remembers to keep track of the focus setting used for each image to avoid accidentally trying to calibrate a set of images where multiple focus settings were used. (The symptom the user will observe in this case is an inability to bring the calibration accuracy down to the 0.1–0.2 pixel range mentioned previously.)

Another is to simply create calibrations at a range of focus distances and use one that fits best, especially for jobs where the accuracy of the calibration is generally far higher than the accuracy required for the job and so a small bit of calibration error doesn't really matter.

Another factor that affects the calibration's validity is the aperture. Changing the aperture has a small scaling effect — a few pixels at worst — and so we recommend to our customers to use a different calibration for each aperture setting if accuracy is absolutely critical. Fortunately, if surveyed camera stations are *not* being used, a small scaling effect is one of the easiest calibration errors for the exterior orientation to compensate for, because the exterior orientation can move the camera slightly closer or further away from the scene to compensate for the calibration error, retaining accuracy in the area of interest.

*On-line Calibration*

Although calibrations are normally performed using images that have been carefully planned and captured for that purpose, 3DM Analyst Mine Mapping Suite can actually derive a calibration from the same images that are being used for the pit wall mapping project. If something has changed optically in the camera (e.g. the focus), not only can this be detected but also an ad-hoc calibration can be performed so that the new images can still be used. With enough images, it is even possible to perform a calibration without any control points or surveyed camera positions at all.

The process of performing a calibration (or *interior orientation*) in 3DM Analyst Mine Mapping Suite is exactly the same as determining the exterior orientation. In fact, the same routines are used internally for both — the only difference is that the interior orientation parameters are automatically fixed when the exterior orientation alone is desired.

In addition to deriving the interior orientation parameters, the software is also capable of analysing the parameters and generating a report that indicates if any of the parameters are correlated (which affects how reliable the derived parameters are) and how accurately it thinks each parameter has been determined, which allows the user to judge the quality of the calibration.

The software also allows the user to easily compare two calibrations visually.

Although performing a calibration is fairly straightforward, it would be nice if we could simply calibrate each type of camera and lens that our customers were likely to use and supply a generic calibration for them. Unfortunately, comparing the calibrations of identical model lenses and cameras, we have found that this is not possible.

In one trial, for example, one of our customers calibrated two Nikon D2x cameras with the same model 60mm lenses and found that the difference between the calibrations was almost as large as the difference between each calibration and no calibration at all. (This should not be completely surprising — the calibration accuracies that the software achieves amount to less than a micron on a digital SLR; the manufacturers of digital cameras certainly have manufacturing tolerances in the placement of the image sensor or lens elements much greater than that!)

As a consequence we always recommend to each customer that they calibrate each camera + lens combination separately and we normally calibrate their camera and lenses for them during training.

## PITFALLS

Although photogrammetry has many advantages as mentioned earlier, things *can* go wrong, and it is important that users not only be aware of the problems that can arise, but also know how to deal with them once they have occurred and, ideally, how to avoid them in the first place.

### *Bad Imagery*

Bad imagery includes both images that actually have something wrong with them (blurry, over- or under-exposed, optically different from the calibration, etc.) and perfectly good images that simply fail to capture the entire area being mapped.

The first problem can be addressed by having good procedures. Ensuring the calibration always matches the camera/lens combination, for example, can be as easy as using a digital SLR with prime lenses and taping the focus ring. If that is not possible or desirable, the problem can be avoided by capturing additional images so an ad-hoc calibration can be performed on a project-by-project basis. (As long as the camera hasn't changed since the images were captured, this can even be done after the event.)

Motion blur can be fixed either by ensuring the shutter speed is high enough or by using a tripod and possibly a remote shutter release. Aperture priority mode will ensure that the images are not over- or under-exposed, and the camera will show what shutter speed is required for the shot allowing a decision to be made about how to capture it. Using a tripod by default means the photographer doesn't need to worry about that at all.

To avoid the problem of failing to completely capture the area that needs to be mapped requires careful planning. ADAM Technology supply a spreadsheet that can be used to calculate the number of images that will be required to capture an area with a given camera and lens combination, calculate the required distance from the wall to the camera stations, and determine how far apart the camera stations need to be in order to achieve the desired distance:base ratios.

Using image merging also greatly reduces the risk of areas not being captured in at least two images — when capturing the images from each camera station, the photographer can overlap them as much as they like because excessive overlap won't affect the size of the final merged image (and hence processing time). Using a great deal of overlap is therefore encouraged, minimizing the risk of gaps.

When capturing image strips, especially from the air, ADAM encourages customers to capture images at least twice as frequently as required — the cost of capturing an image with a digital camera is essentially zero, and having a substitute image nearby can sometimes be *very* useful, as customers who have flown through small clouds at the wrong time can attest.

### *Bad Observations*

There are two types of observational errors that users will encounter:

**(i)** Bad control point or camera station co-ordinates used for an absolute orientation, usually supplied by another party.

**(ii)** Incorrectly identified control points or relative-only points observed by the user of the software or by the software itself.

To address the first problem requires redundancy — if there are only three known locations in the whole

project then the software cannot tell if they are wrong. However, if there are more than three, the software has very robust and sophisticated mechanisms that can detect bad control data.

One customer's project featured over 40 images captured from four camera stations, mapping the pit wall of an iron ore mine from 850 m away. The photography had initially been captured for use in another package that processed each model individually and therefore needed a control point for each pair of images, so there were more than 20 control points placed around the bottom of the pit wall.

The customer found, however, that although the generated 3D images lined up well at the bottom of the pit wall where the control points were, there was a 20 m discrepancy at the top of the wall between the 3D images generated by images captured from the first two camera stations and those generated by images captured from the second two.

3DM Analyst Mine Mapping Suite detected that the problem was with two of the camera stations, and predicted that they should have been over 100 m higher than the survey data indicated.

Checking the original survey data indicated that the customer had actually copied the survey data incorrectly, and that our software had predicted the correct location of those two cameras to within 0.5 meters — at a range of 850 m from the pit wall!

Another customer working on an aerial mapping project had the locations of 15 control points supplied by their surveyor. Our software was able to immediately identify that three of them were wrong — including the one with the 2 km error mentioned earlier. (The surveyor had transposed some digits.)

With some customers experiencing an error rate of up to 1 in 5 with the supplied survey data, it is obviously essential that they be able to verify that it is correct. One of the strengths of our software is that it is able to do just that. (There is a long-standing enmity between surveyors and photogrammetrists; one of the reasons for that is the ability of photogrammetrists to detect when surveyors provide incorrect data!)

The second problem manifests itself in a variety of ways: we have seen one case where two control points were close to each other on a pit wall, and the customer had labelled one of them with a particular ID in one image but used the same ID for the other one in the other image; more commonly the customer simply labels a control point with the wrong ID. In either case the software will detect that the derived 3D co-ordinate for the control point is inconsistent with the supplied survey data. (One good idea is to actually *paint* the number of the control point on the wall next to it so it can be seen in the images!)

The other problem is bad relative-only points — either digitised manually by the user or generated automatically by the software. Fortunately, when generating relative-only points automatically, the software tends to find between 100 and 200 points (manually digitising six to nine points was common in the days before automation) and so bad points are relatively easy to detect due to their large residuals. (In fact, the software actually includes a menu item "Edit | Remove Bad Relative-only Points" to identify and remove these points automatically.)

*DTM Generation*

Most of the earlier problems manifest themselves when the user attempts to determine the camera orientations. Once that has been done, the next step is to generate the DTMs. Fortunately, if the orientations are successful, there aren't many things that can go wrong at this point.

One of the things that *can* go wrong is the generation of "bad points". These fall into two categories:

(i) Points that the software has incorrectly identified as belonging to the same point in the scene.

(ii) Points that the software has correctly identified as belonging to the same point, but that point is undesirable for some reason. (This is more common in aerial photography — examples include points on vehicles that have moved between images, or points on the tops of trees or buildings where the user is trying to model the ground's surface.)

The software has two ways of dealing with points of the first type. Firstly, there is a "matching tolerance" setting that the user can use to specify how similar two points must be before they should be considered a match. If many bad points are being generated, the user should consider raising this setting to make it harder to match. (The default setting generally doesn't create many bad points — the problem usually occurs when the user has

lowered the tolerance because they are getting insufficient coverage, e.g. because of very noisy images making matching difficult.) Secondly, bad points of this type generally have 3D co-ordinates that differ markedly from their neighbours, resulting in "spikes". The software takes advantage of this fact to identify bad points and weed them out. The user can also manually perform a "spike removal" operation with a user-defined level of aggressiveness (i.e. how "spiky" a point must be before it is removed).

Points of the second type are more difficult to deal with (unless the point is on a moving vehicle and it moved far enough that it results in a spike — they can be filtered out in the same way as mismatched points). There are various methods, but unfortunately it is very difficult to explain to the software that you only want points on the ground and not on man-made objects. (Fortunately this problem does not occur much when mapping pit walls!)

Another problem that can occur is that the software simply doesn't find many points at all. One reason could be an excessive distance:base ratio; another could be excessive noise in the images. Both of these should be avoidable with proper planning. Lowering the matching tolerance is a good first step, keeping an eye out for incorrectly matched points. Using the Stereo View and digitizing the data by hand is sometimes a last resort, although if the problem is excessive convergence (due to a large base) then it might be difficult for a human to visualize the scene as well.

The final problem that can occur is that coverage of the area being mapped is incomplete, which is a symptom of bad planning.

EXAMPLE

Ekati Diamond Mine, situated 200km south of the Arctic Circle, is BHP Billiton's only diamond mine. The extreme weather conditions make field work challenging and highlight the importance of safe data collection techniques.

Using a Nikon D1x with a 135 mm lens from 680 m away on the opposite side of the pit, our customer captured a 500 m x 250 m section of pit wall, representing about 1/3$^{rd}$ of the pit, from just two locations (Figure 12).

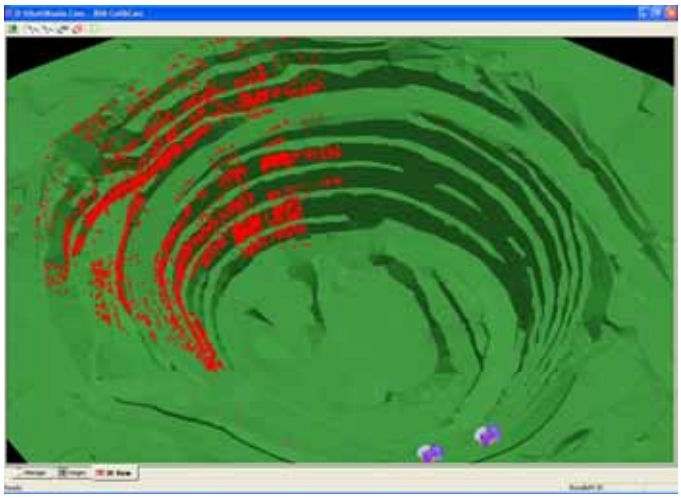

**Figure 12. Mapping a pit wall.**

By mounting the camera on a tripod and panning it up and down to create image fans the pit wall was captured at a ground pixel size of 3 cm x 3 cm (for a detailed structural analysis) within a few minutes. Seven permanent ground control points placed around the outside rim of the pit were used in addition to the surveyed camera stations to provide data accurate to 0.1 m all the way down to the pit floor without any need to place control points there.

Merging the images removed the need to carefully align the images captured from the right camera station with the corresponding images captured from the left camera station, simplifying the field work and reducing the time required (Figure 13).

DTMs and 3D Images were generated in batch mode and imported into VULCAN for geotechnical analysis (Figure 2).

The entire process, from loading the images onto the PC, to having a complete 3D model of the pit wall geo-referenced in the real-world co-ordinate system, ready for geotechnical analysis, took four hours, of which 3 hours 50 minutes was automated. Creating a 3D model of the entire pit would therefore take about 12 hours, almost all of which is automated and could therefore be performed without the user being present (e.g. overnight).

**Figure 13. 24 megapixel merged image of a pit wall at Ekati.**

FIELD EXERCISE

As part of the Golden Rocks workshop, presenters were asked to conduct a field exercise that involved capturing a rock face 50 m × 20 m in size with at least three models along the bottom and two models along the top, in order to demonstrate how a larger project that required multiple models would be approached (Figure 14).

For this exercise, ADAM Technology used the following equipment:

(i) A six megapixel Canon EOS 10D digital SLR camera manufactured in 2003. (At the time of writing, the ten megapixel Canon EOS 400D is available for approximately US$800.)

(ii) A Canon EF 50 mm f/1.8 II lens (worth approximately US$100).

(iii) A Canon EF 28 mm f/2.8 lens (worth about US$200).

To illustrate both image fans and image strips, two separate projects were completed, one using the 28 mm lens and the image strip technique, the other using the 50 mm lens and the image fanning technique. An aperture of f/8 was used for all images.

*28 mm Image Strips*

For the 28 mm project a total of ten images were captured from five different locations at a distance of approximately 25 metres from the base of the rock face in a time of 1 minute 18 seconds (Figure 15). Two strips of images were captured — the lower strip using all five locations, the upper strip using the last three, captured by tilting the camera upwards to create a "mini-fan". The camera was handheld and the appropriate distance between camera stations (~5 metres) was simply paced out according to the distance calculated beforehand using the Object Distance spreadsheet that is supplied with the software. (One of the strengths of 3DM Analyst Mine Mapping Suite is that it is not necessary for overlaps and camera positions to be absolutely perfect, so walking along a rock face

**Figure 14. Site for the Golden Rocks field exercise. (Image is a 33 megapixel merged image created from the 50mm image fans. Control points are visible as white circles on black backgrounds. Nine control points were placed by the organisers so they could check the accuracy of the various systems being demonstrated; only three are actually required for orientation.)**

capturing images by hand is a perfectly reasonable approach to take.)

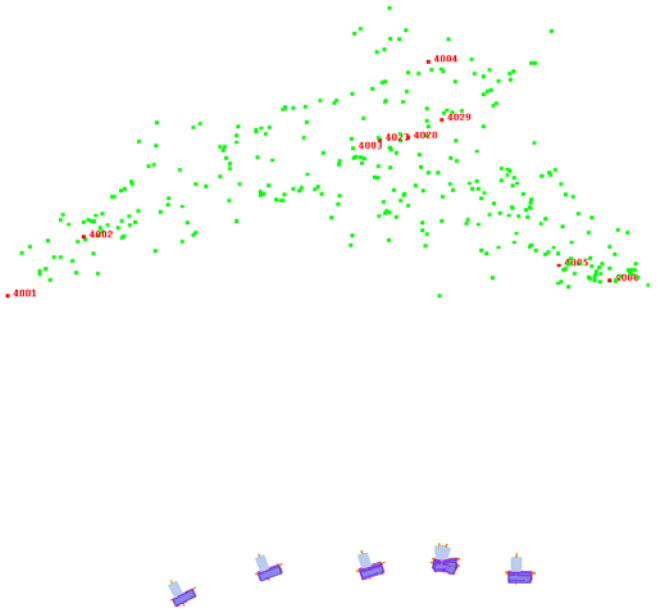


**Figure 15. Configuration of the cameras for the 28 mm project. (Green dots are automatically generated relative-only points; red dots are the supplied control points.)**

After loading the images onto the PC, the following steps were performed:

(i) Set up a new project in 3DM CalibCam, importing images and control point data: 30 seconds.

(ii) Automatically generate relative-only points between all images with no "hinting" at image relationships: 1 minute 49 seconds.

(iii) Digitise three control points in two images and perform an absolute orientation: 40 seconds.

(iv) Use the driveback feature to automatically digitise the remaining control points, then check each to make sure they were all digitised, and perform a final absolute orientation: 2 minutes.

(v) Create projects and launch DTM Generator: 30 seconds.

(vi) Process all five projects: 5 minutes 10 seconds (555,144 points created).

Total time taken: 10 minutes 40 seconds. (All timings are from a PC with a 2.4GHz AMD Athlon X2 4600+ processor and 2GB of RAM.)

At this point, less than 15 minutes after the first image was captured, the software has fully generated the five DTMs, ready for performing geotechnical analysis, all fully oriented in the desired co-ordinate system. No further post-processing is necessary prior to characterising the rock face.

The derived camera orientations are given in Table 1. (Note that the co-ordinate system chosen was in feet, not metres, and the orientations are in degrees but the estimated accuracies of the angles are in arc-minutes.)

The average distance between camera positions was about 5 metres; the distance from the rock face ranged from about 20 metres at the bottom to about 35 metres at the top, so the distance:base ratio for the models in this project was between 4:1 and 7:1.

The ground pixel size ranged from 5 mm to 9 mm, so the expected planimetric accuracy (from Equation 1) is between 2.5 mm and 4.5 mm, assuming an image accuracy of 0.5 pixels. The expected depth accuracy (from Equation 2) is therefore between 10 mm and 30 mm.

According to the Bundle Adjustment Report, the

**Table 1. Camera locations and orientations for the 28 mm project.**

| Image | Camera Location | | | | | | Camera Orientation | | | | | |
|---|---|---|---|---|---|---|---|---|---|---|---|---|
| | X | Y | Z | $\delta_X$ | $\delta_Y$ | $\delta_Z$ | ω (°) | φ (°) | κ (°) | $\delta_\omega$ (') | $\delta_\varphi$ (') | $\delta_\kappa$ (') |
| IMG_6023.JPG | 3076402.96 | 1665424.18 | 6257.77 | 0.02 | 0.02 | 0.02 | -113.259 | 84.531 | 156.806 | 0.9 | 0.4 | 1.1 |
| IMG_6024.JPG | 3076397.91 | 1665406.73 | 6257.99 | 0.01 | 0.02 | 0.02 | -121.230 | 76.387 | 151.020 | 0.7 | 0.4 | 0.7 |
| IMG_6025.JPG | 3076387.19 | 1665389.10 | 6258.38 | 0.01 | 0.02 | 0.02 | -106.741 | 73.153 | 163.914 | 0.7 | 0.3 | 0.7 |
| IMG_6026.JPG | 3076387.08 | 1665389.16 | 6258.44 | 0.01 | 0.02 | 0.02 | -135.391 | 69.229 | 136.832 | 0.7 | 0.3 | 0.7 |
| IMG_6027.JPG | 3076380.26 | 1665375.67 | 6258.93 | 0.01 | 0.02 | 0.02 | -103.177 | 63.543 | 168.799 | 0.7 | 0.3 | 0.6 |
| IMG_6028.JPG | 3076380.08 | 1665375.78 | 6259.01 | 0.01 | 0.02 | 0.02 | -118.793 | 61.034 | 155.726 | 0.7 | 0.3 | 0.6 |
| IMG_6029.JPG | 3076380.09 | 1665375.52 | 6258.90 | 0.01 | 0.02 | 0.02 | -97.030 | 41.978 | 174.866 | 0.7 | 0.4 | 0.6 |
| IMG_6030.JPG | 3076380.03 | 1665375.60 | 6259.00 | 0.01 | 0.02 | 0.02 | -110.304 | 39.847 | 166.376 | 0.6 | 0.4 | 0.6 |
| IMG_6031.JPG | 3076370.07 | 1665364.11 | 6259.57 | 0.01 | 0.02 | 0.02 | -97.180 | 56.062 | 175.444 | 0.7 | 0.3 | 0.6 |
| IMG_6032.JPG | 3076369.88 | 1665364.26 | 6259.69 | 0.01 | 0.02 | 0.02 | -115.819 | 54.110 | 160.363 | 0.7 | 0.3 | 0.6 |

RMS's of the control point residuals for this project are 2.4 mm in X, 2.4 mm in Y, and 3.8 mm in Z. We should not be surprised that the depth accuracy is better than our estimate for the data we will generate later because each control point is centroided and observed in multiple images, making them more accurate.

*50 mm Image Fans*

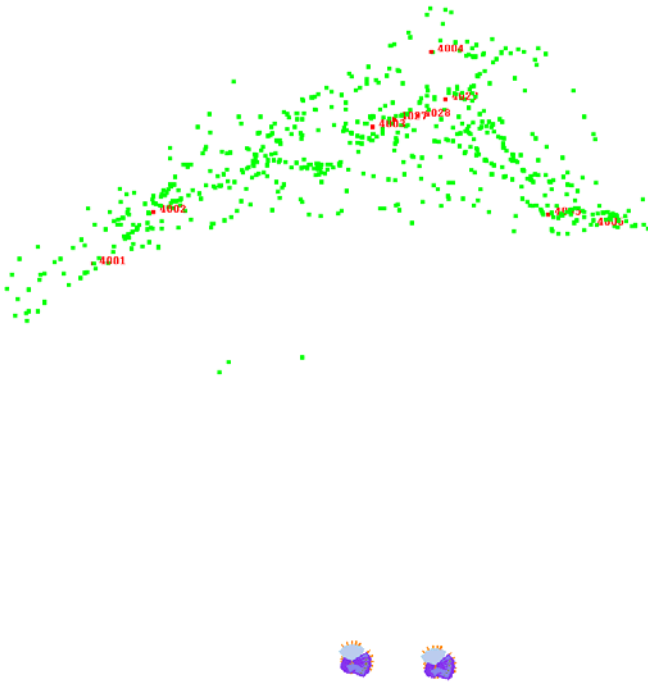


**Figure 16. Configuration of the cameras for the 50 mm project.**

Two fans of nine images each were captured in 2 minutes 4 seconds for the 50 mm project. The two camera positions were approximately 35 metres from the base of the rock face (50 metres from the top) and approximately 6 metres apart, giving a distance:base ratio ranging from 6:1 at the bottom to 8:1 at the top (Figure 16). (As before, nominal distances required to achieve the desired number of models were calculated using the Object Distance spreadsheet and the locations were simply paced out.) To process the images, the following steps were performed:

(i) Set up a new project in 3DM CalibCam, importing images and control point data, including two camera stations of unknown location with the appropriate images under each: 35 seconds.

(ii) Automatically generate relative-only points between all images with no "hinting" at image relationships (other than placing them under the appropriate camera station): 3 minutes.

(iii) Digitise three control points in two images and perform an absolute orientation: 1 minute 10 seconds.

(iv) Use the driveback feature to automatically digitise the remaining control points, then check each to make sure they were all digitised, and perform a final absolute orientation: 1 minute 5 seconds.[2]

(v) Generate two 33 megapixel merged images: 2 minutes 45 seconds.

(vi) Create a single 3DM Analyst project, generate DTM: 12 minutes 30 seconds (606,153 points). (More points were generated in this project because the ground pixel size is slightly smaller.)

Total time taken: 21 minutes 5 seconds.

This project took longer because of the additional image-merging step and because working with larger data sets slows the computer down, but the advantage is that now the entire rock face can be processed as a single 3D image. On a large scale project, where the time required to move from one camera station to another is much longer, the time required to capture the images using the image fanning technique will be much less than the time required to capture them using the strip technique, more than compensating for any extra time required to process the images.

The ground pixel size ranged from 5 mm at the base of the rock face to about 7.5 mm towards the top, so the expected planimetric accuracy (from Equation 1) is between 2.6 mm at the base and 3.7 mm at the top, assuming an image accuracy of 0.5 pixels. The expected depth accuracies (from Equation 2) are therefore about 15 mm and 30 mm at the base and top, respectively.

According to the Bundle Adjustment Report, the RMS's of the control point residuals for this project are 3.0 mm in X, 4.1 mm in Y, and 1.7 mm in Z.

[2] The checking was much faster in this project because the driveback feature was successful in digitising all control points in the project. The targets were a little too small for the software to digitise all of them automatically in the 28 mm project, so some were digitised manually although the software was still used to predict their locations accurately.

**Table 2. Camera locations and orientations for the 50 mm project.**

| Image | Camera Location | | | | | | Camera Orientation | | | | | |
|---|---|---|---|---|---|---|---|---|---|---|---|---|
| | X | Y | Z | $\delta_X$ | $\delta_Y$ | $\delta_Z$ | ω (°) | Φ (°) | κ (°) | $\delta_\omega$ (') | $\delta_\varphi$ (') | $\delta_\kappa$ (') |
| IMG_6062.JPG | 3076356.92 | 1665425.93 | 6260.41 | 0.04 | 0.04 | 0.07 | -92.889 | 86.615 | 176.110 | 1.9 | 1.2 | 1.2 |
| IMG_6063.JPG | 3076356.92 | 1665425.93 | 6260.41 | 0.04 | 0.04 | 0.07 | -89.998 | 69.778 | -179.987 | 2.1 | 1.0 | 1.2 |
| IMG_6064.JPG | 3076356.92 | 1665425.93 | 6260.41 | 0.04 | 0.04 | 0.07 | -106.852 | 68.959 | 164.577 | 2.1 | 1.0 | 1.2 |
| IMG_6065.JPG | 3076356.92 | 1665425.93 | 6260.41 | 0.04 | 0.04 | 0.07 | -92.664 | 54.011 | 179.014 | 2.0 | 1.0 | 1.2 |
| IMG_6066.JPG | 3076356.92 | 1665425.93 | 6260.41 | 0.04 | 0.04 | 0.07 | -106.142 | 53.185 | 168.618 | 2.0 | 1.0 | 1.2 |
| IMG_6067.JPG | 3076356.92 | 1665425.93 | 6260.41 | 0.04 | 0.04 | 0.07 | -91.968 | 43.220 | -179.147 | 2.0 | 1.1 | 1.2 |
| IMG_6068.JPG | 3076356.92 | 1665425.93 | 6260.41 | 0.04 | 0.04 | 0.07 | -104.150 | 42.689 | 172.840 | 2.0 | 1.1 | 1.2 |
| IMG_6069.JPG | 3076356.92 | 1665425.93 | 6260.41 | 0.04 | 0.04 | 0.07 | -92.748 | 29.956 | -178.351 | 1.8 | 1.4 | 1.2 |
| IMG_6070.JPG | 3076356.92 | 1665425.93 | 6260.41 | 0.04 | 0.04 | 0.07 | -102.962 | 31.815 | 176.315 | 1.8 | 1.4 | 1.2 |
| IMG_6071.JPG | 3076344.21 | 1665410.03 | 6260.82 | 0.04 | 0.04 | 0.08 | 89.348 | 85.266 | -2.706 | 1.8 | 1.3 | 1.2 |
| IMG_6072.JPG | 3076344.21 | 1665410.03 | 6260.82 | 0.04 | 0.04 | 0.08 | -87.673 | 78.202 | -178.548 | 2.0 | 1.0 | 1.2 |
| IMG_6073.JPG | 3076344.21 | 1665410.03 | 6260.82 | 0.04 | 0.04 | 0.08 | -114.827 | 76.854 | 155.140 | 2.0 | 1.0 | 1.2 |
| IMG_6074.JPG | 3076344.21 | 1665410.03 | 6260.82 | 0.04 | 0.04 | 0.08 | -92.864 | 62.108 | 177.751 | 2.1 | 0.9 | 1.2 |
| IMG_6075.JPG | 3076344.21 | 1665410.03 | 6260.82 | 0.04 | 0.04 | 0.08 | -110.377 | 60.673 | 162.644 | 2.1 | 0.9 | 1.2 |
| IMG_6076.JPG | 3076344.21 | 1665410.03 | 6260.82 | 0.04 | 0.04 | 0.08 | -92.588 | 49.037 | 179.393 | 2.0 | 1.1 | 1.2 |
| IMG_6077.JPG | 3076344.21 | 1665410.03 | 6260.82 | 0.04 | 0.04 | 0.08 | -106.243 | 48.084 | 169.260 | 2.0 | 1.1 | 1.2 |
| IMG_6078.JPG | 3076344.21 | 1665410.03 | 6260.82 | 0.04 | 0.04 | 0.08 | -92.535 | 37.515 | -179.479 | 1.9 | 1.2 | 1.2 |
| IMG_6079.JPG | 3076344.21 | 1665410.03 | 6260.82 | 0.04 | 0.04 | 0.08 | -103.005 | 38.995 | 173.911 | 1.9 | 1.2 | 1.2 |

If we compare the derived co-ordinates of the control points between the two projects, the RMS's are 3.2 mm in X, 4.0 mm in Y, and 3.6 mm in Z, giving us confidence that the accuracies we are actually achieving are in line with what we expect.

*Rock Face Characterisation*

Having generated the 3D surface model, the next task was to digitise a total of 160 discontinuities on the rock face — 80 of them visible as traces, the other 80 visible as faces (Figure 17).

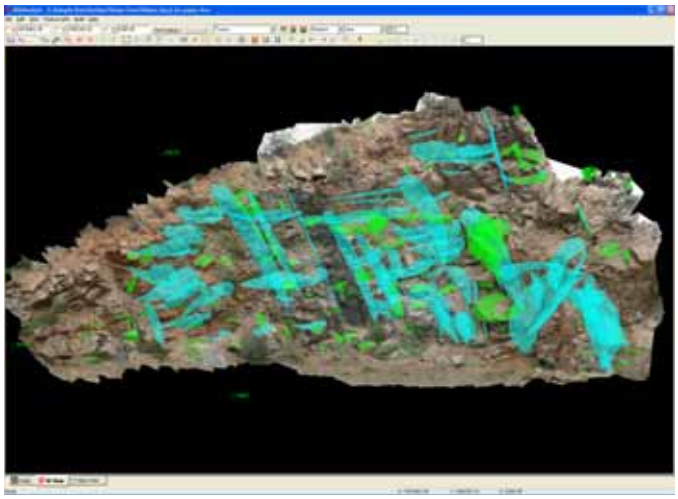

**Figure 17. The joints requested by the organisers. Traces are shown in cyan, faces are shown in green.**

For this task we used the new geotechnical support in 3DM Analyst Mine Mapping Suite 2.2. In total it took approximately 1.5 days, largely because of the time required to identify the features on the images supplied by the organisers. An experienced user collecting features that they identified themselves, rather than trying to locate and digitise the features marked on a totally different image by someone else, should be able to perform this task in a couple of hours. To verify this, we re-digitised a set of 20 traces and faces in just over two minutes, so the actual mechanical act of digitising the structures is not very time-consuming at all.

Once all 160 features were digitised, the next step was to identify the largest set of structures (Figure 18), determine their mean orientation, and ensure only those structures within 10 degrees of the mean orientation were included in the set using the Advanced Operations dialog in 3DM Analyst (Figure 19).

In addition to digitising the features, presenters were also asked to construct a profile of Face 54 in the dip direction using the DTM. (Profiles such as this could be used for roughness calculations.)

Since we had two completely independent projects at our disposal, using different lenses, different

distances, and different image capturing techniques, this was a good opportunity to verify the accuracy of the derived data so we generated the profile using both projects and compared them to each other (Figure 21). The graph depicts the deviation from the dip in the dip direction through the centre of Face 54. The RMS of the differences of the two profiles is 3.7 mm, with a maximum difference of 12 mm. This is an excellent validation of the accuracy we are actually achieving because it derives from the DTM itself.

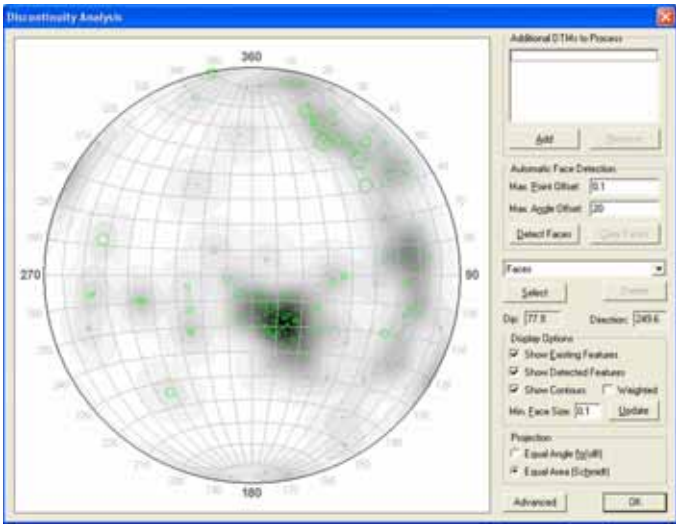

**Figure 18. Pole plot of all 160 digitised features shown in 3DM Analyst (equal area, lower hemisphere projection) with greyscale contours. The largest set consists of the nearly horizontal structures with an unweighted mean orientation of 22.5º dip, 328.3º dip direction.**

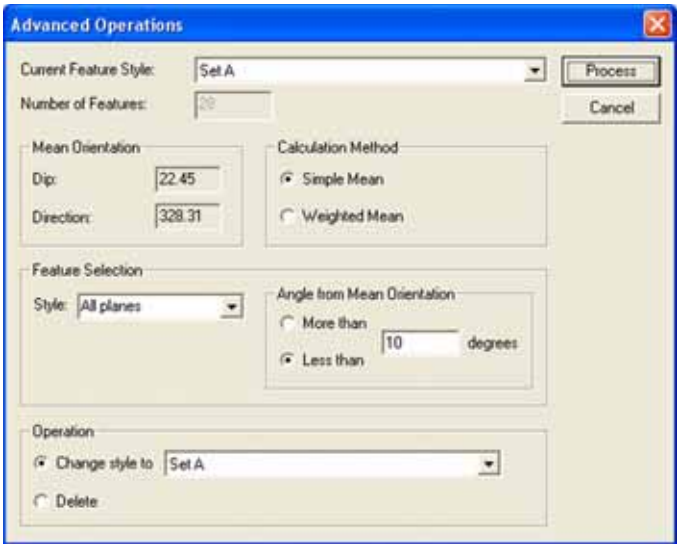


**Figure 19. Adding all features within 10 degrees of the set mean to the set. (The Simple Mean is the average orientation of all features in the set; the Weighted Mean gives greater importance to larger features on the basis that (a) larger features are likely to be more important, and (b) larger features should be more accurate.)**

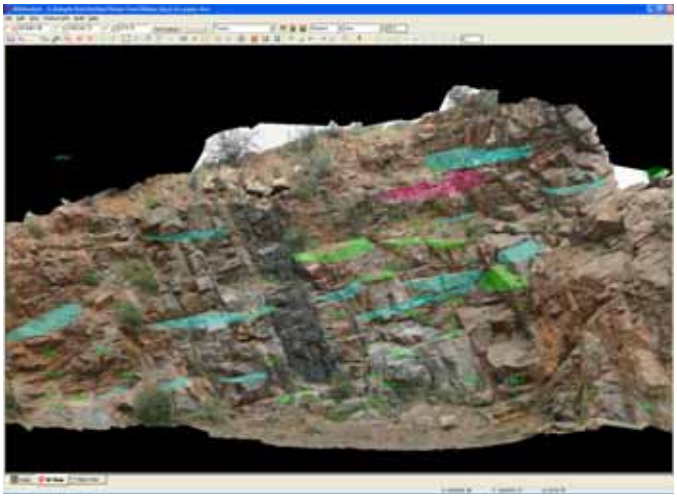

**Figure 20. Largest set (other joints excluded).**

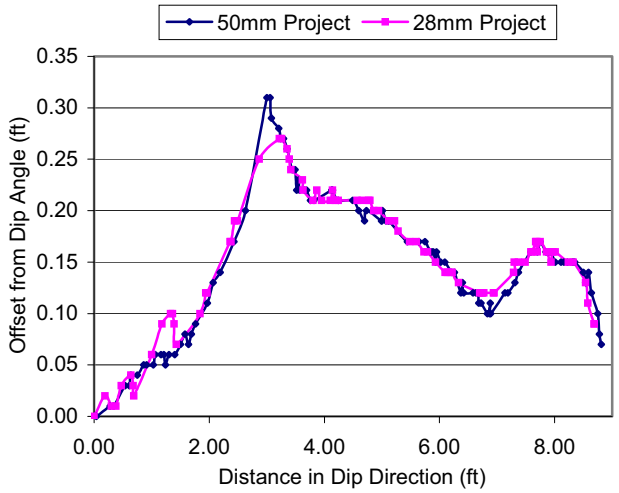


**Figure 21. Profile of Face 54 in two different projects.**

## CONCLUSION

After decades of being restricted to aerial mapping and other esoteric applications, photogrammetry is rapidly expanding into new markets as people become increasingly aware of the advancements that digital cameras and faster computers have made possible.

Building on 20 years of experience in the photogrammetric industry, ADAM Technology has developed a tool that sets new standards in automation, user-friendliness, and performance.

3DM Analyst Mine Mapping Suite has proven itself to be a valuable tool for many applications, with one of the fastest growing areas being rock face characterisation. With a level of detail, accuracy, range, and price that is difficult to match using any other technology, ADAM is convinced that the use of 3DM Analyst for face mapping will continue to grow rapidly in the future.

# Basics and application of 3D imaging systems with conventional and high-resolution cameras

Gaich, A.
*3G Software & Measurement GmbH., Graz, Austria*
Pötsch, M. & Schubert, W.
*Institute for Rock Mechanics and Tunnelling, Graz University of Technology, Graz, Austria*

Copyright 2006, ARMA, American Rock Mechanics Association

This paper was prepared for presentation at the workshop: "Laser and Photogrammetric Methods for Rock Face Characterization" organized by F. Tonon and J. Kottenstette, held in Golden, Colorado, June 17-18, 2006.

This paper was selected for presentation by F. Tonon and J.T. Kottenstette following review of information contained in an abstract submitted earlier by the author(s). Contents of the paper, as presented, have not been reviewed by F. Tonon and J. Kottenstette, and are subject to correction by the author(s). The material, as presented, does not necessarily reflect any position of USRMS, ARMA, their officers, or members. Electronic reproduction, distribution, or storage of any part of this paper for commercial purposes without the written consent of ARMA is prohibited. Permission to reproduce in print is restricted to an abstract of not more than 300 words; illustrations may not be copied. The abstract must contain conspicuous acknowledgement of where and by whom the paper was presented.

**ABSTRACT:** The contribution shows the benefits of supplementing conventional geological data acquisition with contact free measurement and assessment techniques. It shows the use of 3D images originating from standard and very high resolution digital cameras, their processing and the tools for the geometrical and geological assessment. Without the sake of completeness, special attention is given on two commercially available systems named JointMetriX3D and ShapeMetriX3D. Several applications of the technology conclude the article.

## 1. INTRODUCTION

The acquisition and evaluation of geotechnical data are integral parts during the investigation and design stage of construction works in rock masses. Geotechnical data serve as input for decision making processes during different phases of projects, ranging from feasibility studies to construction and maintenance.

For example, in conventional tunneling continuous adaptation of the excavation and support method to the actual ground conditions is required in order to obtain an economical and safe construction [1]. This observational approach needs, among others, the continuous collection of information on rock mass type, structure, and quality, as well as the system behavior.

Also in surface applications, such as stability analyses for slopes, open pit mining, or quarry management, geometric properties of the rock mass and the discontinuity network have an impact on the rock mass behavior. Together with descriptive parameters they allow to establish a consistent rock mass model.

Traditional geological documentation can be seen as a combination of manual and visual methods. Depending on the type of work, the documented area usually consists of a rock face (foundation area, cut slope, pit wall, tunnel face, dam abutment), or of wall, crown and invert area of an underground opening.

Relevant parameters particularly important for rock mass modeling are related to discontinuities, such as orientation, spacing, frequency, size, aperture, filling width, termination index, or the geo-referenced position, as well as the rock surface geometry. These data are completed by information concerning distribution of rock types, weathering, and specific local phenomena like karst. All these data can be acquired by visual methods when measuring, positions, distances, and orientations within a known 3D co-ordinate system [2].

Figure 1 shows excellent working conditions for geological data acquisition during excavation works in a tunnel. It still outlines one major problem: without additional support areas above

approximately 2 m off the ground cannot be reached.

Besides, normal working conditions are characterized by the interference of the documentation work with other construction activities such as excavation, mucking, support installation or drilling and charging for the next blast. Consequently, the documentation work has to be performed while machinery like boomers, excavators or muck loading and hauling equipment is operating.

Finally, when unstable rock mass conditions are encountered, there is no opportunity to enter the unsupported areas at all. In that case a direct collection of data is impossible

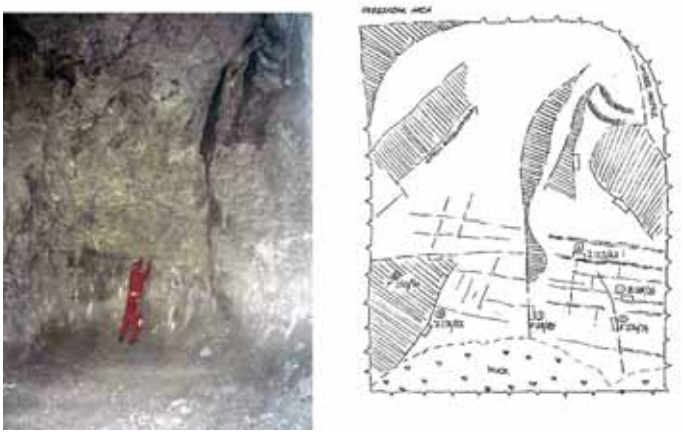

Figure 1: Present practice of acquiring discontinuity orientation data at an underground opening (left). The picture shows an approx. 7.5m high drift tunnel in a magnesite mine in Austria. Manual sketch with six discontinuity orientation measurements (right). Hatched areas represent slickensided fault planes, lines depict discontinuity traces.

Figure 2 outlines the problem of needed access in surface applications. When mapping has to be done in a larger scale rock mass, e.g. in a quarry, at pit walls, or at slopes, it might take considerable efforts to get access. However, usually inaccessible areas remain. Another issue at larger outcrops is that the relevance of a discontinuity for geotechnical analysis is more difficult to assess when inspecting it from close range.

Additionally to access and time restriction problems, traditional methods of geological data acquisition are prone to errors [3] due to sampling difficulties, human bias, and instrument errors.

Therefore the resulting mapping represents a rather subjective description of the actual rock mass conditions. And if the rock faces are subject to changes, e.g. from excavation, exploitation, movements, or erosion, information that not immediately captured is lost.

Figure 2: Mapping in a limestone quarry in Austria. It took the geologist a considerable time to access all areas for getting a significant number of orientation measurements.

To overcome existing drawbacks of conventional mapping, systems were developed that capture the actual conditions, providing the visual and geometric information for the assessment of the rock mass including measurement possibilities. This entails that a major part of the mapping process is transferred to the computer. The basis for mapping on the computer is a realistic representation of the rock face as it is which leads to the use of two-dimensional images and more recently, three-dimensional (3D) images.

3D images allow recording the visible rock mass structures completely and specially developed software enables to measure geometric data on the rock surface and the discontinuity network without physical contact and at an arbitrary number. Measurements are performed directly on the 3D image displayed on the computer screen. There are no access restrictions and results are instantly available for further processing. The 3D image itself is an objective documentation of the rock mass conditions which makes analyses possible even if a specific rock face no longer exists.

The presented systems JointMetriX3D and ShapeMetriX3D open new possibilities for optimization concerning safety, productivity,

design, and construction. Both systems base on the generation of metric 3D images of a rock surface which are then analyzed and assessed on a computer. Both systems allow measuring rock mass features such as orientations or spacing, and provide analyses such as joint statistics or stereonets.

The major difference between the two systems is related to the imaging system and the image resolution. ShapeMetriX3D uses a calibrated off-the-shelf SLR camera while JointMetriX3D relies on 100 Megapixel images taken by a panoramic line-scan camera.

Notwithstanding existing drawbacks, field work is still the source of prime importance for gathering information on a rock mass, especially, as parameters remain that cannot be determined by visual or contact-free methods. Within this context modern methods for geological data collection shall be seen as a support to the field work and not as a substitute.

## 2. BASICS OF 3D IMAGING

### *2.1 Background*

A 3D image can be seen as the combination of a real (digital) photograph with the geometric information on the objects it shows. In the actual cases the objects are rock faces and walls.

*Photogrammetry* is the art and science to measure from images and dates back to the beginning of photography [4, 5]. Stereoscopic photogrammetry deals with the measurement of three-dimensional (spatial) information from two images showing the same object or surface but taken from different angles. This principle is also referred to as Shape from Stereo (see Figure 3). An important prerequisite to Shape from Stereo is the knowledge of the following:

(i) Precise information on the image formation process of the camera (interior camera orientation).

(ii) Precise information on the camera position and viewing direction when taking the pictures (exterior camera orientation)

Point (i) led to purpose built cameras (metric cameras) relying on mechanically accurate imaging, thus being expensive. Issue (ii) was realized either by observation of control points, i.e. points with known co-ordinates, or determining the exterior orientation by additional external measurements which is cumbersome for field applications.

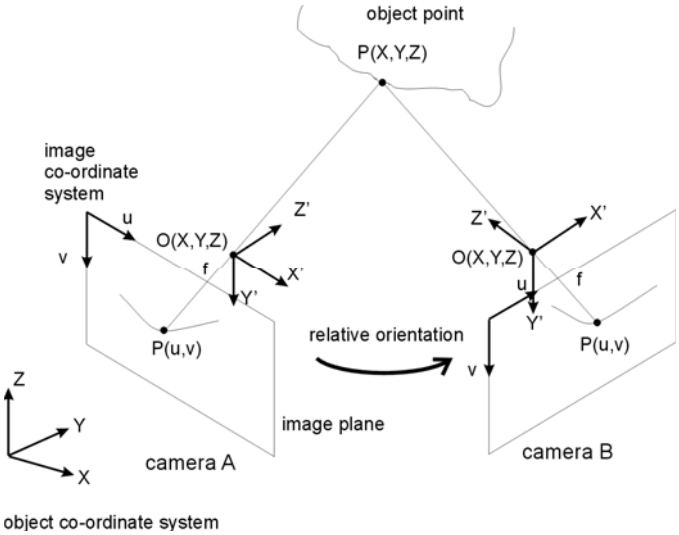


Figure 3: Shape from Stereo principle.

More recent approaches to the same topic are related with the term *Computer Vision* where among others the calibration of off-the-shelf cameras was addressed [6].

Improvements within computer vision led to the possibility of fully automatically determining the relative orientation of the two images to each other without any control points [7] resulting in some consequences:

(i) Picture taking is eased (freehand) since measurements are possible without any surveying of the exterior camera orientations.

(ii) 3D images can be generated also from uncalibrated cameras. The results are qualitatively correct 3D images (generic 3D image). Calibration is required as soon as geometric measurements are needed.

(iii) Metric 3D images can be generated just by observing an object with known geometry, e.g. a scale pole visible in the image pair. If in addition information on the pose of the scale object is available (e.g. it is posed vertical) then 3D images with the according reference (verticality) can be generated.

As mentioned, two pictures from different standpoints are required to get a 3D image. The (virtual) connection between the two standpoints is referred to as baseline (see Figure 4). Practical

experience showed that the length of the baseline (base-length) is reasonably chosen to be 1/5 – 1/10 of the mean imaging distance. The chosen base-length is a compromise. The larger the base-length the better the (theoretically) achievable accuracy due to the intersection angle of imaging rays (see Figure 4) but also the more is the perspective change between the images which complicates the automatic identification of corresponding points (image matching –see below).

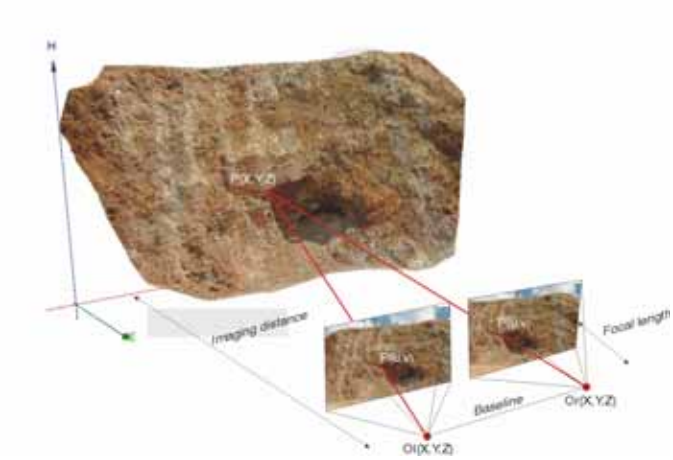


Figure 4: Stereoscopic image pair. Two corresponding image points P(u,v) relate to one three-dimensional object point P(X,Y,Z). Note that modern algorithms do not require the baseline to be known.

If the measurements should be related to a superior co-ordinate system, so-called control points or reference points are used (3 to 6). These points are placed somewhere in the imaging area and their co-ordinates are determined by external measurements, e.g. total station or accurate GPS.

Other applications might require only local co-ordinates. In this case it is possible to omit the use of control points and their survey. A vertically established range pole is sufficient.

For both methods it is possible to take the pictures freehand, which allows a high degree of flexibility for the imaging (see Figure 5).

*2.2 Generation of a generic 3D image*

The generation of a 3D image is performed using a specially designed software component. The user specifies the two images forming the stereoscopic image pair, the used camera and lens, and which area of the images is the region of interest. This suffices to generate a generic 3D image.

A generic 3D image refers to a 3D image that is not yet scaled or referenced but showing qualitatively correctly the 3D surface. With generic 3D images relative analyses, e.g. relative dipping of discontinuities towards the rock face or relative spacing can be performed.

Figure 5 Application of the ShapeMetriX3D system in a magnesite mine. Note that the pictures are taken freehand.

An essential component that allows this automatic computation of the generic 3D image is the automatic identification of corresponding points (image matching). A proprietary algorithm exists that allows a robust (few to no errors), dense (up to every image pixel if required), accurate, and fast image matching.

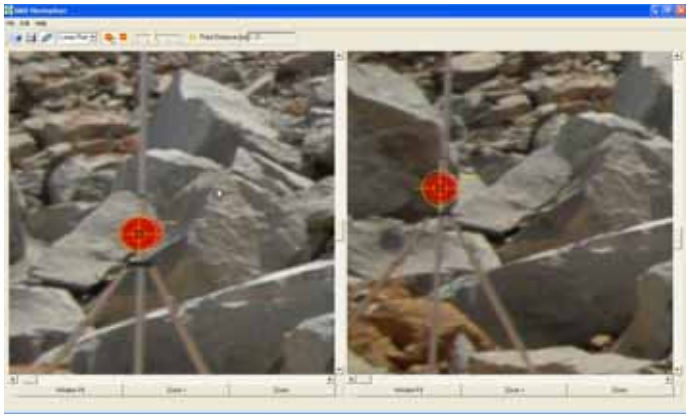

Figure 6: Software component supporting the identification of target points mounted on a range pole.

*2.3 From a generic to a metric 3D image*

The upgrade from a generic to a metric 3D image can be done by different referencing methods:

(i) If surveyed control points are used the result is within the same (global) co-ordinate system. Total station measurements or accurate GPS are commonly used.

(ii) Using a vertically established scale pole (see Figure 6) the 3D image is related a local-coordinate system. By introducing conventional compass reading the 3D image can be related to north.

*2.4 Camera calibration*

Camera calibration refers to the interior camera orientation describing the actual image formation process by parameters, such as precise focal length, precise image center, pixel size, and lens distortion. By camera calibration the determined deviations of the real image formation are corrected usually by introducing correction polynomials [4, 5].

Some manufacturers provide a measure of lens quality. One way to specify this is to determine the position of ideally located points in a real image:

Assuming $h$ to be the ideal paraxial distance of an image point to the image centre:

$$h = \sqrt{x^2 + y^2} \qquad (1)$$

and $h'$ to be real distance, then the lens distortion can be specified by

$$V = \frac{h' - h}{h} \cdot 100[\%] \qquad (2)$$

Special lenses used in aerial photogrammetry show deviations of 0.1% whereas standard lens are in the range of 0.5-1.5%. Further information can be found in textbooks on optics such as [9].

Since standard lenses show poorer quality, calibration is crucial. A series of comparative tests with standard off-the-shelf cameras and lens showed deviations of 1.3 – 2.2%. Distortions in the images especially at the border regions can reach some 10 pixels for an off-the-shelf SLR camera (especially at shorter focal lengths). Figure 7 depicts a plot showing such deviations.

From literature it is known (e.g. [9]) that a larger variation in lens quality is due to variations in the manufacturing process. These variations become relevant when using such cameras for measurement purposes. Therefore, every camera should be calibrated individually together with the used lens when aiming on 3D measurements.

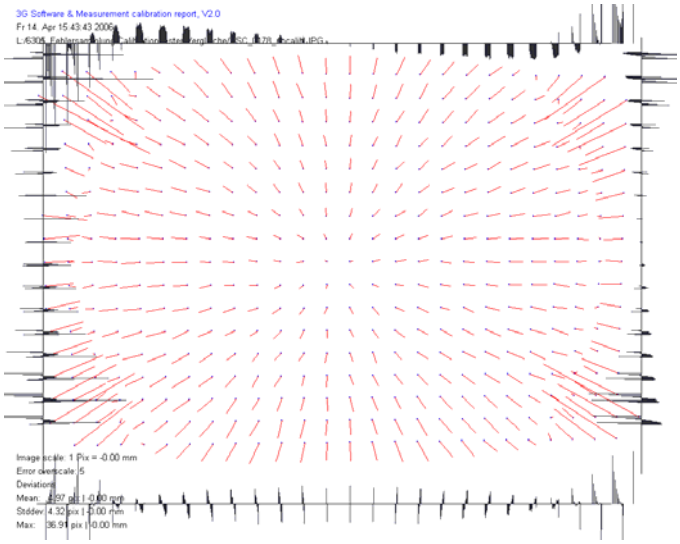

Figure 7: Lens distortion (5 times overscaled) of an uncalibrated SLR camera with 10 mm lens. The maximum error is about 40 pixels.

## Error simulation

In order to determine the influence of optical deviations, the geometric model for reconstructing a single point in 3D as illustrated in Figure 3 was implemented. Furthermore, the introduction of optical deviations was allowed in order to check the effect on depth errors (meaning the distance of the 3D point from the cameras). Table 1 reflects some of the found values. The image arrangement was chosen to be typical for close range use in rock face characterization.

**Table 1: Resulting depth error according to different imaging situations assuming an uncalibrated camera and an image pixel deviation of 40 pixel.**

| Distance to the rock wall [m] | Base length [m] | Deviation [pix] | Focal length [mm] | Resulting depth error [m] |
|---|---|---|---|---|
| 20 | 4 | 40 | 10 | 2.7 |
| 20 | 2 | 40 | 10 | 4.8 |
| 30 | 6 | 40 | 10 | 4.0 |
| 30 | 6 | 40 | 20 | 2.2 |
| 30 | 4 | 40 | 20 | 3.1 |

## Camera stability

Due to mechanical stability of a SLR camera and proper treatment it is possible to keep the calibration valid for a camera-lens pair. But it is important to be able to check the actual condition of the calibration during field operation (see Figure 8).

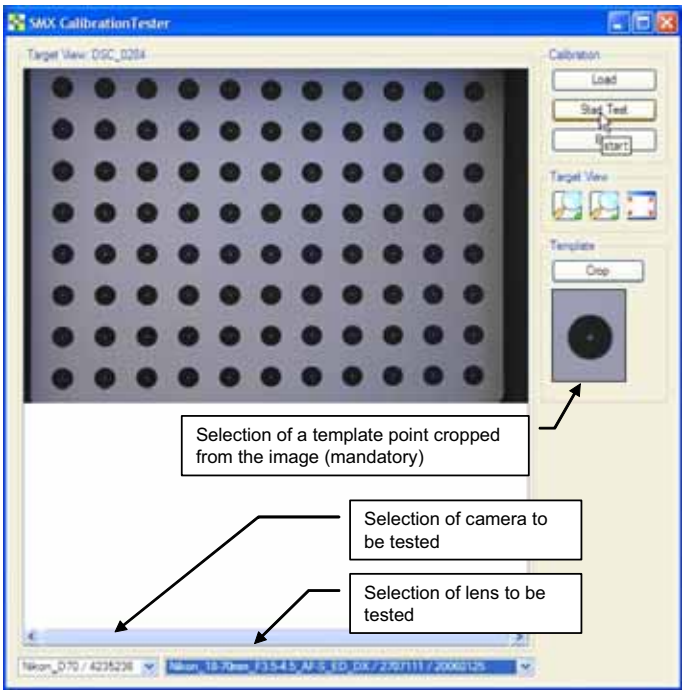


Figure 8: Snapshot of the tool for testing the actual camera calibration on site. The test image shows a planar calibration target containing a regular pattern of dots.

*2.5 Quality measures*

Quality of a 3D rock mass image can be seen from various aspects. Depending on the actual project, several of the following issues are more or less important for the geotechnical analysis:

**Geometric accuracy**

*Accuracy* is a measure of the nearness of a measured value to the true value. This must not be mixed up with *precision* which refers to the degree of repeatability of a measurement. The *absolute error* of a measurement is defined as its deviation from the true value of the location. If the true value is not known, the *residual error* is used instead. It is defined as the deviation of a measurement from the most probable value, e.g. the mean value of a set of samples. The relative error is the quotient of the absolute error and the true value.

For practical field applications the absolute position of certain locations of the rock wall is known only for surveyed control points. Consequently, the true error can be determined only at those locations. Although surveying itself is not error-free, control points can be assumed to have true values, if their accuracy is higher than the values to be compared. In this case deviations are assumed to be absolute errors. According to this, the achieved accuracy strongly depends on the quality of the surveyed reference points.

Practical applications with the JointMetriX3D system (described below) showed a typical absolute error of 2-3 cm (standard deviation) in space for imaging distances between 10 and 1,000 meters.

Note that the accuracy is not a direct function of the working (imaging) distance.

**Geometric image resolution**

For geological/geotechnical analyses image resolution is a key parameter. Depending on the desired level of detail, the structural information on the rock mass has to be visible. The higher the number of pixels that map a certain area, the higher is the geometric image resolution (specified in mm/pixel).

A simple method to estimate the geometric image resolution is to estimate the height of the rock wall that is captured, and divide it by the number of (vertical) pixels (if the camera is used in landscape mode).

Example: assuming a rock wall height of 25 m and a 10,2 Megapixel camera having 3872 x 2592 pixel the estimated geometric image resolution is 25,000/2,600 ~ 10 mm/pixel.

**3D point density**

The actual shape of the rock wall is described more accurately, the denser the 3D point cloud is. The parameter is specified by points/m$^2$, or also by its opposite, the mean distance between surface measurements given in mm.

However, for data handling reasons it might be required not to address a 3D surface to every image pixel, especially when the size of the digital images increases, e.g. 100 Megapixel as with the JointMetriX3D system.

**Radiometric image resolution**

The radiometric image resolution describes the amount of color information that is available for every image point. For geological/geotechnical analyses at least 3x8 bit/pixel is recommended (color).

**Field of view**

A key parameter for an imaging/measurement system is the vertical and horizontal field of view. When having little space for taking images, a wide angle lens is required, while imaging locations with large distances to the rock wall need the opposite. At best a system has a wide operational range for a flexible application.

**Application range**

In opposite to active measurement techniques passive ones such as photogrammetry do not have principle limitations that relate to the reflective character of a surface or the distance from which measurements can be taken. Nevertheless, limits exist mainly related to the possibility of taking the stereoscopic image pair at visibly acceptable quality, or the requirement of having structural information in the images (which is normally the case when taking pictures of rock surfaces). However, free sight between the imaging locations and the rock surface is obviously required.

## 3. 3D IMAGING SYSTEMS

In the following two commercial systems are briefly addressed. One is designed for taking very high resolution images (when used for larger areas and/or very detailed analysis), the other one for highly flexible applications.

### *3.1 JointMetriX3D*

The system bases on a rotating CCD line-scan camera and software components for generating 3D images and allowing geotechnical assessments.

The imaging system is mounted on a tripod acquiring the image line by line while the rotation unit is turning the line sensor. Digital images of even more than 100 Megapixel are possible. Another particularity of this scanning camera is that the horizontal field of view can be changed (by the rotation unit) independently from the vertical one (zoom lens) which allows panoramic images with the region of interest at best resolution. Figure 9 shows the application of the system in an open pit in Sweden. Note that it is not necessary to survey the imaging standpoints and the viewing direction of the scanner.

From the taken stereoscopic image pair a generic 3D image is computed which is then referenced using surveyed control points. The metric 3D image is then ready for geometrical, geological, and geotechnical analysis to be done on the computer (see also Section 4). Processing and analysis is usually performed in the office.

Figure 9: Application of the JointMetriX3D system in an open pit mine in the North of Sweden. Note that a ruggedized portable computer is used in order to control the scanner and save the acquired data instantly.

Figure 10: ShapeMetriX3D imaging system consisting of a calibrated SLR camera and changeable zoom lenses.

### *3.2 ShapeMetriX3D*

ShapeMetriX3D works analogously to Joint-MetriX3D but using a calibrated SLR camera as the imaging unit. This entails a smaller geometric area for the typical application but increases flexibility on site as only a standard camera without any tripod

is used. Figure 10 shows the imaging system. Note that the system is applied freehand as depicted in Figure 5.

*3.3 Combination*

The combination of the two systems is reasonable when facing large and complex geometries, e.g. having large outcrops and the need for thorough analyses. JointMetriX3D is used to produce a 3D base (reference) model of large parts or the whole area and with ShapeMetriX3D detailed 3D images are supplemented. The detailed 3D images can be referenced to the base model by corresponding image information, thus no additional reference points or surveying is required.

Corresponding image information of overlapping regions is also used when merging 3D images. This is used for (i) completing information on complex surface geometries (see case study in Section 6), (ii) increasing geometric image resolution, or (iii) increasing the field of view at the same image resolution.

## 4. ASSESSMENT OF 3D IMAGES

*4.1 Navigation*

Navigation "through" a 3D image means that the 3D image can be inspected from any designated view by changing the observing position. This can be done interactively by using the computer mouse. For assessments, structural features of the rock mass can be investigated and marked by clicking the appropriate location directly on the 3D image. Since the markers are set on a 3D image, spatial measurements are instantly available.

Interaction with the 3D image alleviates rock mass assessments since structures can be inspected from different angles. A quick zoom between a close-up view and an overview is possible which supports the identification of geologically significant locations especially at larger outcrops.

*4.2 Co-ordinates and distances*

Basic magnitudes are related to surface point measurements (x,y,z coordinates) and the determination of the Euclidean distance between arbitrary surface points which correlates to a virtual tape measure. By clicking on the designated position the software instantly provides the metric information.

*4.3 Individual orientations*

Any location on the 3D image can be touched with a special kind of cursor. It follows the actual 3D shape of the reconstructed surface and changes its pointing direction according to the actual orientation of the surface (see Figure 11). In this way orientation measurements are possible corresponding to the application of a compass-clinometer device on any particular location.

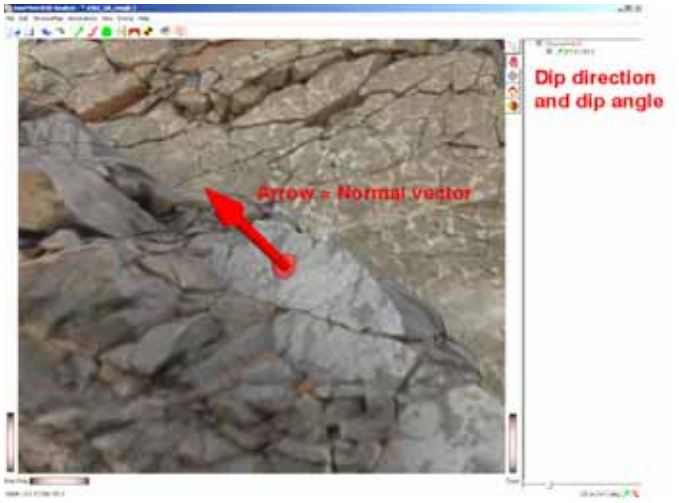


Figure 11: Orientations can be measured at arbitrary locations on the 3D image. Dip angle and dip direction are provided instantly.

*4.4 Linear features*

The measurement of linear rock mass features such as joints, lithological bundaries, or strata is also performed by marking the joint trace on the 3D image.

The result of these markings is a three-dimensional poly-line. It consists of 3D surface point measurements. If the 3D poly-line shows a significant change in depth, a plane can be fitted automatically to the set of surface points. The orientation of the fitted plane corresponds to the spatial orientation of the discontinuity that was marked, thus the three-dimensional orientation is determined only by marking the joint trace (see Figure 12).

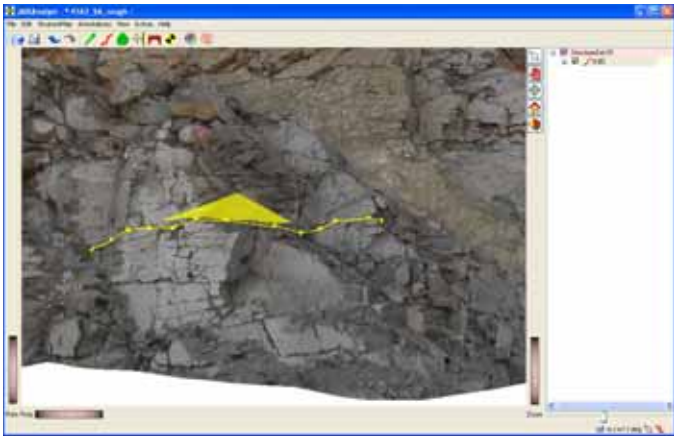

Figure 12: A 3D poly-line marks a discontinuity trace. A plane is fitted to the poly-line. Its orientation corresponds with the orientation of the discontinuity.

*4.5 Areas*

Regions of similar geological attributes (e.g. lithology or same degree of fracturing) or joint surfaces are marked with areas. An area is defined by marking a closed poly-line on the 3D surface. From the marked part of the 3D surface the mean orientation is computed and instantly provided as dip angle and dip direction.

Figure 13 shows an example of a marked area and the resulting surface normal that indicates the spatial orientation of that area.

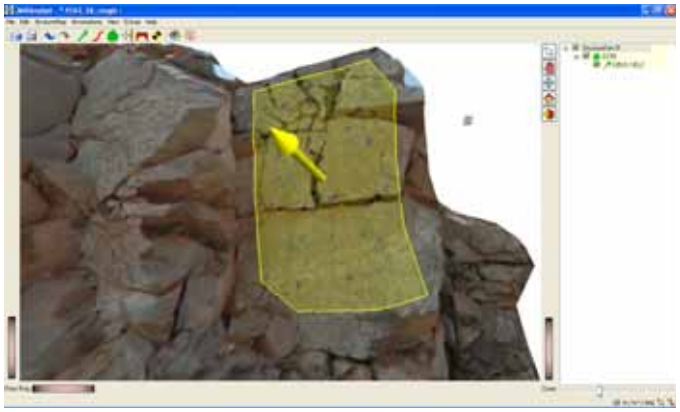

Figure 13: Measurement of joint orientations at joint surfaces. By marking points on the 3D surface and calculating the mean orientation of the surface normal the orientation vector is determined.

*4.6 Structure maps*

Basic features, such as joints and areas, orientations, as well as co-ordinates, or distances are combined to structure maps that represent geological units, e.g. a discontinuity set. Structure sets enable to handle a various number of and various types of measurements. Figure 14 shows an example of a 3D image with several structure sets marked.

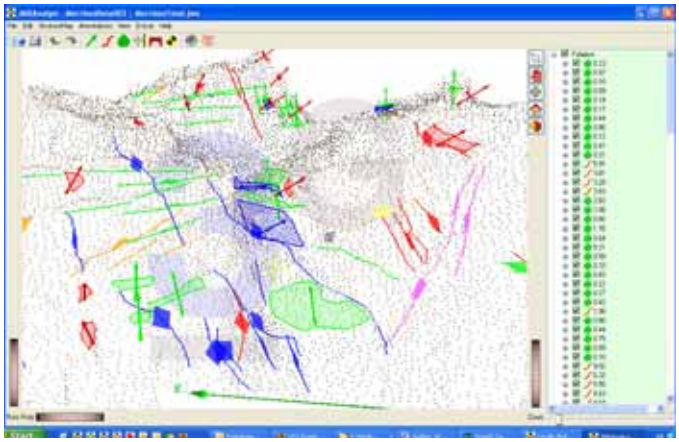

Figure 14: Snapshot of the JMX Analyst software used for interactive assessment of 3D images and the determination of descriptive rock mass parameters.

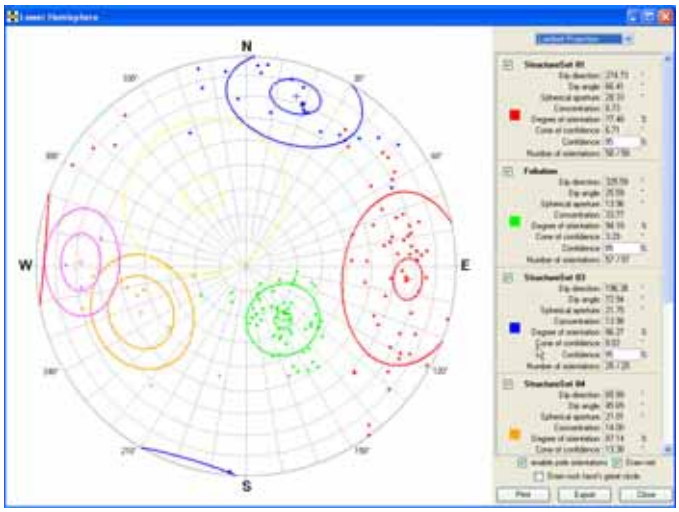


Figure 15: Lower hemisphere equal-area projection polar plot of identified discontinuity sets. Measured orientations are instantly displayed together with statistics on the distribution of the orientations.

*4.7 Hemispherical plots*

The measurements taken from the 3D image are grouped to sets by the user. Each set can be instantly visualized in hemispherical plots (stereonets) in order to get an impression of the spatial relationships of the set orientations instantly.

The stereonets deliver also some statistical parameters, such as the spherical aperture or the cone of confidence for each discontinuity set. Figure 15 outlines such a plot. The output is instantly updated when new orientation measurements are applied.

*4.8 Spacing*

As orientation measurements are assigned to joints, it is possible to determine the true spacing between joints traces within a structure set. Spacing in this context is referred to as normal spacing, according to definitions given by Priest [10]. True spacing means to determine the real spatial distance between subsequent discontinuities of a set. Conventional scanline sampling or analysis of a single image normally leads just to the apparent spacing that depends on the orientation of the discontinuities and their intersection with the free surface.

By using 3D information real spacing can be computed analytically based on the marked discontinuity traces and their orientation.

The procedure first intersects the discontinuity traces with a plane of projection and then determines the distances between adjacent intersection lines. Figure 16 shows an example of an automatically generated sketch for visually checking the spacing calculation.

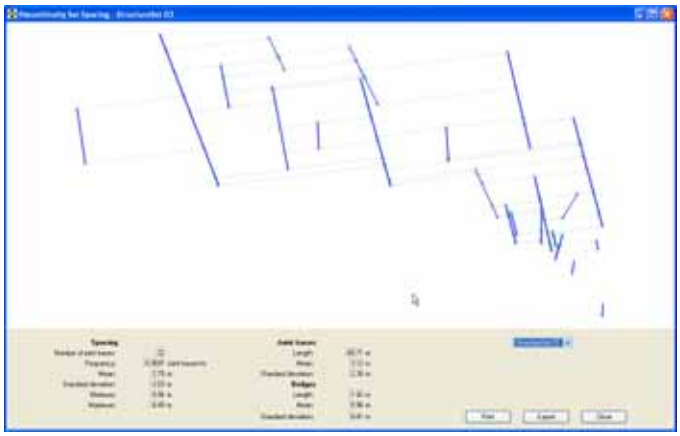

Figure 16: Computer generated sketch of a discontinuity network and statistics on the traces. The dashed lines indicate the scanline direction for determining the spacing and frequency.

*4.9 Histograms*

Structural information that is annotated on the 3D image is stored as 3D information. Therefore, true lengths of discontinuity traces are available and exportable (see Figure 17).

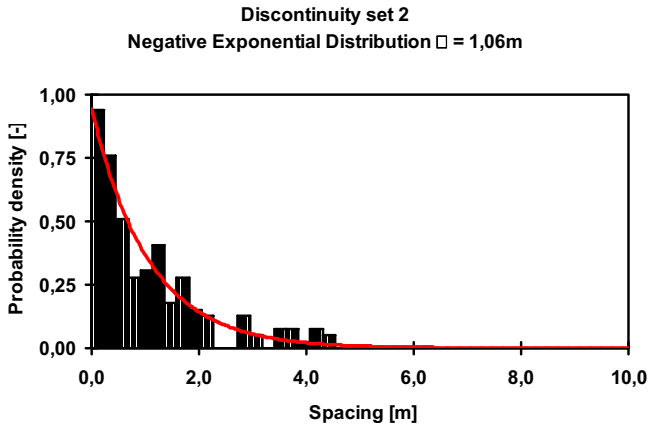


Figure 17: Discontinuity trace length distribution of two sets from a quarry assessment visualized with third party software.

*4.10 Automatisms*

Fully automatic analysis of rock mass features seems to have limits for the detection of rock mass properties encountered during practical work, especially when facing on changing rock mass conditions. Observed problems so far include:

(i) Artificial lineaments might be more representative than natural ones, e.g. excavator traces or traces from drilling in tunneling or underground excavation. Even boundaries between light and shadow are often more prominent than rock mass features. This most probably confuses image processing automatisms and requires some effort to check whether a structure was identified correctly or not.

(ii) The automatic identification of joint sets based on topographic surface analysis is only reasonable when a blocky rock mass is present.

A semi-automatic approach that supports the interactive assessment is therefore proposed for practical applications. Following automatisms are used:

(i) Accurate detection of lineaments by “guided” image processing: only a few sample points are marked on the 3D image and the points belonging to the same geological structure in-between are detected automatically based on image processing algorithms. This approach is based on an algorithm called “live wire” [11].

(ii) Automatic detection of the extension of a joint surface and its orientation based on one single marked location on the joint surface.

(iii) Automatic discrimination of structure sets based on mean orientation values. As the orientation measurements from a 3D image provide the information on dip angle and dip direction instantly, it is simple to define a new structure set containing the actual orientation measurement based on an (adjustable) angular discrimination.

The mentioned automatisms speed up interactive marking of geological features by concurrently keeping the decisions on geological relevance of features to the human operator.

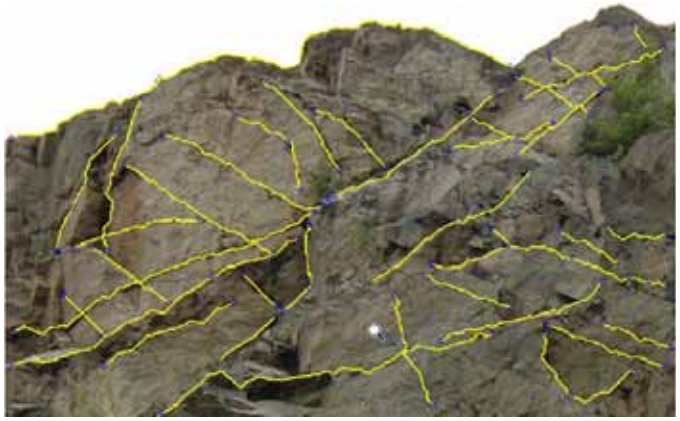

Figure 18: Trace detection results based on guided image processing.

## 5. CASE STUDIES

In the following some selected applications of the described systems are given:

### *5.1 Rock mass characterization*

**Rock slope**

The stability of a rock slope with a height of about 150 m was to be assessed. Several parts were not accessible safely, so contact-free measurements were the only way for reasonable quantitative geometric information on the discontinuity network and the free surface. Using JointMetriX3D two large scale images were used to generate a highly detailed 3D image from which a thorough geological assessment was performed. Results are shown in Figure 19, Figure 20, and Figure 21, respectively.

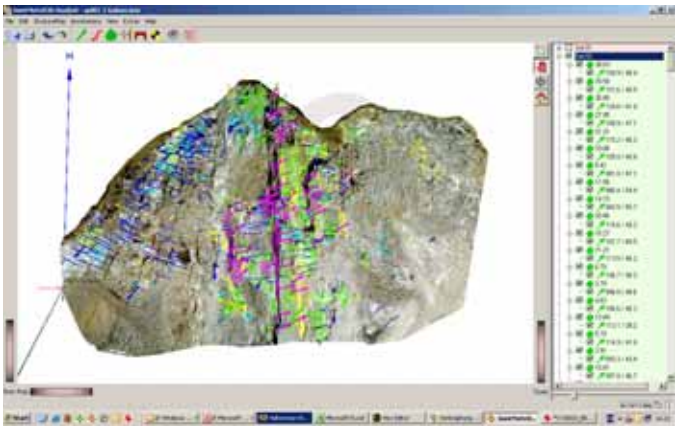

Figure 19: Application of the JointMetriX3D system for analyzing a 150m rock slope.

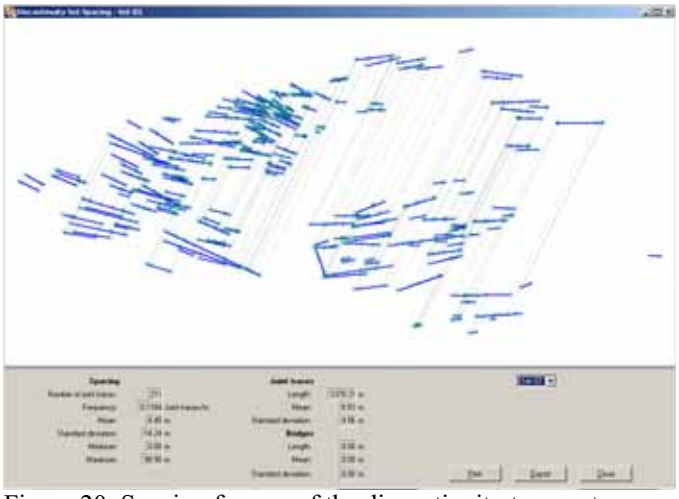

Figure 20: Spacing for one of the discontinuity trace sets.

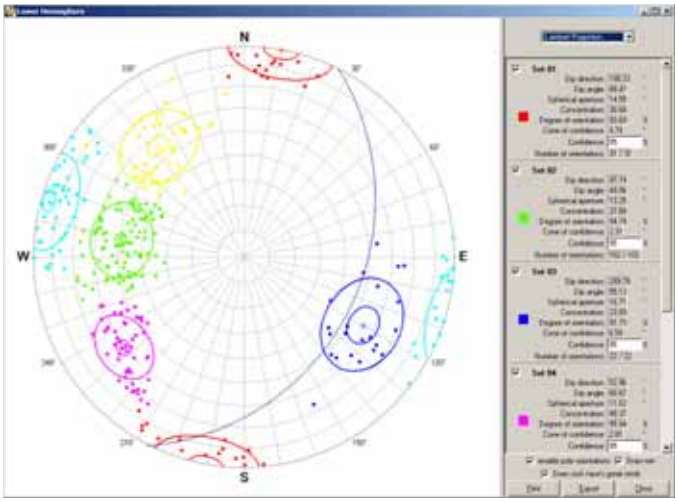


Figure 21: Hemispherical plot

**Tunnel face mapping**

In conventional tunneling face mapping has to be performed quickly. Using the ShapeMetriX3D system the geometry of the tunnel face can be acquired in quickly, e.g. within a minute. Assessments are then performed on the computer

without further time and access restrictions. This provides the geologists with more time on site for the analysis of other than geometric rock mass parameters such as filling, interlocking, or water phenomena. Subsequent 3D images of tunnel faces represent an objective, reproducible record of the rock mass conditions encountered during excavation.

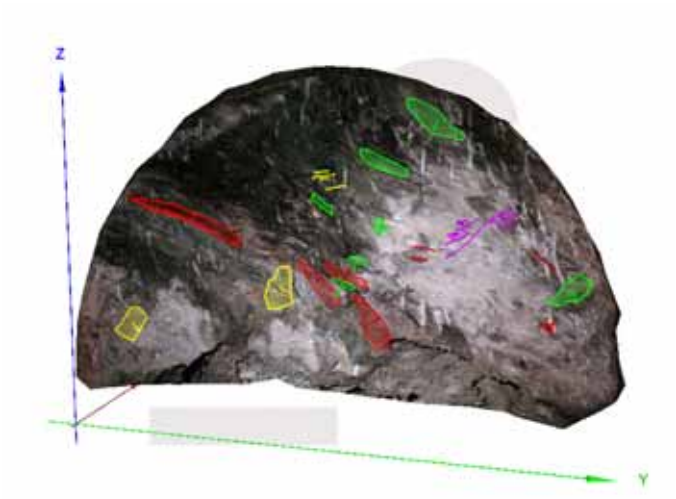


Figure 22: 3D image of a tunnel face and brief geological assessment using special tailored 3D software.

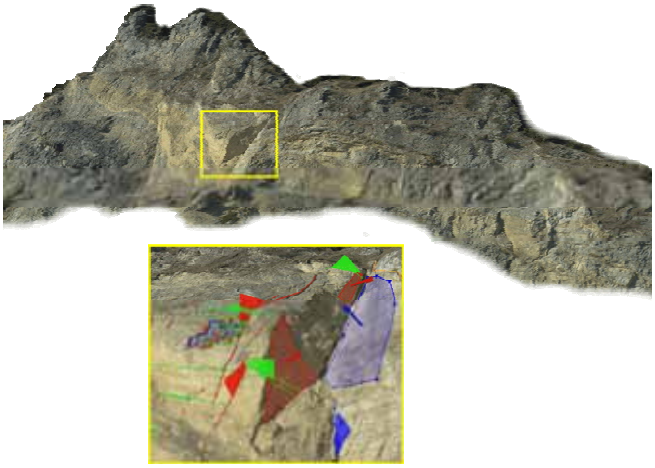

Figure 23: 3D image of a quarry acquired from about 700 m distance. The marked area shows a movable block whose kinematical properties were analyzed based on the remote measurements.

**Block stability**

Both systems can be used for the identification of kinematically free blocks. From the 3D image(s) of the site comprehensive analysis of the visible discontinuities are performed (see Figure 23). Based on the measured discontinuities and their position intersections are computed and analyzed. The analysis includes the determination of movability, failure modes, and stability assessment.

The establishment of a discontinuity model also allows the prediction of unstable blocks ahead of an underground excavation (see Figure 24)

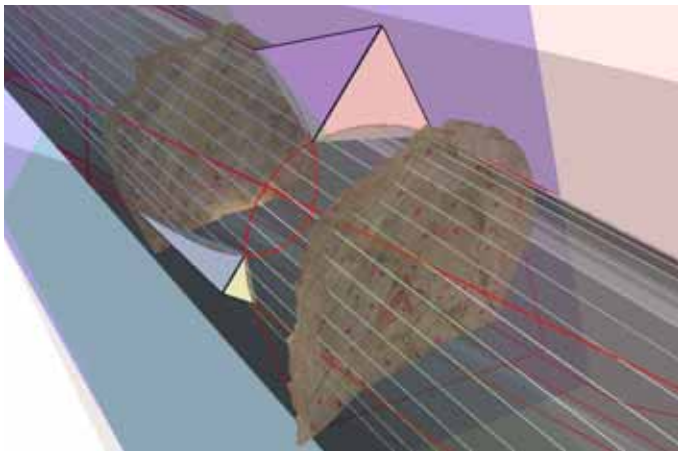

Figure 24: Identified blocks with kinematical freedom in a drift excavation derived from a discontinuity model which is based on sequential face imaging.

*5.2 Survey of open pit mines*

Especially for more complex excavation geometries the combined use of the two mentioned systems is beneficial. With JointMetriX3D high resolution overview 3D image(s) and with the flexible ShapeMetriX3D supplemental detailed 3D images are generated. This results in a common 3D surface model that reflects the actual geometry of an outcrop but allows additionally performing geological analysis.

A consequent use of this information allows geotechnical engineers to increase wall inclinations by keeping safety.

Repeated application allows the determination of the excavated volume directly from the 3D images.

*5.3 Blast engineering*

**Bench face surveying and planning of blasts**

Another application deals with the determination of the geometry of the bench faces and the planning of the blast layout in surface mining and quarries. The ShapeMetriX3D system is used for taking images of the area to blast and within a short time the blast layout can be planned on site based on the actual geometry (height, inclination) of the bench face. This way optimum borehole positions and/or

optimum loading conditions can be found which leads to reduced excavation costs, reduced danger for rock fly, reduced blasting vibrations [12]. Figure 25 shows an example.

Figure 25: 3D image of a bench face in a quarry and planned borehole positions. The system provides the blasting engineer with the required geometric information on the rock wall, as well as the distance between boreholes and surface (burden).

**Underground blasting**

In an underground mine the blasting layout was to be optimized. By regularly using ShapeMetriX3D, 3D images of subsequent excavation rounds were acquired. On each of the 3D images the borehole scheme was visualized and the locations measured in a mine co-ordinate system. By combining borehole measurements of subsequent tunnel faces together with determined surface quality, the actual blasting could be analyzed and improved step-by-step [13].

The analysis also included so-called critical burden tests. The investigated rock volume was surveyed by ShapeMetriX3D before and after the blast. The difference between the two 3D images allowed the quantification of effectiveness of different borehole-explosive systems.

Figure 26: Subsequent 3D images of drift tunnel excavation in an underground mine. The marked points represent the borehole positions that were measured together with the geometry of the tunnel face and the geological conditions.

## 6. TEST AT MORRISON SITE

### *6.1 General information*

During the Golden Rocks conference 2006 a workshop on rock face characterization was held. A rock face at Morrison site was chosen to be acquired and analyzed by different systems amongst others with ShapeMetriX3D.

The ShapeMetriX3D systems consists of a pre-calibrated SLR camera (Nikon D70, D80, or D200), or Canon Series) in a protective case, marking element(s), and a mobile computer running the measurement and assessment software, thus a complete system ready to go (see Figure 27).

### *6.2 Used hardware*

For the actual imaging on site a standard off-the-shelf Nikon D70s was used. The camera was pre-calibrated by 3G Software & Measurement. From the available zoom lens on site (10-20mm and 18-70mm), the 35 mm position was chosen.

For the actual photo shooting on June, 16 the automatic program of the camera was used resulting in an aperture of 5.6.


Figure 27: Components of the ShapeMetriX3D system.

*6.3 Image related information*

A set of six stereoscopic image pairs was taken. As imaging locations can be chosen freely (see Figure 28) they were selected in order to maximize the area to measure and thus the geometric image resolution on the rock surface. Therefore, the distances to the rock face are significantly different between the single stereo pairs.

Photos were taken freehand; the approximate length of the baseline was chosen to be around 1/8 to 1/10 of the distance to the rock face. The resulting lengths of the baseline showed to be between 1.5 m and 3.5 m.

Figure 28: Image taking at Morrison site.

Geometric image resolution (ground pixel size) varies between 1.1 and 2.1 cm.

The (adjustable) resolution of the surface grid ranges from 2.5 to 7.0 cm.

The minimal area for reliable orientation measurements at discontinuity surfaces is related to the resolution of the surface grid. In the current case the minimal area is 0.012m$^2$ (mean value for the merged 3D image and the chosen resolution of the surface grid).

*6.4 Exterior camera orientations*

Choosing the imaging locations is highly flexible due to the possibility of using zoom lens and taking the picture freehand. No external determination of the exterior camera orientation is required explicitly. However, the software is able to determine those locations based on the provided surveyed reference points.

Table 2 and Figure 30 show the determined exterior camera orientations for six stereoscopic image pairs taken at Morrison site. Each exterior orientation is provided by six parameters: three describing the location of the centre of projection and three providing rotation angles around the axes of the camera frame (see Figure 29).

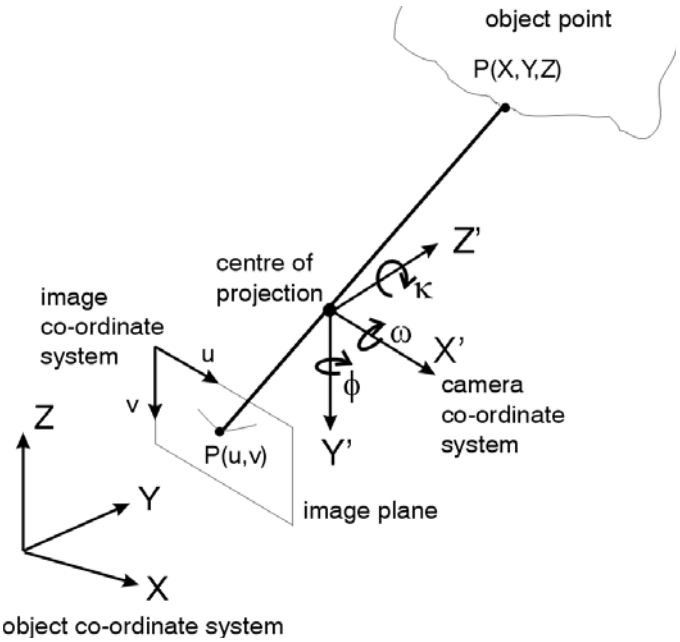


Figure 29: Co-ordinate systems and rotation angles.

The order of rotation for the rotation angles is: (i) rotation around the x-axis of the camera (omega ω), (ii) rotation around the y-axis (phi ϕ), and (iii) rotation around the z-axis (kappa κ).

Table 2: Exterior camera orientations (positions and rotation angles) for the 6 stereoscopic image pairs taken at Morrison site.

| Location [m] | Easting | Northing | Elevation |
|---|---|---|---|
| 1 Left | 937.678,408 | 507.615,045 | 1.908,102 |
| 1 Right | 937.675,239 | 507.613,171 | 1.908,213 |
| 2 Left | 937.678,894 | 507.611,799 | 1.907,425 |
| 2 Right | 937.677,165 | 507.608,944 | 1.907,482 |
| 3 Left | 937.677,429 | 507.605,923 | 1.908,190 |
| 3 Right | 937.677,279 | 507.603,494 | 1.908,259 |
| 4 Left | 937.686,768 | 507.619,616 | 1.907,741 |
| 4 Right | 937.686,159 | 507.617,545 | 1.907,775 |
| 5 Left | 937.694,890 | 507.626,383 | 1.907,339 |
| 5 Right | 937.694,592 | 507.625,065 | 1.907,329 |
| 6 Left | 937.682,791 | 507.614,838 | 1.907,083 |
| 6 Right | 937.679,817 | 507.612,445 | 1.907,215 |

| Orientation [deg] | Omega | Phi | Kappa |
|---|---|---|---|
| 1 Left | 75,30 | -57,20 | 167,35 |
| 1 Right | 77,68 | -50,12 | 170,12 |
| 2 Left | 78,10 | -29,23 | 173,54 |
| 2 Right | 79,21 | -26,05 | 174,78 |
| 3 Left | 81,39 | -4,15 | 179,16 |
| 3 Right | 80,85 | 0,33 | 179,49 |
| 4 Left | 83,39 | -7,56 | 177,72 |
| 4 Right | 82,51 | -3,24 | 177,85 |
| 5 Left | 85,26 | -7,16 | 179,21 |
| 5 Right | 85,23 | -6,30 | 178,93 |
| 6 Left | 56,87 | -49,74 | 154,26 |
| 6 Right | 59,62 | -45,11 | 159,17 |

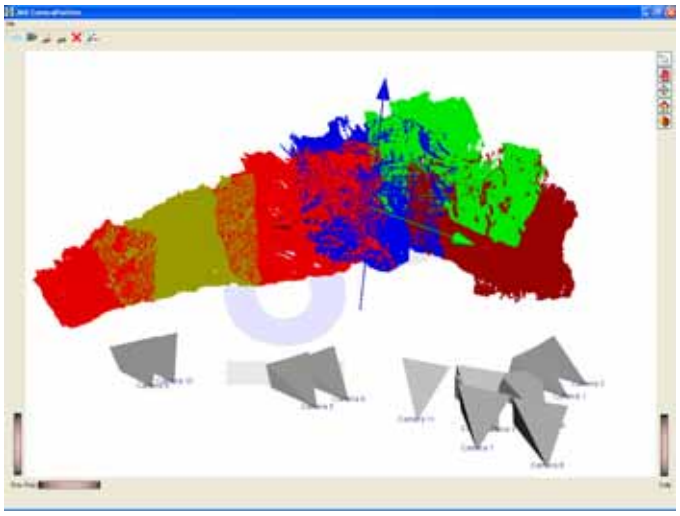

Figure 30: Snapshot of the geometric arrangement for imaging at Morrison site. All pictures were taken freehand. The software determines all camera locations and viewing directions based on the provided 6 reference points and relative orientations between the images computed automatically based on corresponding image points.

*6.5 Model merging*

The stereoscopic image pairs are processed individually leading to so-called generic 3D images which are true three-dimensional images showing the 3D surface qualitatively but providing no metric measurements. No reference points or exterior camera orientations, or any rigid setup are required.

The six generic 3D images are then combined based on common image information (corresponding points) in overlapping regions, i.e. those parts of the images showing the same part of the rock surface. The procedure currently relies on manual interaction but bears the capability for more algorithmic support using automatic image matching techniques which are already in use for generating the generic 3D image.

The merged 3D image is related to the provided reference points using Bundle Adjustment well known from classical photogrammetry [4]. This step transforms the generic 3D images into a metric 3D image.

*6.6 Workflow and time*

Imaging on site takes seconds for a pair of images as pictures can be taken freehand. It is important to take care on providing overlapping areas when the entire rock face is captured by several images.

The generation of the merged 3D image model comprises the following steps:

(i) Generation of the generic 3D images taking about 5 minutes per individual part.

(ii) Identification of corresponding points in overlapping regions of the individual parts taking currently some user interaction. At least three points per merge are to be marked. In the actual case six points per merge were used taking about 10 minutes per individual part.

(iii) Overall time: 6 x 5 + 6 x 10 = 90 minutes.

*6.7 Achieved accuracy*

Accuracy was checked using the provided 6 reference points. The standard deviations of the residuals are specified in Table 3.

**Table 3: Residuals**

| X [cm] | Y [cm] | Z [cm] | Total [cm] |
|---|---|---|---|
| 1.9 | 1.4 | 1.3 | 2.0 |

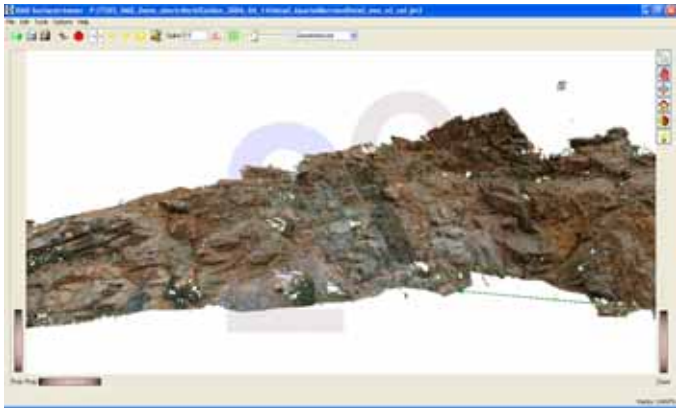

Figure 31: Geo-referenced 3D image of Morrison site merged from 6 individual parts. The overall 3D image contains about 700,000 surface measurements.

Figure 32: Detailed view of the merged 3D image from Morrison site.

### *6.8 Final remarks*

ShapeMetriX3D and JointMetriX3D use a strategy different from classical photogrammetry for the reconstruction of three-dimensional information from two-dimensional images.

Both systems firstly computes a generic 3D image that does not require any information from surveying or marked points (or even on the camera) and then transforms the generic into a metric 3D image using surveyed reference points or scaling elements.

The consequences of using this "photogrammetry plus computer vision" approach are grave: picture taking allows highest flexibility and 3D image processing runs with very less user interaction.

The ShapeMetriX3D system showed to be a valuable tool in both surface and underground mining, as well as in (conventional) tunneling, and in general for the acquisition and assessment of rock and terrain surfaces for various rock engineering projects.

## REFERENCES


1. Schubert, W., Goricki, A., Riedmueller, G. 2003. The Guideline for the Geomechanical Design of Underground Structures with Conventional Excavation. *Felsbau-Rock and Soil Engineering* 21, Nr. 4, Glueckauf Press, Essen.
2. Gaich, A., Fasching, A., Schubert, W. 2003. Improved site investigation. Acquisition of geotechnical rock mass parameters based on 3D computer vision. In Beer, G. (ed.) *Numerical Simulation in Tunnelling*: 13-46, Springer, Wien.
3. Fasching, A. 2001. Improvement of Acquisition Methods for Geotechnical Data. PhD thesis. In Riedmüller, G., Schubert, W., Semprich, S. (eds.) *Schriftenreihe Gruppe Geotechnik Graz Heft 12b*, Graz University of Technology.
4. Slama, Ch.C. (ed.) 1980. *Manual of Photogrammetry*. 4th edition. American Society of Photogrammetry, Falls Church, VA.
5. Wolf, P.R., Dewitt, B.A. 2000. *Elements of Photogrammetry,* Third Edition. McGraw-Hill, Boston.
6. Faugeras, O. 1993. Three-*Dimensional Computer Vision*. MIT Press, Boston, MA.
7. 3G Software & Measurement, 2003. Automatic identification of camera orientations. Internal report.
8. Sonka, M. Hlavac, V., Boyle, R. 1999. Image Processing, Analysis, and Machine Vision, 2nd ed., Pacific Grove et al.: PWS Publishing.
9. Naumann, H, Schroeder, G. 1992. *Bauelemente der Optik*, 6. Auflage, Carl Hanser Verlag München Wien.
10. Priest, S.D. 1993. *Discontinuity Analysis for Rock Engineering*. Chapman and Hall, London.
11. Falcao, A.X., J.K. Udupa, F.K. Miyazawa, 2000. An ultra-fast user-steered image segmentation paradigm: Live-wire-on-the-fly. IEEE Trans. on Medical Imaging, 19(1):55–62.
12. P. Moser, A. Gaich, E. Zechmann, A. Grasedieck, BlastMetriX3D – A new tool to determine the geometrical parameters of a blast based on 3D imaging, *ISEE 2006, Texas, USA.*
13. Wimmer, M. 2006. *Optimisation of the Drill and Blast Work in the Underground Marble Mine Sterzing of Omya S.p.A.* Diploma Thesis, Department of Mineral Resources and Petroleum Engineering, Montanistic University of Leoben, Austria.

# LIDAR for Rock Mass Characterization: Hardware, Software, Accuracy and Best-Practices

John Kemeny
*Department of Mining and Geological Engineering, University of Arizona, Tucson, AZ USA*
Keith Turner
*Dept. Geology and Geological Engineering, Colorado School of Mines, Golden, CO USA*
Brian Norton
*Split Engineering LLC, Tucson, AZ USA*

Copyright 2006, ARMA, American Rock Mechanics Association

This paper was prepared for presentation at the workshop: "Laser and Photogrammetric Methods for Rock Face Characterization" organized by F. Tonon and J. Kottenstette, held in Golden, Colorado, June 17-18, 2006.

This paper was selected for presentation by F. Tonon and J.T. Kottenstette following review of information contained in an abstract submitted earlier by the author(s). Contents of the paper, as presented, have not been reviewed by F. Tonon and J. Kottenstette, and are subject to correction by the author(s). The material, as presented, does not necessarily reflect any position of USRMS, ARMA, their officers, or members. Electronic reproduction, distribution, or storage of any part of this paper for commercial purposes without the written consent of ARMA is prohibited. Permission to reproduce in print is restricted to an abstract of not more than 300 words; illustrations may not be copied. The abstract must contain conspicuous acknowledgement of where and by whom the paper was presented.

**ABSTRACT:** This paper discusses the use of Ground-based LIDAR and digital image processing for rock mass characterization. Ground-based LIDAR (also referred to as 3D laser scanning) consists of a compact instrument that rapidly sends out laser pulses and calculates the three dimensional position of reflected objects. A typical scan takes 5-15 minutes and results in a three-dimensional point cloud containing 1 – 1.5 million points. Laser scanners have a range of up to 1 km and an accuracy of ± 3-10 mm. Along with the laser measurements, a high-resolution digital image can also be taken of the same scene. In the past several years LIDAR has gained acceptance as a potentially valuable new technology for rock mass characterization. In that period of time the LIDAR hardware has improved, automated point cloud processing software has been developed specifically for rock mass characterization, and best-practices are starting to be developed for field scanning and 3D data processing. Overall, it is felt that LIDAR surveys, along with automated point cloud processing, is accurate and cost effective and can now be used on engineering projects to assist with rock mass characterization and other rock engineering tasks.

## 1. INTRODUCTION

Engineering in rock masses includes the design of tunnels, slopes, bridge and dam foundations, underground and surface mines, and other types of rock excavations. In general, rock masses are very complex and consist of small and large-scale heterogeneities, changes in lithology, complex in-situ and induced stresses, and the presence of water and pore pressure. Many of the challenges with rock engineering design have to do with medium- to large-scale discontinuities present in the rock, including joints, faults, bedding planes and other types of fractures. With the exception of the small-scale frictional properties, the properties of the discontinuities must be determined in the field, from boreholes, excavations, and natural outcrops. Discontinuity properties to be determined in the field include orientation, length, spacing, roughness, persistence, aperture, filling, termination, and others (Priest [1], Hudson and Harrison [2], Nicholas and Sims [3]). Rock mass characterization is the process of compiling information and data on a rock mass for the purpose of engineering design. The results of rock mass characterization go on to be used in blast and excavation design, determination of support requirements, cost analyses, numerical modeling, and many other aspects of the design process. At a minimum, rock mass characterization usually involves borehole logging and sampling, laboratory testing, and field mapping and data collection.

Due to access problems, safety concerns, and time and cost concerns, there are many uncertainties and inconsistencies associated with the field activities associated with rock mass characterization. For example, consider the widening of a highway that involves additional excavation along an existing rock slope. It is traditional to conduct cell mapping or scanline surveying to collect rock mass information, which involves making detailed measurements along the slope (Priest [1]; Nicholas and Sims [3]). Some information can be gathered

from the base of the slope, but if the slope is high or unstable, the collection of data is hazardous as well as being time consuming and costly. As another example, in tunneling through difficult and varying rock conditions, it is necessary to characterize the rock mass continually as the tunneling progresses in order to properly design the tunnel support. It is difficult with traditional methods to properly characterize the rock mass while at the same time doing it in a timely manner so that the tunneling can progress without delays. As a third example, consider a large open-pit mine. It would useful both for blast design and slope stability to be able to completely characterize the rock on all the exposed rock faces as mining progresses. This information could then be input into the mine database along with geology, grade, throughput, cost and other information. However, because of the large number of new rock faces that are created each week in a large mine, this is an unreachable goal using traditional field methods.

The examples given above illustrate some of the problems with traditional field methods associated with rock characterization. New technologies have the potential for greatly assisting with the field mapping and data collection activities associated with rock mass characterization. These include the technologies of digital imaging / digital image processing (Gonzalez and Wintz [4]; Russ [5], Hadjigeorgiou [6]), laser-based imaging (Feng [7]; Slob et al. [8]; Kemeny et al. [9]), stereo-vision (Pötsch et al. [21], Roberts and Poropat [25], Faugeras [10]), geophysics (Boadu [11]; Hopkins and Kemeny [12]), and others. These technologies offer the potential for gathering fracture and associated information in a semi-automatic or automatic fashion at a distance from the face. The automated procedures can reduce the errors associated with gathering field fracture data by eliminating human bias and by standardizing the sampling procedure. These automated procedures can also be used to increase the amount of fracture information that is routinely collected, thereby allowing probabilistic engineering design to be carried out on projects where such a detailed analysis was not cost effective previously. Also, by imaging rock faces from a distance, both safety and access problems are reduced or eliminated.

This paper focuses on two of the technologies described above, ground-based Lidar and digital image processing. Ground-based LIDAR (also referred to as 3D laser scanning) consists of a compact instrument that rapidly sends out laser pulses and calculates the three dimensional position of reflected objects. A typical scan takes 5-15 minutes and results in a three-dimensional point cloud containing 1 – 1.5 million points. Laser scanners have a range of up to 1 km and an accuracy of ± 3-10 mm. Laser scanners weigh about 10 to 15 kg and are very portable, as shown in Figure 1. In the past several years LIDAR has gained acceptance as a potentially valuable new technology for rock mass characterization. In that period of time the LIDAR hardware has improved, automated point cloud processing software has been developed specifically for rock mass characterization, and best-practices are starting to be developed for field scanning and 3D data processing. Lidar alone cannot usually obtain all the necessary information for rock mass characterization. The usual procedure is to take high-resolution digital images of the same scene at the same time that a Lidar survey is being conducted. The digital images can then be processed to obtain additional rock mass characterization data.

This paper is broken up into seven sections. In the section that follows (Section 2), Lidar hardware is described. In Section 3, software for processing point clouds to obtain rock mass characterization information is described. Section 4 describes the use of digital image processing to obtain rock mass characterization information, and Section 5 discusses accuracy issues. Section 6 discusses the issue of best-practices, and Section 7 gives conclusions.

Figure 1. Examples of rock mass characterization using Lidar, a) dam foundation, b) quarry, c) highway, d) mountain environment. Scanner in all images is Optech Ilris 3D

## 2. LIDAR HARDWARE

The use of lasers to determine distances to objects is based on the same principles as ordinary radar; but "laser radar", or "Lidar," systems send out a narrow pulsed beam of light rather than broad radio waves. The systems utilize the speed of light and very precise timing devices to calculate the distance between a laser emitter/receiver device and an object reflecting the beam. Laser ranging devices have been developed for use in mobile (airborne) platforms and are fairly widely used to develop accurate terrain models. Around 1998, a new class of laser scanning instruments was developed for use in ground-based near-range and highly accurate surveying applications. These instruments undertook a "progressive scan" of a desired scene by sending out a sequence of narrowly focussed laser beams with gradually changing orientations. Thus, provided the base unit was in a stable configuration during the scanning operation, a series of closely spaced but slightly offset objects would be illuminated by the laser and located by range and orientation to the instrument location. These devices were capable of generating dense "clouds of points" that could be processed to yield three-dimensional [x, y, z] definitions of the features being scanned. More importantly, these ground-based laser scanners could assess vertical, or near-vertical, rock faces that could not be accurately measured from the airborne sensors.

### *2.1 Technological and Economic Developments*

The early devices were somewhat limited by current standards, but were the subject of considerable interest. Rapid improvements in the timing hardware allowed much more rapid sequencing of the pulses, and hence the more rapid collection of larger numbers of individual points. At the same time, improvements in laser technologies increased the focus of the beam and also reduced its tendency to enlarge (spread) with distance. Also the power of the laser, while maintaining visual safety issues, was adjusted so that maximum ranges of these instruments grew from a few hundred meters to over a kilometre. As these capabilities developed, in particular the longer maximum range, geologists and geotechnical engineers became increasingly interested in applying these instruments to rock slope assessments.

Table 1 summarizes the important characteristics of three ground-based laser scanners commonly used in North America. The data is mostly reproduced from technical literature provided by the manufacturers, although a few values (noted in the table) were estimated in order to assist the making of comparisons. These data reveal that current instruments are capable of collecting data at rates over 2000 points per second, with a position accuracy of about 5 mm at distances up to 800 meters. There are several trade-offs between accuracy, maximum distance and precision (Jacobs [13]). The output from a typical laser-scanner survey is a "point cloud" consisting of millions of reflection points. These points will have 3D coordinates, plus a reflected laser intensity value. In addition, all manufactures now offer high-quality digital cameras, usually of 6 mega pixels or more, that are "bore sighted" with the laser scanner instrument. A technique called texture mapping or photo draping can be used to overlay this high resolution color information from digital camera images onto the 3D points, so each has additional R, G, B attributes.

These ground-based laser scanners have remained relatively expensive since their inception. A single scanner costs roughly ten-times the cost of a total station survey instrument. In spite of this cost difference, private, state and federal agencies have purchased ground-based laser scanners, often for a variety of appliations. A large number of scanners have also been purchased by private surveying firms, who have found their productivity increase over traditional approaches more than offsets their purchase cost (Jacobs [14]). Experience by the authors demonstrates that these economic assessments are also valid for rock slope studies. For example, in 2003 a series of laser scans were used on a roadway widening project in Arizona and compared to traditional assessment methods that were also undertaken at the same locations. The total cost of the traditional methods was about $6250.00 (mostly manpower), while the laser scanning surveys cost about $5000.00 (one-third manpower, two-thirds equipment and software expenses). In addition, the traditional surveys required 10 man-days to complete, while the laser scanned products were available in two days. The conclusion that can be drawn from this comparative study is that laser scan-based survey and automated analysis can be considerably faster, less labor-intensive and therefore cheaper than traditional

survey and analysis (Slob et al. [15]).

**Table 1.** Basic Characteristics of Popular 3D Laser Scanners (Source: Manufacturer's literature and Poboline [16])

| **Performance** | Optech **ILRIS-3D** | Riegl **LMS-Z420i** | Leica **HDS3000** |
|---|---|---|---|
| Laser wavelength (nanometers) | 1,500 | 1,550 | 532 |
| Beam Diameter at 100m distance | 27mm | 25mm | 12mm* |
| Average Data Acquisition Rate (pt/sec) | 2,000 | 8,000 | 1,400 |
| Maximum Data Acquisition Rate (pt/sec) | 2,000 | 12,000 | 1,800 |
| Distance Accuracy at 100m distance | 7mm | 5mm | 8mm* |
| Position Accuracy at 100m distance | 10mm | 6mm | 12mm* |
| Minimum Range | 3m | 2m | < 1m |
| Maximum Range [range limit depends on target albedo (0-100%)] | 1500m @ 80%<br>700m @ 10%*<br>350m @ 4% | 1000m @ 80%<br>350m @ 10% | 400m @ 80%*<br>100m @ 5% |
| Digital Camera [externally mounted and boresighted] | 6 megapixel | 6.1 or 8.2 megapixel | 6+ megapixel |

* These values estimated from available published values.

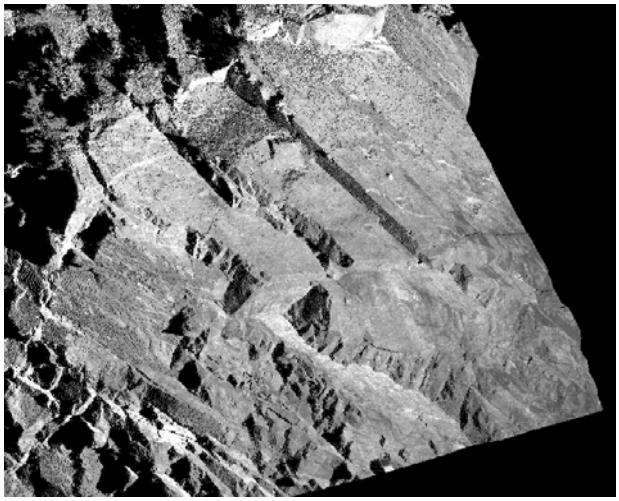

**(a)**

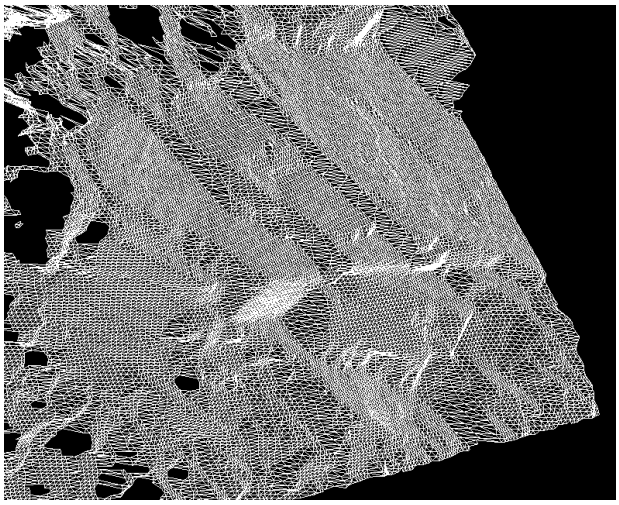

**(b)**

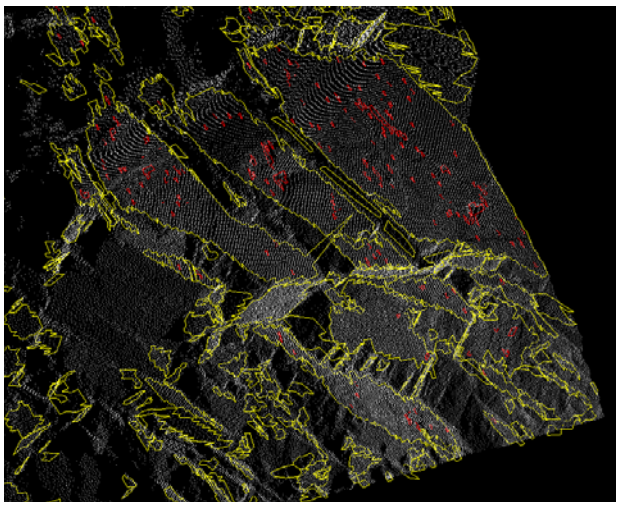

**(c)**

## 3. POINT CLOUD PROCESSING SOFTWARE

The output from a laser scanner survey is a "point cloud" consisting of millions of reflection points that represent the 3D surface that was scanned. After some data cleaning, a triangulated surface can be rendered from the point cloud data, and many subsequent calculations and visualizations can be made using the 3D surface. In addition, a technique called texture mapping or photo draping can be used to overlay high-resolution color information from digital images onto the 3D surface. An example of a point cloud of a rock face is shown in Figure 2a (taken along a highway south of Ouray, Colorado). This point cloud has about 1.5 million points and the scanning took about 15 minutes using an Optech Ilris3D scanner.

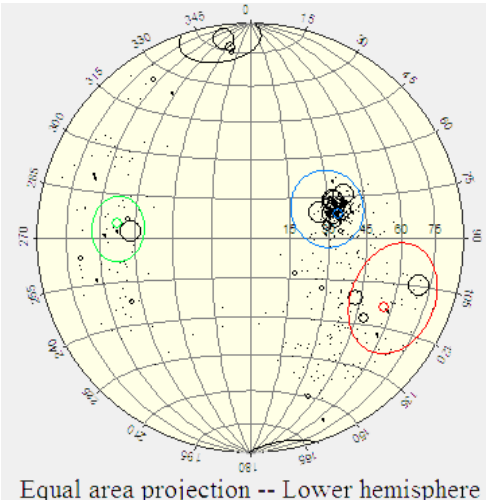


**(d)**

Figure 2. Basic steps in rock mass characterization using Lidar, a) point cloud, b) triangulated mesh, c) automatic delineation of fracture patches, d) plotting patch information on a stereonet and delineating fracture sets.

This section describes the use of automated point cloud software for extracting rock mass characterization information. Point cloud processing software is capable of automatically extracting valuable information about discontinuities, including 3D orientation, spacing, size, roughness and block size. Point cloud processing software can often utilize information from digital images as well as from point clouds, and can plot information on stereonets and histograms as well as export data in various formats. We show specific examples from the Split FX software that is currently being developed at Split Engineering LLC (Split [17]). However, similar features can be found in other point cloud processing programs. Some key features of automated point cloud processing software are described below.

*3.1 Point cloud registration*

The first step in point cloud processing is to orient the point cloud into the real world coordinate system based on data that was taken in the field. Point cloud software usually includes several methods for point cloud registration. The most common method is to register the point cloud based on 3 targets of known position (three point registration method). However, for some applications (such as slope stability), only the orientation registration is required. In these instances, simpler methods are possible, such as only measuring the orientation of the scanner (orient by scanner method) without any position surveying.

*3.2 Triangulated mesh generation*

The second step in point cloud processing is to create a surface mesh from the point cloud data. In the process of creating a surface mesh, erroneous data points in the point cloud can be filtering. Figure 2b shows a triangulated mesh of part of the point cloud shown in Figure 2a.

*3.3 Automatic Fracture Delineation*

The most important processing step is the delineation of fracture "patches" from the triangulated surface mesh. The term patch is used rather than fracture, because a single large fracture may be delineated into several smaller patches, depending on the flatness and roughness of the fracture. Fractures are detected by using the basic property that they are flat. Flat surfaces are automatically found in the triangulated mesh by first calculating the normal to each triangle, and then finding groups of adjacent triangles that satisfy a flatness criterion. This criterion has parameters that can be adjusted by the user. Figure 2c shows the patches that were found in the point cloud shown in Figure 2a, using the criterion that a patch must be at least 5 triangles, and neighboring triangles in a patch must not deviate in orientation by more than 10 degrees. The patches are outlined in yellow and holes in patches are outlined in red. Overall this simple criterion results in a good delineation of the major fractures at the site. Patches can also be manually added, deleted and edited.

*3.4 Stereonet plotting*

Once the patches have been found, their average orientations can be plotted on a stereonet. Each patch plots as one point on the stereonet. However the size of the point can be adjusted based on other parameters such as the patch area or roughness. We have found that large patches are a good indication of important fractures and fracture sets. Small patches, on the other hand, may not actually be a fracture but only a small portion of the surface that happens to be flat. Thus it is useful to weight the points by area, and plot the smallest fractures as only a small dot. Figure 2d is a plot of the patches from Figure 2a. In Figure 2d the points have been weighted by patch area, and several prominent joint sets are visible. At this point fracture sets can be

defined, and the statistical properties of each set (mean orientation, Fisher constant, etc.) can be calculated. The data can also be exported to slope stability and underground stability software.

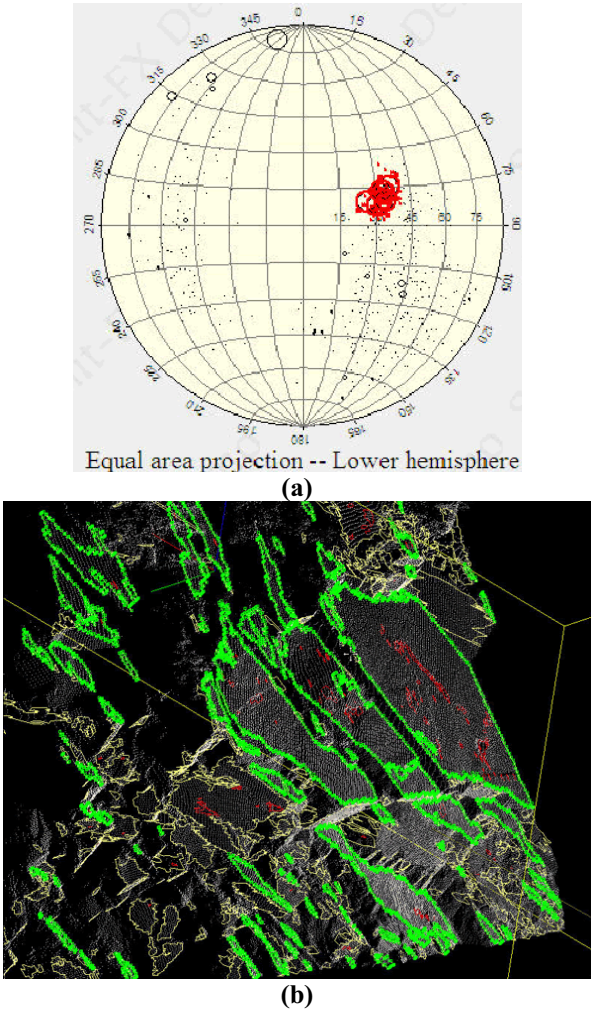


**(a)**

**(b)**

Figure 3. Selection of a group of fractures on the stereonet (a), followed by an investigation of those fractures on the point cloud (b) (this can also be done the other way around).

A particularly useful feature of point cloud processing software is the interaction it allows between the stereonet and the point cloud. Delineating joint sets from stereonet data is difficult and necessitates professional expertise. Normally the data is taken in the field and the delineation of joint sets is accomplished at a later time and location. Therefore, any difficulties with interpretation of the data cannot be resolved without additional field work. With access to the point cloud, however, additional analysis can be conducted off site. For instance, a group of patches can be selected on the stereonet and then viewed on the point cloud, as shown in Figures 3a and 3b. This allows the user to go back and forth between the stereonet and the point cloud to determine with a great deal of precision the delineation of important fractures and fracture sets.

The number of laser points that strike a fracture surface will depend on many factors, including the laser resolution, the size of the fracture, the distance of the fracture, and the orientation of the fracture relative to the scanner orientation. Fractures that are sub-parallel to the direction of scanning may be under-represented on the stereonet because fewer laser points will strike those surfaces. However, a careful evaluation of the point cloud and the sterenet can reveal those under-represented areas in the stereonet, and patches can be added accordingly using hand-editing tools in the point cloud processing software. The scanner can only detect surfaces that are in the scanner's line of sight, and the portion of the surface that is not in the scanner's line of site is referred to as the scanner "shadow zone". In some circumstances, an entire joint set may be in the scanner shadow zone, and in these cases several scans need to be taken at different angles to the face in order to adequately represent the structural conditions at the site (see Donovan et al. [18]).

## 4. PROCESSING DIGITAL IMAGES

Discontinuities appear in two forms in exposed outcrops, as fracture traces and as fracture surfaces. A fracture trace is the intersection of a discontinuity with a rock outcrop or the intersection of two discontinuities. In a relatively smooth rock outcrop or tunnel wall, most of the discontinuities will appear as fracture traces, such as the digital image shown in Figure 4a. In rough rock outcrops and tunnel walls, on the other hand, most of the discontinuities will appear as fracture surfaces, as shown in Figure 4b. Both Figures 4a and 4b are from the same location and have identical geology and rock mass characteristics. Digital images containing fracture traces (such as Figure 4a) can be analyzed using digital image processing techniques, as described in Kemeny and Post [5], Hadjigeorgiou et al. [6] and others. In general these techniques are useful for extracting trace length, trace spacing, trace large-scale roughness, and block area. In addition, by utilizing texture algorithms or multi-spectral imaging, information about weathering and joint condition can also be extracted (Monte [26]).

Except in cases where multiple non-parallel images are taken, it is not possible to reliably extract information on fracture orientation or three-dimensional block volumes using two-dimensional image processing techniques.

**(a)** **(b)**

Figure 4. a) Digital image of a relatively flat portion of a rock outcrop, which is ideal for 2D image processing, b) another portion of the same rock mass that shows significant relief, which is ideal for ground-based Lidar.

The first step is to delineate the fracture traces in a digital image. This can be done either automatically or by using hand-editing features in a digital image program. Figure 5a shows a digital image from a bench in an open-pit mine in Arizona, and Figure 5b shows the delineation of the fracture traces using hand-editing features in the public-domain ImageJ image processing program (Rasband [19]).


**(a)**

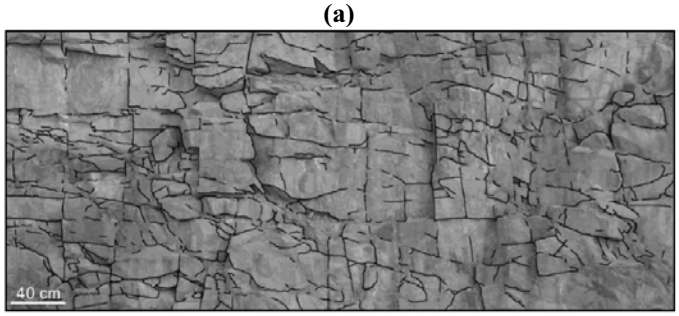


**(b)**

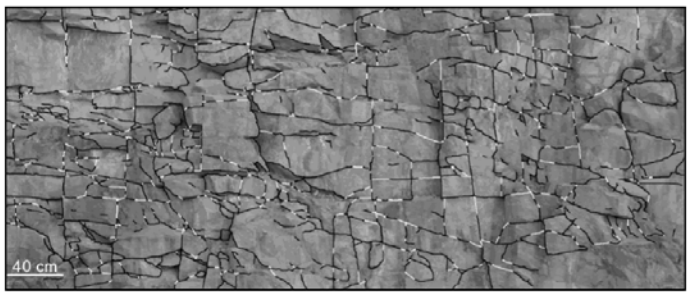


**(c)**

Figure 5. a) Digital image of a bench from an open-pit mine, b) delineation of fracture traces using hand-editing tools, c) delineation of rock bridges (gray) in addition to fracture traces in order to determine block size.

There are several pieces of information that can be obtained from each delineated fracture trace. First of all the trace orientation can be measured. Since the trace may not be perfectly linear, the trace angle is usually taken as the angle of the best-fit line through the fracture trace. The convention used here is to measure the rake, which is defined as the clockwise angle measured from horizontal. The rake measured from a fracture trace in a digital image is the apparent rake due to the angle between the normal to the face and the axis of the camera. The actual rake as would be measured in the plane of the rock face can be calculated using trigonometric functions.

The other parameters of the fracture trace are the length and some measure of the roughness. The fracture length can either be the straight-line length from one end of the fracture to the other, or the total arc-length as traveled along the fracture. Following delineation, standard image processing programs will output a detailed profile of each fracture consisting of the x,y coordinates for the center of each pixel making up the trace. This data can be used to calculate large-scale roughness. Measures of fracture roughness that can be calculated from the profile information include $Z_2$ (Tse and Cruden [20]), fractal properties, Fourier coefficients, and other measures. Also, from these roughness measures standard joint roughness parameters such as the Joint Roughness Coefficient (JRC) can be estimated (Tse and Cruden [20]).

*4.1 Analysis of fracture information for individual sets*

One set of information comes from each fracture set analyzed separately. Rock joints in particular usually occur in sets, and this is reflected in clusters of trace angles, referred to as trace sets. The first step is to determine the number of trace sets. The next step is to separate the traces by trace set and analyze each set separately. The information that can be extracted for each set includes the distributions of trace angles, lengths, large-scale roughnesses and spacings. The distributions of the first three (angle, length, roughness) are straightforward and are merely the distributions of the information gathered on each trace. The distribution of joint spacing, on the other hand, is problematic due to the fact that the individual traces from a given set are not parallel. For two parallel traces, the spacing is the distance between the traces measured perpendicular to the trace direction. For non-parallel traces, on the other hand, the spacing between any two traces depends on where it is measured and along what direction it is measured. The approach taken here to measure the distribution of fracture spacing is illustrated in Figure 6a. As illustrated in Figure 6a, spacing measurements are made from a series of scanlines perpendicular to the average orientation of the traces. This method for estimating the joint spacing will provide a measure of the degree of persistence of the joints, which is an important aspect of block interlocking. The joint spacing distributions for the two trace sets are shown in Figure 6b.

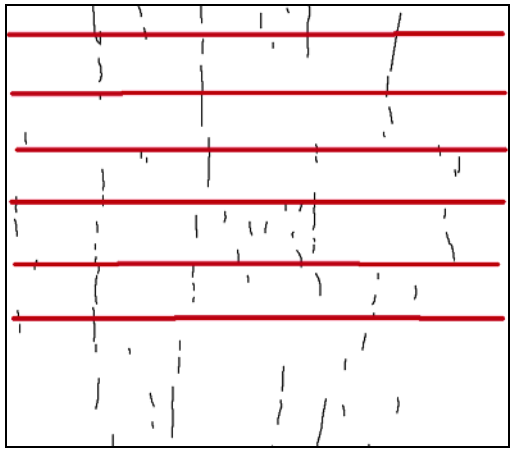

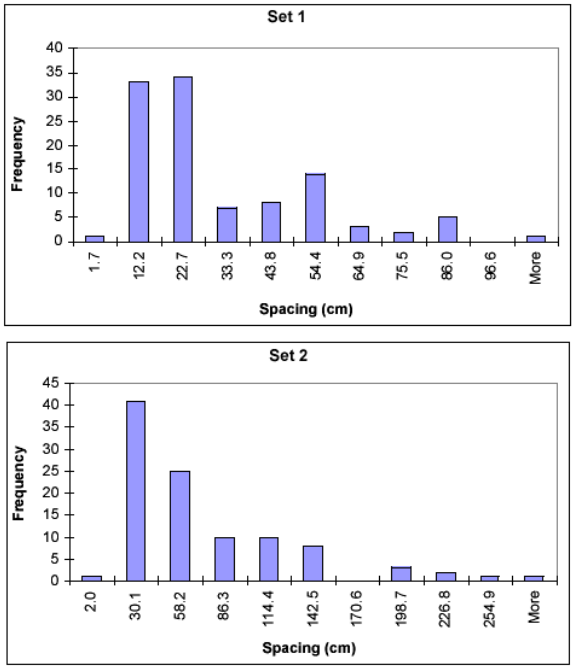


Figure 6. a) Method for determining the distribution of fracture spacing for a joint set, b) fracture spacing distributions for the horizontal (set 1) and vertical (set 2) sets from Figure 5b.

*4.2 Analysis of fracture network information*

The second set of information comes from the combined fracture network. The combined fracture network for Figure 5a is shown in Figure 5c. There are two important kinds of information here, the distribution of block sizes (or areas) and the distribution of rock bridge sizes. A block is defined as a region bounded on all sides by traces. Any small gap in the boundary will prevent the block from being delineated as a separate block. These small gaps are referred to as rock bridges (Einstein [23], Goodman and Kieffer [24]), and many rock bridges are apparent in Figure 5a. In some cases, these gaps may be due to inaccuracies in either hand or automatic trace delineation. In other cases, the gaps may be real and represent regions of intact rock that must be broken before the block could be removed. In either case, the first step is to delineate the rock bridges and thereby complete the boundary of each block. Then the block size distribution can be easily determined using standard "analyze particles" features in most standard image processing programs. It should be noted that the exact way in which the bridges would fail cannot be determined without knowing the material properties and boundary conditions of the rock mass being studied. Here we assume that the bridges would fail by making the shortest

connection between the traces bounding each rock bridge. After delineation of the rock bridges, the size distribution of both the blocks and the rock bridges can be determined, as shown in Figures 6c and 6d respectively for the network shown in Figure 6b. In Figure 6c, the block volumes are calculated by multiplying the area of each block by the average diameter of a best-fitting ellipse through each block (i.e., the third dimension of each block is assumed to be equal to the average dimension of the block in the plane of the image).

## 5. ACCURACY

An important aspect of the use of 3D laserscanners for rock mass characterization is understanding the errors associated with 1) the instrument, 2) the procedures for scanning in the field, and 3) processing the resulting point clouds. The errors associated with the scanner itself were discussed in Section 2. For extracting fracture information from point clouds, a key measure of accuracy is the error in the estimation of a fracture's strike and dip (or dip and dip direction). For a typical scan of a rock face, often over 1000 laser points will intersect large fracture surfaces, while less than 50 points may intersect smaller surfaces. It is important to understand how the number of laser points intersecting a fracture surface and the error of the laser impact the accuracy in the estimation of the strike and dip of the plane. For this purpose a computer model has been developed to determine the error in the calculation of strike and dip, based on a laserscanner with given distance and position accuracies and a fracture plane with a given size and distance from the scanner. Below we show results for a 1 m x 1 m fracture plane at a distance of 100 meters from the scanner with a dip of 62.581 degrees and dip direction of 26.565. For scanner accuracy, position and distance accuracies of ± 1.5 cm were used. This is a large error, and most 3D laserscanners are capable of scan accuracies less that this. Two cases were considered. In the first case 91 laser points intersected the plane, and in the second case only 11 laser points intersected the plane.

The program works by first calculating the exact intersections between the laser rays and the plane. x, y and z errors are then added to each intersection xyz, based on a uniform random number with bounds ± the laser accuracy. Figure 7 shows the distribution of radial error (i.e., the distance between the actual intersection point and the one with the xyz errors added) for the case of 91 laser points hitting the plane. It shows that most of the radial errors vary from 1.5 to 3 cm for this case. A least squares plane is then fit through the intersection points with the error, and the dip and dip direction of this plane is calculated and compared with the actual orientation. This process is repeated in a Monte Carlo fashion. Figures 8a and 8b show the distributions of dip and dip direction for 30 Monte Carlo simulations for the case of 91 laser points hitting the plane. It shows variations in dip of about ±0.18 degrees from the actual, and variations in dip direction of about ±0.1 degrees from the actual. Figures 9a and 9b show the distributions of dip and dip direction for 30 Monte Carlo simulations for the case of only 11 laser points hitting the plane. It shows variations in dip of about ±0.5 degrees from the actual, and variations in dip direction of about ±0.35 degrees from the actual. Overall these results are very promising and indicate that errors in the strike and dip less than 0.5 degrees should be able to be attained with fractures containing as little as 20 laser intersections and using almost any of the laser scanners available today. It should be noted that the model does not consider some important sources of possible error, including atmospheric and temperature errors. It also does not include the error associated with spatially orienting the point cloud, which is discussed below.

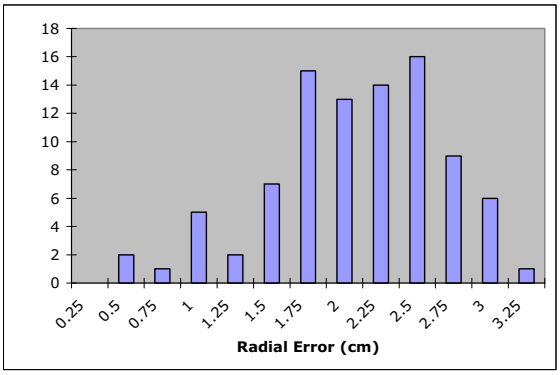


Figure 7. Distribution of radial error for a simulation of 91 laser points hitting a fracture plane with a scan accuracy of ±1.5 cm.

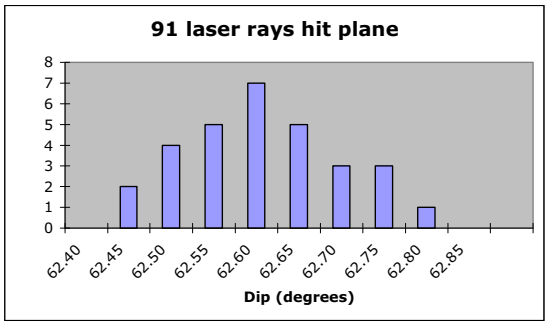


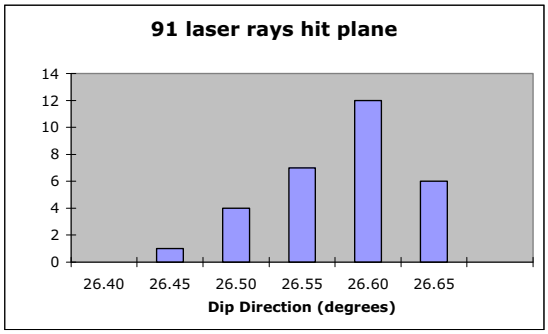


Figure 8. Distributions of dip and dip direction from 30 Monte Carlo simulations, where 91 laser rays hit the fracture plane and using a scan accuracy of ±1.5 cm.

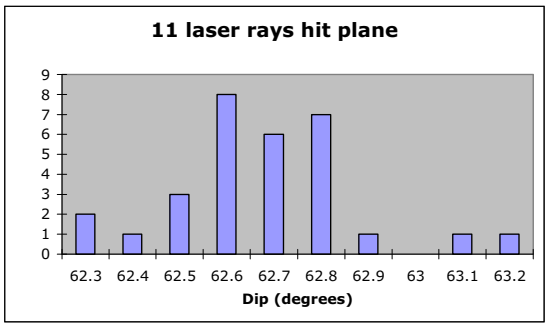


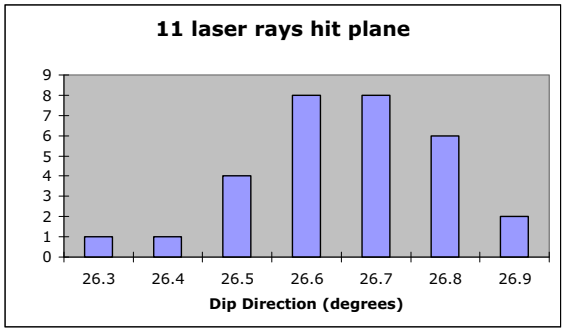


Figure 9. Distributions of dip and dip direction from 30 Monte Carlo simulations, where 11 laser rays hit the fracture plane and using a scan accuracy of ±1.5 cm.

One of the most important steps in processing the point cloud is reorienting the point cloud to the real world coordinate system. This is typically done by placing targets in the images and using standard surveying equipment such as a total station or laser rangefinder. There are several problems associated with this technique. First of all, this can be a costly and time consuming step, especially if scanning surveys are conducted in remote areas. Secondly, there could be safety hazards associated with putting targets on the rock faces. To alleviate some of these problems, an alternative method has been developed. For the purpose of fracture characterization, the point cloud needs to be oriented correctly, but not necessarily positioned correctly. For such cases, a technique has been developed where the orientation of an object in the image is measured accurately using a compass. The flat object can either be a natural object already in the image, or a non-natural object can be placed in the image. The object can also be the scanner itself (orient by scanner method described in Section 4). The placed object does not have to be on the rock face being scanned. The accuracy of this technique should be as good as the accuracy in measuring the orientation of the flat object with a compass, about ±2 degrees. A test using this technique was conducted on the University of Arizona campus. A flat rock surface was scanned from several orientations and distances. In each scan, a flat object with known orientation was placed in a position so that it would be part of the point cloud. Figure 10 shows the results of this test on a lower hemisphere stereonet. It shows the actual orientation of the object as well as the results from the scans. The scanned results are within 2-4 degrees from the actual orientation.

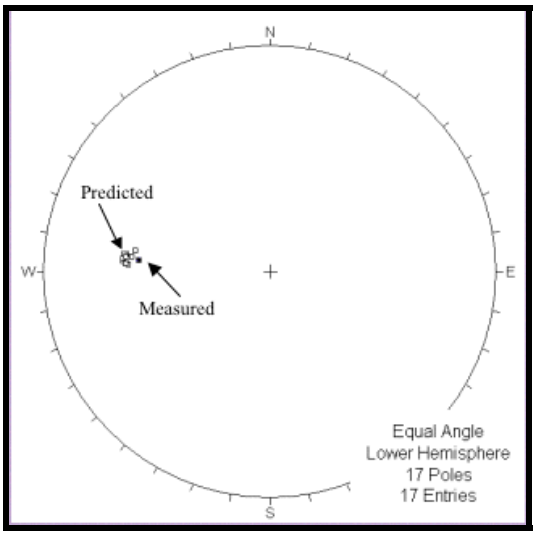


Figure 10. A comparison between the actual orientation of a rock face, and numerous predictions using a 3D laserscanner positioned at different

angles and distances from the face. The point cloud was oriented using a technique where a flat object of known orientation was placed in the scan.

*5.2 Case study: Mt Lemmon field test site, Tucson, Arizona*

One way to assess the error in the estimation of strike and dip is to compare orientation measurements extracted from the point cloud with measurements made using manual scanline or cell mapping. Figure 11 shows one such comparison made at a field site in the mountains northeast of Tucson, Arizona. As shown in Figure 11, 50 manual measurements were made and 441 fractures were extracted from the point cloud. The results shown in Figure 11 are typical of the results of these kinds of comparisons. Overall, there is a good correlation between the measured and extracted orientations. More important however, the extraction of almost 10 times as many joint orientations results in a much more accurate assessment of the structural conditions at the site.

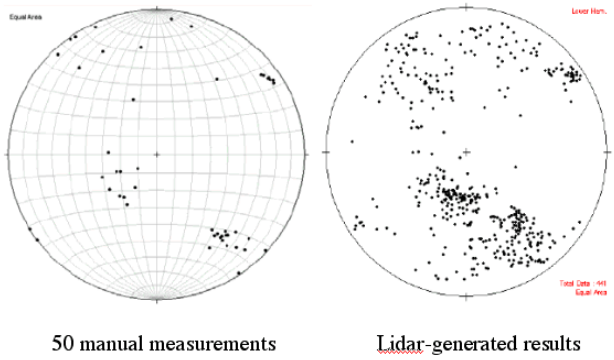


Figure 11. Comparison between field and LIDAR-generated results from a site at Mt. Lemmon, Arizona.

*5.2 Case study: Morrison field test site, Colorado*

As a second validation, a case study was conducted at the US Bureau of Reclamation test site near Morrison, Colorado. This test site was previously used to test out photogrammatic procedures for estimating discontinuity orientations, as described in Kottenstette [22]. Six locations were chosen where discontinuity orientations were estimated by the Bureau of Reclamation. For the Bureau of Reclamation analysis, 17 surveyed points on the slope were used for control. The results for the Bureau of Reclamation analysis using photogrammetry are shown in the upper hemisphere stereonet shown in Figure 12a (from Kottenstette, [22]). For the analysis using Lidar and the Split FX program, several scans were made using an Optech ILRIS3D scanner. The results are shown for the first of these scans. The point clouds were registered by carefully measuring the orientation of the scanner (orient by scanner method described in Section 3.0). In the Split FX program, patches were inserted in roughly the same locations as in Bureau of Reclamation analysis. The orientation results for the selected patches are shown in the upper hemisphere stereonet in Figure 12b. Overall there is a good match between the results by the Bureau of Reclamation (photogrammetry and PhotoModeler software) and the results of this study (Lidar and Split FX). The biggest difference occurs for location D1. Initially patches could not be inserted in location D1 due to the non-planarity of the discontinuity at this location. Eventually, the planarity criterion was reduced, and four patches were inserted at location D1 to show the large variation at this location. An analysis of all the joint sets at the Morrison site using the FX data indicated that fracture D1 is likely an undulating blast-induced fracture rather than a natural discontinuity.

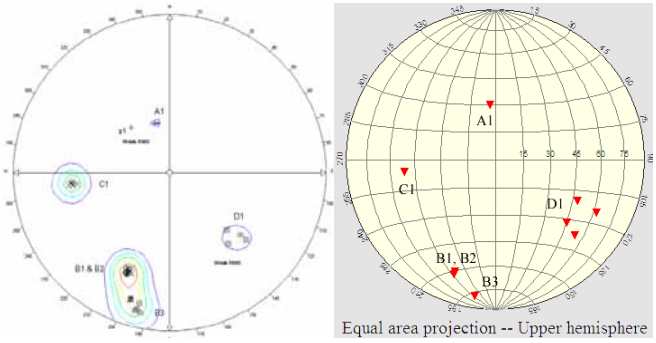


Figure 12. a) Upper hemisphere plot of fracture orientations at 6 locations (A1, B1, B2, B3, C1, D1) determined using photogrammetry from the Morrison site, b) Upper hemisphere plot of orientations for six patches inserted in a Lidar point cloud of the Morrison site to roughly match the locations in Figure 12a.

## 6. BEST PRACTICES

As hardware and software solutions are being developed for rock mass characterization using Lidar and digital image processing, an important issue has to do with specific procedures and best-practices associated with the practical application of the technique. Guidance is still needed on specific and appropriate procedures involved to conduct

ground-based LIDAR surveys, as well as the appropriate data validation, processing and management procedures. In the field, appropriate procedures must be specified concerning a) the suitability of a site for LIDAR surveying, b) the procedures for scanning (number of scans, point spacing, resolution, etc.), c) establishing surveying control points, d) taking digital images, and e) collecting non-digital types of information. After a survey is conducted, data processing and management procedures include a) the specific steps that should be taken to process the data using various software packages for specific outcomes (i.e., calculate the slope hazard at a particular site), and b) the appropriate standards and formats for the various kinds of data from a LIDAR survey, including the raw scanner files, point cloud files, rendered surface files, and calculations and interpretations made on this data.

Best-practices are currently being developed based on case studies in a variety of rock types and environmental conditions. With each new case study in a new type of rock or environment, knowledge is gained. For instance, initially it was thought that the scanner shadow zone was going to be a major issue, and that scans of a rock face would need to be conducted at many different angles. However, with improvements in hardware and software, and an awareness that the location of the scanner must be selected with this in mind, multiple scans of a rock face are now only necessary in certain cases. Case studies have also revealed that the requirements (point spacing and resolution) for obtaining geotechnical data from a highway slope using Lidar are much different than, say, obtaining volume information related to a slope. For rock masses containing complex structure, a point spacing of 2 cm or less is recommended. Case studies have also revealed the importance of point cloud registration, and the problems associated with integrating survey information and point cloud information. These are just a few examples, and a complete discussion of best-practices for field scanning and data analysis is currently being compiled.

## 7. CONCLUSIONS

This paper discusses the use of Ground-based LIDAR and digital image processing for rock mass characterization. Ground-based LIDAR (also referred to as 3D laser scanning) consists of a compact instrument that rapidly sends out laser pulses and calculates the three dimensional position of reflected objects. A typical scan takes 5-15 minutes and results in a three-dimensional point cloud containing 1 – 1.5 million points. Laser scanners have a range of up to 1 km and an accuracy of ± 3-10 mm. Along with the laser measurements, a high-resolution digital image can also be taken of the same scene. In the past several years LIDAR has gained acceptance as a potentially valuable new technology for rock mass characterization. In that period of time the LIDAR hardware has improved, automated point cloud processing software has been developed specifically for rock mass characterization, and best-practices are starting to be developed for field scanning and 3D data processing. Overall, it is felt that LIDAR surveys, along with automated point cloud processing, is accurate and cost effective and can now be used on engineering projects to assist with rock mass characterization and other rock engineering tasks.

## REFERENCES


1. Priest, S. D. 1993. Discontinuity Analysis for Rock Engineering, London, Chapman & Hall.
2. Hudson, J. and J. Harrison. 2000. Engineering Rock Mechanics. Pergamon Press, 896 pages.
3. Nicholas, D.E. and D.B. Sims. 2001. Collecting and using geologic structure data for slope design, in Slope Stability in Surface Mining, ed. by W.A. Hustrulid, M.K. McCarter and D.J.A. Van Zyl, SME, Littleton, CO, pp11-26.
4. Gonzalez, R. C., Wintz, P. 1987. Digital image processing, 2 edn. Addison-Wesley, Boston.
5. Russ, J.C. 1999. The Image Processing Handbook , CRC Press.
6. Hadjigeorgiou, J., Lemy, F., Co te´, P., and X. Maldague. 2003. An Evaluation of Image Analysis Algorithms for Constructing Discontinuity Trace Maps Rock Mech. Rock Engng., 36 (2), 163–179.
7. Feng, Q. 2001. Novel Methods for 3D semi-automatic mapping of fracture geometry at exposed rock faces, Doctoral Thesis, Royal Institute of Technology, Stockholm, Sweden.
8. Slob, S., Hack, R., and K. Turner. 2002. An approach to automate discontinuity measurement of rock faces using laser scanning techniques, ISRM International Symposium on

Rock Engineering for Mountainous Regions – Eurock 2002 Funchal, November 25-28th.
9. Kemeny, J., Mofya, E. and J. Handy. 2003. The use of digital imaging and laser scanning technologies for field rock fracture characterization, Proceedings of Soil and Rock America 2003 (12th PanAmerican Conference on Soil Mechanics and Geotechnical Engineering and the 39th US Rock Mechanics Symposium), Eds. J. Culligan, H. Einstein, A. White, Massachusetts Institute of Technology, Cambridge, MA, pp. 117-122.
10. Faugeras, O. 1996. Three Dimensional Computer Vision: A Geometrical Viewpoint", The MIT Press, Cambridge, Mass.
11. Boadu, F. K. 1997. Fractured rock mass characterization parameters and seismic properties: Analytical studies Journal of Applied Geophysics, Vol. 37 (1), pp. 1-19
12. Hopkins, D. and J. Kemeny. (2002). Drilling and blasting optimization through integration of geophysical, mineral-content, and drilling data, NARMS-TAC 2002, University of Toronto, pp. 987-994.
13. Jacobs, G. 2005a. Understanding Laser Scanning Terminology. Professional Surveyor, Vol. 25, no. 2, pp. 26-31.
14. Jacobs, G. 2005b. Laser Scanning: Big Advantages, Even for Small Projects. Professional Surveyor, Vol. 25, no. 10, pp. 30-35.
15. Slob, S., Hack, H.R.G.K., van Knapen, B., Turner, K. and Kemeny, J. (2005) A method for automated discontinuity analysis of rock slopes with 3D laser scanning. In: Transportation Research Record, 1913(2005)1, pp. 187-208
16. Poboline. 2005. 2005 3D Laser Scanner Hardware & Software Surveys. http://www.pobonline.com/FILES/HTML/ProductSurveys/
17. Split Engineering LLC, www.spliteng.com
18. Donovan, J., Kemeny, J., and J. Handy. 2005, The Application of Three-Dimensional Imaging to Rock Discontinuity Characterization, Alaska Rocks 2005: The 40th U.S. Symposium on Rock Mechanics, Anchorage, AL.
19. Rasband, Wayne. 2004. ImageJ, http://rsb.info.nih.gov/ij/
20. Tse, R. and D. M. Cruden. 1979. Estimating joint roughness coefficients, Int. J. Rock Mech. Min. Sci., 16:303-307.
21. M. Pötsch, W. Schubert, A. Gaich, Application of metric 3D images of rock faces for the determination of the response of rock slopes to excavation, EUROCK 2005, Brno, Czech. Rep.
22. Kottenstette, J.T. 2005. Measurement of Geologic Features using Close Range Terrestrial Photogrammetry, The 40th U.S. Symposium on Rock Mechanics (USRMS): Rock Mechanics for Energy, Mineral and Infrastructure Development in the Northern Regions, held in Anchorage, Alaska, June 25-29, 2005.
23. Einstein, H. 1993. Modern Developments in Discontinuity Analysis – the Persistence-Connectivity Problem, In Comprehensive Rock Engineering, Principles, Practice, & Projects. Volume 3: Rock Testing and Site Characterization, pp. 193-213, Oxford, Pergamon Press.
24. Goodman, R. and S. Kieffer. 2000. Behavior of rock in slopes, J. Geotech. Geoenv. Eng., Vol. 126, No. 8, pp. 675-684.
25. Roberts, G. & Poropat, G. 2000. Highwall joint mapping in 3D at the Moura mine using using SIROJOINT. Bowen Basin Symposium 2000 Coal and Mining The New Millennium, Rockhampton, Oct. 2000.
26. Monte, J. 2004. Rock mass characterization using laser scanning and digital imaging data collection techniques, M.S. Thesis, University of Arizona.

# Remote 3D Mapping Of Rock Mass Structure

Poropat, George V.
*Commonwealth Scientific & Industrial Research Organisation,*
*Division of Exploration & Mining, Brisbane, Qld., Australia*

Copyright 2005, ARMA, American Rock Mechanics Association

This paper was prepared for presentation at the workshop: "Laser and Photogrammetric Methods for Rock Face Characterization" organized by F. Tonon and J. Kottenstette, held in Golden, Colorado, June 17-18, 2006.

This paper was selected for presentation by F. Tonon and J.T. Kottenstette following review of information contained in an abstract submitted earlier by the author(s). Contents of the paper, as presented, have not been reviewed by F. Tonon and J. Kottenstette, and are subject to correction by the author(s). The material, as presented, does not necessarily reflect any position of USRMS, ARMA, their officers, or members. Electronic reproduction, distribution, or storage of any part of this paper for commercial purposes without the written consent of ARMA is prohibited. Permission to reproduce in print is restricted to an abstract of not more than 300 words; illustrations may not be copied. The abstract must contain conspicuous acknowledgement of where and by whom the paper was presented.

**ABSTRACT:** Remote sensing techniques can now be used routinely to identify and measure features of a rock mass that manifest in the surface topography and visual character. Remote sensing techniques allow users to acquire data from rock masses when physical access is not possible and can provide more accurate data than can be obtained using traditional measurement methods. Remote sensing techniques can be used to map large areas rapidly with high precision. This paper reviews aspects of methods for remote mapping of rock mass structure and describes computer analysis of the data acquired.
Computer analysis of remotely sensed spatial data can provide precise estimates of the position and orientation of features such as discontinuities. Three-dimensional imaging systems have been developed specifically for mapping mine rock faces (walls) and are now being used to acquire accurate 3D data defining surface structure at a number of sites. The paper discusses some of the advantages and limitations of the sensing and analysis techniques that enable accurate mapping to be performed rapidly and enable mapping of inaccessible sections of a rock mass.

## INTRODUCTION

The prediction and control of the behaviour of rock masses are critical tasks in mining and construction engineering. Controlling and predicting rock mass behaviour is based on the determination of rock mass structure. Mapping of the surface structure of a rock mass is an essential input to these tasks and provides mining and civil engineering projects with critical design information. This information includes descriptions of the observed rock mass structure as well as physical properties of the rock mass and enables inferences about the structure of the rock mass in areas not accessible to surface or subsurface mapping.

Mapping of rock mass structure is a complex task subject to a range of measurement errors, human errors and is subject to sampling bias. It is conventionally undertaken using established techniques that have been developed to provide consistent results under a wide range of conditions. Mapping techniques have been 'designed to take advantage of the many benefits of on site personal sampling' [1]. However, in many operations safety considerations may limit the scope of mapping and such limitations will increase as bench heights in mines increase.

The value of the data acquired from mapping a rock mass and any information produced from the data depends on the quality of the data and how amenable the data are to subsequent analysis. In particular the quality of these data depends on:

- the accuracy of the measurements and
- the sampling processes associated with the measurements.

Improving the quality and consistency of the measurement of discontinuities in a rock mass requires both improved accuracy of measurement and improved sampling. The outcomes from the use of the data can be improved by better data management and improved data accessibility. To improve safety requires a means of determining the surface topography and physical characteristics of a rock mass from a distance.

A number of methods can be used to achieve these improvements, one very effective method being the use of three-dimensional (3D) imaging. A 3D image is a composite data set obtained by fusing 3D

spatial data (a 3D surface map) and spectral data accurately registered to the spatial data to create a spatially accurate 'model' of a physical entity. The spectral data is usually a video image however 3D imaging with high resolution spectral data from other wavelength regions has been demonstrated. Three-dimensional imaging is more than a three-dimensional analogue of photography or electronic imaging. Three-dimensional imaging inherently implies the measurement of the position in space of a physical entity and the acquisition of data representing the visual or spectral characteristics of the entity such that the visual (spectral) data is accurately registered in space.

## BACKGROUND

### *3D Imaging*

Three-dimensional imaging has been developed over a considerable period and a number of imaging (measurement) technologies are now available. These techniques can provide 'dense' accurate spatial data defining the position of features in 3D space and are ideally suited to the remote mapping of the surface topography of a rock mass. Photogrammetry is perhaps the oldest technology that can be used for 3D imaging. More recently 3D imaging based on the use of laser ranging has been developed.

These methods produce a digital representation of the surface of the rock mass and a computer can be used to extract measurements characterising the discontinuities visible at the surface of the rock mass. The analysis of surface structure can be performed manually, or automated but both methods require accurate 3D data.

For mining applications, 3D imaging systems must be able to determine the 3D surface structure over a large volume with good accuracy. Here 'large' implies a measurement volume of the order of 50 $m^3$ and may mean a volume of up to 5,000,000 $m^3$. For mapping typical discontinuities in a rock mass, the required measurement volume will be of the of the order of 50 $m^3$ to 50,000 $m^3$.

In this context, accuracy refers to a combination of the 'density' of measurement points and the precision with which the location of each point is determined. The role of the density of data points may be described by a simple example; a sphere may be described parametrically or by specifying the position of a finite number of points on the surface of the sphere. In the latter case, the 'density' of measurement points determines the accuracy of the description when the density is low. For example, as few as four points may be used to produce a topologically 'correct' model but the 'sphere' will then be unrecognisable since it will look like a tetrahedron. As more points are added the 'sphere' becomes easily recognisable as illustrated in Figure 1.

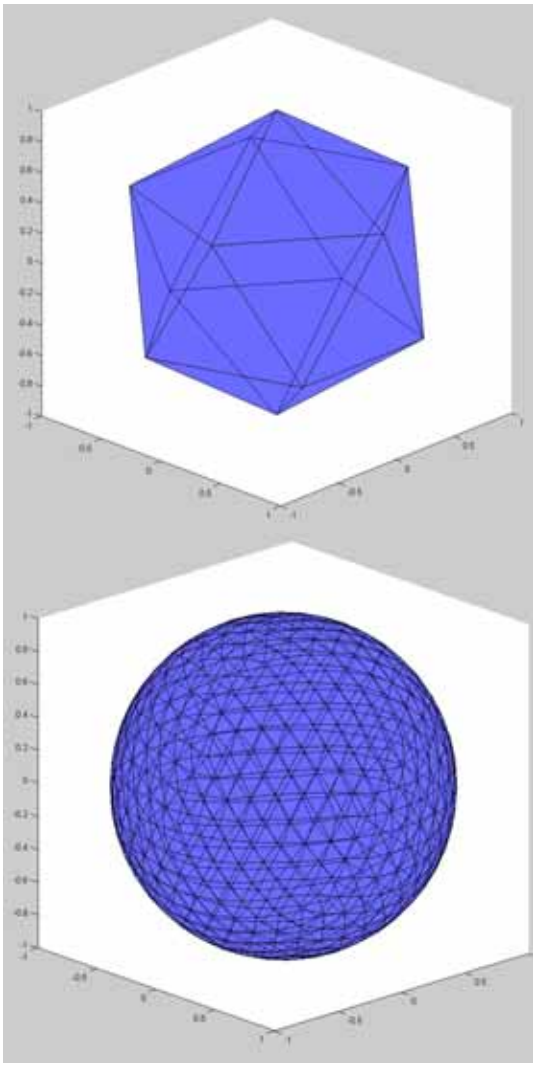

Figure 1: Representation of a sphere using a finite set of triangulated points

Measurement of the characteristics of complex structures is similarly dependent on dense, accurate 3D mapping. Surveying produces 3D data, however traditional survey systems produce this data at relatively widely separated points. Three-dimensional imaging systems acquire much greater volumes of spatial data in less time than conventional survey techniques and produce a 'dense' 3D map or image. Spatial measurement technologies have reached a stage of development where routine application to mining operations is

now feasible. Excluding holography, the major methods of obtaining 3D data are:

- triangulation (either passive or active);
- measurement of distance either by direct measurement e.g. radar, laser ranging systems, or indirect measurement e.g. depth by defocus using imaging systems or
- Moire techniques.

Moire techniques are not generally used for measuring objects with discontinuities and will not be considered further here. Triangulation has been used for many years in passive 'photogrammetric' systems such as 'conventional', ie stereo image based, photogrammetric systems and in active photogrammetry where techniques such as structured lighting using lasers or alternative energy sources provide 3D data.

Two approaches to 3D mapping that are currently used in mining are passive photogrammetry and laser based distance measurement. To obtain spatial information quickly and cheaply, major developments in these technologies have been required. The technical advances required in these technologies have been in:

Photogrammetry

- high resolution (> 10,000,000 'true' pixels) CCD cameras;
- high capacity, reliable portable data storage, and
- processing power.

Laser Mapping

- high repetition rate, short pulse, high power, eye safe lasers;
- accurate, high precision timing systems, and
- robust beam scanning systems.

These requirements have been largely met in the last few years. To support the acquisition of spatial data and ensure that the data can be utilised effectively the data must be integrated into a known spatial reference system. Modern computer systems and software now readily support these tasks.

A good, general review of active 3D mapping systems is provided in a review article by P.J. Besl [2]. This review describes many of the then available measurement approaches and provides a figure of merit for the comparison of 3D mapping systems. The figure of merit is defined as

$$M = \frac{1}{\sqrt{T}} \cdot \left( \frac{L_x L_y L_z}{\sigma_x \sigma_y \sigma_z} \right)^{\frac{1}{3}} \qquad (1)$$

where $L_x L_y L_z$ is the working volume of the sensor, $\sigma_x$, $\sigma_y$, $\sigma_z$ are the root mean square measurement errors in the x, y and z directions and T is the time taken to acquire a single spatial measurement. When used in mining applications, laser based survey systems will have (or should have) a figure of merit of the order of $10^6$ to $10^8$ in the field. This figure of merit will be reduced by the overheads of data handling. The time taken to process film and extract the measurement data effectively precludes the use of this figure of merit for conventional film based photogrammetry. However automated digital photogrammetry may produce 3D data with a figure of merit of the order of $10^4$ to $10^6$.

The figure of merit is dominated by rate of data acquisition, for example the laser repetition rate. The figure of merit does not reflect the impact of any 'measures' of safety, for example the possible requirement for eye safe operation over large measurement ranges and other operational considerations. The requirements of low cost and eye safe operation prevented the development 3D imaging systems using laser ranging for mining applications in the past.

The figure of merit above ignores the impost of equipment set-up, data preparation times and, as in the case of photogrammetry, additional data processing time that may be required. These factors reduce the performance differential between laser ranging and photogrammetric systems. For typical mining applications the figures of merit for laser ranging systems and photogrammetric systems may be reduced significantly.

The figure of merit does not provide any means of incorporating the capital cost of the sensor or operating costs. Depending on the implementation and patterns of use, automated digital photogrammetry may be cheaper than laser based 3D imaging. The differential in costs between the two technologies is determined by the capital cost of acquisition and by the costs associated with processing images to produce 3D data.

A figure of merit with more applicability to the mapping of rock mass structure would include total

data acquisition time accommodating set up times etc as well as visual 'resolution'. A brief comparison of passive photogrammetric 3D imaging and 3D imaging using laser based direct range measurement is presented.

*Photogrammetric 3D Imaging*

Two-dimensional imaging is a well known process. In addition to being one of the primary senses possessed by most animals, it is used in many facets of daily life and business operations. By undertaking a set of well known but complex computations three-dimensional information can be extracted from two-dimensional images. The basic principle of stereo photogrammetry is illustrated in Figure 2.

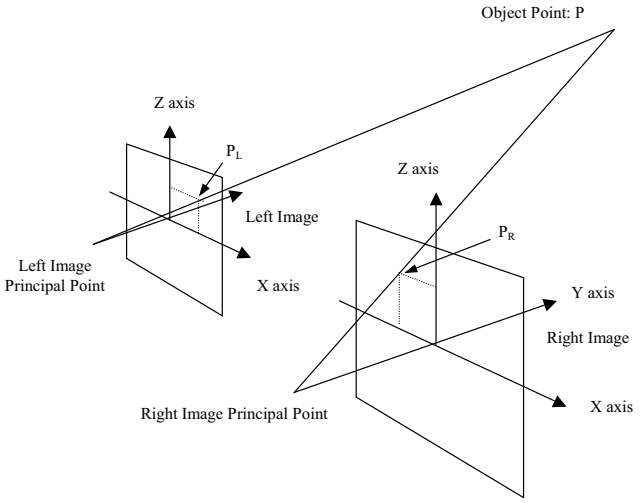


Figure 2: Geometry for the determination of the position of a point in object space using photogrammetry

Using image data from the area of overlap of two images, the equations describing the process of image formation can be used to estimate the spatial location of a point in the image(s) relative to the camera(s).

The application of photogrammetry to terrestrial operations had been limited by the difficulty in automating the computations required to extract 3D data, the computation time required and problems inherent with the use of film based cameras. Traditional, film based systems were limited by the time taken to process the film and extract image data as well as by the characteristics of the film used (shrinkage etc). These limitations have been largely eliminated as a result of the development of new technologies that have produced digital electronic cameras and much greater computational capability.

The results obtained from photogrammetry are dependent on the quality of the image data. Poor image quality will limit measurement accuracy. The diffraction of light in the optical system sets the fundamental limit on performance in terms of image resolution that is a major factor in image quality. In practice, factors such as the quality of the image sensor (either photographic film system or photodiode array in a CCD camera) and environmental factors (eg heat shimmer) will determine the measurement accuracy. The range resolution achievable when using stereo photogrammetry is also limited by the measurement baseline.

'Digital' imaging systems are spatially sampled electronic imaging systems and provide a sampled, quantised representation of the analogue video signal produced by the imaging sensor that is usually a CCD or CMOS image sensor. For a given field of view, the range measurement accuracy is determined by the number of pixels across the field of view, the baseline and the range at which the measurement is taken and the 'quality' of the image registration achieved in aligning the images.

Typically, well-calibrated photogrammetric systems may achieve range measurement accuracy of the order of 1 part in 10,000 to 1 part in 100,000 or more. Robust, accurate image matching algorithms and appropriate calibration enable modern CCD cameras to achieve precision of from one to ten centimetres at distances of the order of 100 metres with moderate focal length lenses. The accuracy of such systems scales with the focal length or pixel size and varies non-linearly with other parameters such as the camera baseline.

*Laser 3D Imaging*

Spatial data can be acquired using laser based distance measurement techniques. These techniques have found application in many mining operations. Many previous systems did not have the attributes of speed of data acquisition (and therefore spatial coverage), measurement precision, spatial resolution and eye safety required for mapping discontinuities. However, the technology required for accurate 3D imaging systems using lasers is now available and a number of systems are now sold commercially.

Spatial data for 3D imaging is acquired by determining the range and bearing of a selected point as viewed from a defined reference point. This

operation is suited to active systems such as laser distance measuring systems since these systems provide the components of the measurement (distance and angle) directly. The principle of 3D imaging using laser based range measurement is illustrated in Figure 3.

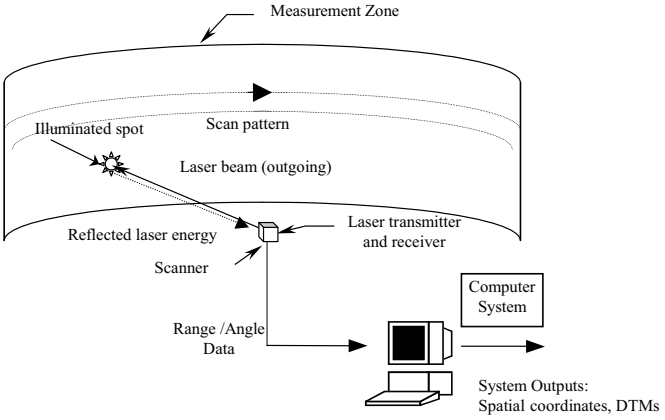


Figure 3: General principle of a 3D imaging system using laser ranging

Active spatial data acquisition based on distance measurement using lasers offers substantial improvements over conventional techniques such as surveying and passive photogrammetry in many applications. In particular, these advantages are:

- broad area coverage;
- centimetre precision independent of range or field of view;
- speed of data acquisition;
- ease of data acquisition and
- relatively 'simple' data processing for some low level tasks.

The ability to acquire spatial data directly substantially reduces the complexity of a 3D imaging system. Direct acquisition of spatial data eliminates the requirement for complex arrangements of multiple sensors and can reduce the amount of computation required to provide spatial data in comparison to photogrammetric systems. However, accurate 3D imaging does require precise positioning and orientation of laser systems and the overheads associated with setting up a laser imaging system in the field must be taken into account.

Laser distance measurement systems used for high-speed measurement as required in 3D imaging can achieve a precision of 5 centimetres (neglecting path effects) over ranges up to a kilometre. Some systems may achieve this accuracy over even longer ranges. Using laser distance measurement it is therefore possible to map structures of the scale of a mine site in 3D with this order of precision over a significant extent of typical mines.

Prior to the development of eye safe high repetition rate lasers range measurement using lasers was only possible at low repetition rates that effectively limited the use of these techniques to single point measurement. Development of new lasers and positioning systems has increased the speed and reduced the cost of data acquisition substantially.

## MEASUREMENT OF DISCONTINUITIES USING 3D IMAGES

Once 3D images have been acquired, software tools can be used to analyse the structure of a rock mass. The CSIRO Division of Exploration and Mining has developed a software package, named Sirovision, that provides an integrated processing environment. This system provides users with the ability to generate and analyse 3D images of the surface of a rock mass (maps of the surface topography of a rock mass). This allows a user to determine the dip, orientation and spacing etc of surface features such as discontinuities. It provides facilities for visualisation and analysis of rock slopes in a real world coordinate system.

To obtain these measurements users interactively analyse the structure of a rock mass using real world data visualised as a 'virtual' model of the surface of the rock mass. The visualisation software provides facilities to measure the position, orientation, length, area and volume of exposed structural features of a rock mass. The 3D position of a point is accessed by placing the mouse cursor at the corresponding position on the 2D digital image or the 3D visualisation of the surface. The orientation of the surface of the rock at any point on the rock mass can be determined from the spatial data integrated with the image. Thus, the position in space, length and orientation of a feature such as a joint trace can be determined easily from the 3D image.

The determination of the orientation of an entire plane is a more complex process. The natural variations in the surfaces of exposed joints and the errors inherent in 3D spatial measurement mean that the determination of the orientation of a joint surface requires considerable care. The software

enables a user to determine the orientation of any (plane) surface feature on the rock mass defined by all the 3D spatial points bounded by a user selected polygon and provides a measure of the 'reliability' of the estimate based on information about the 3D spatial measurement.

The orientation of a surface is provided in the form of dip and dip direction. The orientation of dominant discontinuities can be identified using the stereonet facilities provided by the program. Discontinuities, including bedding planes, joint traces, faults and shears, can be easily highlighted or designated using a mouse. Measurements of orientation can be classified using the facilities provided in the program.

## APPLICATION

To demonstrate the use of 3D imaging to map the surface structure of a rock mass and compare the results to those obtained using conventional techniques a target site was chosen and sections of the site were mapped using both methods. The 3D data presented here was acquired using the photogrammetric 3D imaging system Sirovision and analysed using the same software.

*The Data Acquisition Process*

The data acquisition system in Sirovision is essentially a software toolkit that enables users to generate 3D images from stereo pairs of 2D images (photographs). The 2D images used in this demonstration were acquired using a digital electronic camera. The camera used was a Nikon D1 and standard Nikkor lenses were used. The lenses were previously calibrated to determine their distortion characteristics and the images acquired were corrected to remove the distortion due to the lens.

An example of the 2D images from which the 3D images were created is shown in Figure 4. It should be noted that the Nikon D1 is a superseded model and provides resolution of only 2.7 million pixels whereas newer cameras provide resolution of more than 12 million pixels. Therefore, while the software can be used with much larger images, the resolution and precision of the data presented here is not representative of the current capability of the technology and is used for the purposes of demonstration only.

Figure 4: Full 2D image of the test site

Selection of the areas for mapping, matching image features in the images and creation of the 3D images was performed using standard facilities provided in Sirovision.

*The Analysis Process*

Once the 3D images were generated the parameters of selected joint faces and joint traces were determined using the computer based analysis system provided by Sirovision. The software has been developed specifically for this application and the user interface provides the tools required to quickly designate features in any compatible 3D image.

*Example*

The 3D Image

While Figure 4 shows a 2D image of the test site. Figure 5 and Figure 6 show the visual and spatial components respectively of a 3D image of a portion of the test site. Figure 7 and Figure 8illustrate the detail available in the 3D image, both in the visual data and the spatial data. The system is now used routinely to build 3D images with 500,000 to 1,000,000 3D spatial data points and 5 million to 10 million visual pixels using up-to-date digital cameras. Using a typical personal computer the core calculations performed will produce data points at more than 2,000 points per second. Allowing for data handling overheads and the time taken to set up a task the time to create a typical 3D image is generally less than ten minutes.

Figure 5: Visual component of the 3D image

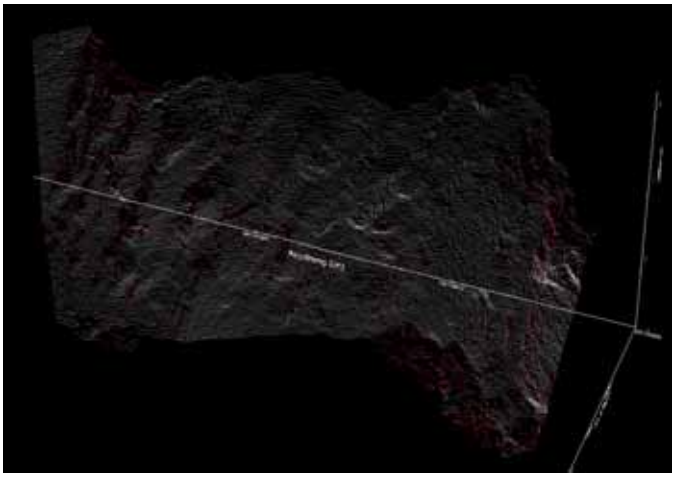

Figure 6: Spatial data component of the 3D image.

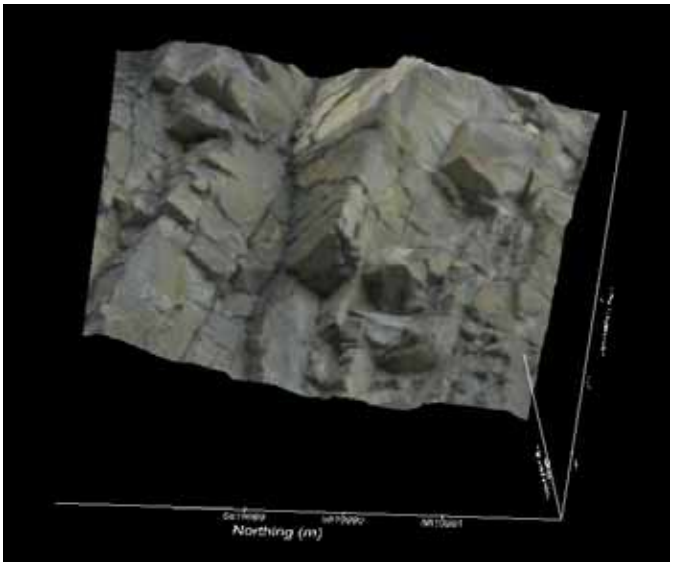


Figure 7: Detail of a section of the 3D image of the test site

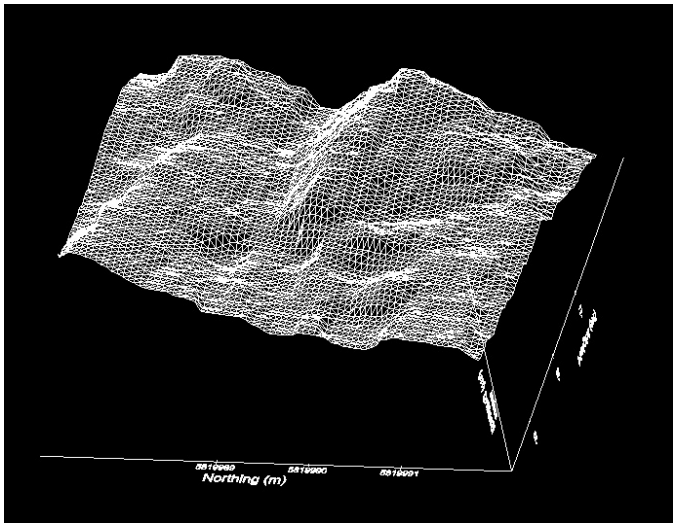


Figure 8: Detail of the spatial data of a section of the 3D image of the test site represented as a wire frame model

## Measurements Using The 3D Image

The orientations of four discontinuity planes in the 3D image have been measured as an example of the techniques used in analysing the data. Figure 9 and Figure 10 show 2D and 3D Images of the discontinuity planes chosen for measurement. It can be readily seen from the 3D image that, while the orientations of the planes are similar, the dip angles vary significantly. The two planes in the middle of the image show an 8-degree difference in dip and a 5-degree difference in dip direction. What is not obvious from the 2D image is that the plane on the left hand side tips towards the viewer. This is clearly seen in the 3D image in Figure 10. Figure 11 shows the orientations of the normals to the planes; the normals have been used for clarity in the visual presentation.

Figure 9: 2D image of the measured discontinuity planes

Figure 10: 3D image of the measured discontinuity planes

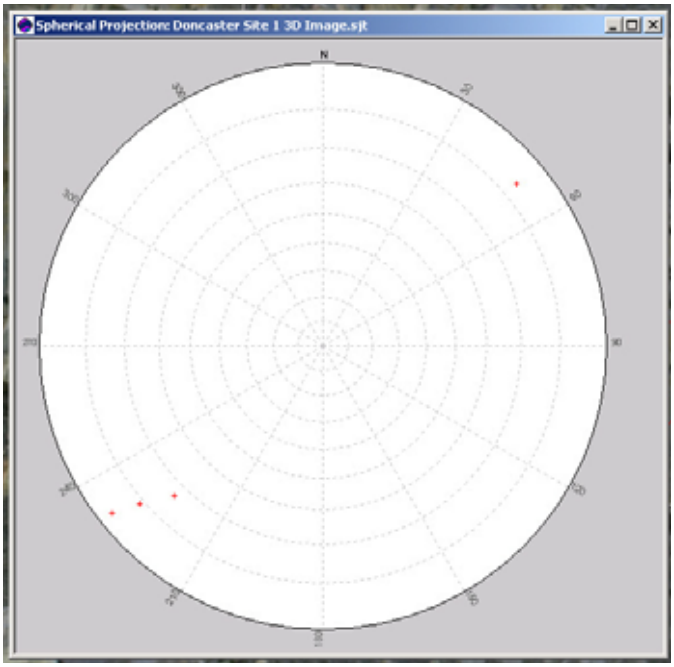


Figure 11: Orientations of the measured discontinuity planes plotted in Sirojoint®

## Measurement Effort

Depending on the size of the image, a typical 3D image requires between 5 and 10 minutes of processing time to build. The time required in the field varies from 15 to 30 minutes for each 3D image depending on the geometry of the area being mapped.

Each measurement of orientation takes approximately 15 seconds to acquire. The system has been used to map over 1,000 discontinuity planes at one site and has been used to map orientations at ranges from 20 metres to over 500 metres.

## Additional Results

Typical results of measurement of the orientation of joint surfaces, in this case obtained in independent use of the system by De Beers Consolidated Mines [3] are shown in Table 1.

Table 1: Comparison between compass and Sirovision® measurements of joint orientations

| Joint Number | Compass Measurement | | Sirovision® Measurement | |
|---|---|---|---|---|
| | Dip | Dip Direction | Dip | Dip Direction |
| J0 | 43 | 333 | 45 | 330 |
| J1 | 90 | 060 | 89 | 240 |
| J2 | 26 | 151 | 33 | 143 |
| J3 | 88 | 131 | 89 | 119 |
| J4 | 46 | 345 | 51 | 336 |

Similar results have been obtained by users world wide over more than 5 years of use of the system, for example as reported in [4] to be presented at this conference. The accuracy of the orientation measurements has been consistently and independently verified in use.

*Measurement Accuracy And Precision*

What Is Meant By Accuracy, Precision And Resolution?

Accuracy is a quantitative estimate of the difference between a measurement of a parameter and the true value of the parameter. Since the 'true' value of a parameter is rarely known precisely, accuracy is only known to the resolution of the 'instrument' used to determine the 'true' value. Some manufacturers 'confuse' accuracy and precision so care is required in interpreting 'accuracy'.

Resolution is the minimum differential measurement that can be made irrespective of accuracy or precision and is the smallest difference between two adjacent measurement values or points that a sensor can determine.

Precision is a measure of the random variation of the measurement of a parameter often expressed as the root mean square deviation about a mean value, usually assumed to be the true value. Repeatability is often used with precision or in the same context. For example, a measurement that can be made with a resolution of 5 centimetres will have a precision of approximately 1.5 centimetres if the uncertainty introduced by the finite resolution is the only source of error.

What Measurement Accuracy Can Be Achieved Using A 3D Image?

The measurement accuracy depends on the type of measurement and depends on whether the measurement is a positional measurement or a measurement of orientation. For the measurement of the orientation and position of structure in a rock mass accuracy of between one part in 5,000 and one part in 10,000 is adequate.

When determining the location of a single point the measurement accuracy has a number of components. These are:

- the accuracy of the measurement of distance from the camera;
- the accuracy of measurement of the azimuth of the projection of the line of sight from the camera on the local horizontal and
- the elevation of the line of sight from the camera.

The local horizontal is effectively the tangent to the earth surface at that point since the horizontal is usually defined by the plane perpendicular to the direction that gravity acts. These are effectively the same accuracy components that arise when considering the use of a laser ranging system except for the influence of the distortion created by the lens when acquiring an image. This distortion is corrected in Sirovision and would otherwise be a major source of error.

When using photogrammetry the measurement of range (distance of a point from the camera) is a function of the baseline between the cameras, the pixel spacings of the sensor array and the focal length. The accuracy of the measurement of the azimuth and elevation is dominated, in part, by the effectiveness of correction of lens distortion and elimination of tilt. It is also determined by the accuracy of the measurements of positions of the camera and the control point used. Human error in selecting the control point in the image will also apply but is not quantifiable.

Typically, when using a Nikon D200 with a 50 mm focal length lens the resolution of the range measurement at 150 metres is 15 cm for a displacement within the 2D image of 1 pixel if the baseline is 25 metres. The corresponding precision of the range measurement is approximately 7 cm.

Many photogrammetric systems use interpolation to improve the accuracy and precision of spatial measurement. In some cases interpolation to $1/100^{th}$ of a pixel is used however this level of interpolation is nonsensical for typical off-the-shelf colour cameras. Using realistic levels of interpolation will enable range measurement resolution of 1 to 2 centimetres to be achieved with corresponding range measurement precision of around 7 millimetres.

The range measurement accuracy will be affected by the precision of the baseline measurement. When using a typical RTK GPS surveying system (properly) the range precision due to baseline error will typically be 1 cm giving a total range

measurement precision of approximately 10 to 15 millimetres.

When used with a 50 mm focal length lens the Nikon D200 will give a base precision in orientation measurement of 0.12 milliradians with a corresponding displacement of the position perpendicular to the line of sight of about 8 millimetres.

These measurements combine in a non-linear way to give the final measurement accuracy but, as a rule of thumb, for an initial estimate, they can be assumed to add in quadrature with a measurement precision of 15 to 20 millimetres at 150 metres.

When making 'compound' measurements such as the orientation of a plane the answer to this question is more complicated. Standard mathematical analyses of the accuracy of linear regression cannot be applied because of the errors inherent in all three spatial variables. However techniques based on probabilistic analysis can be applied and these show that when measuring the orientation of a flat 1 metre square plane using this camera at 150 metres the orientation measurement accuracy will be typically 0.1 degree.

Why Are The Accuracies Of Measurement Different For Points And Plane Orientation?

Point Measurements

The accuracy, resolution and precision of the measurement of a single point in space are determined by a number of factors as discussed. The measurement accuracy is dependent on the camera and the measurement geometry. Measurement accuracy that approaches one part in 10,000 for a Nikon D1X or Nikon D100 with a 35 mm lens at a range of between 90 metres and 100 metres has been demonstrated. The measurement accuracy and precision increase almost linearly with increasing focal length for a given measurement situation.

We have acquired some validated accuracy data for Sirovision using a Nikon D1X to produce 6,000,000 pixel images. Since it is difficult to validate measurements of slope of natural rock faces due to the inherent roughness of such surfaces we went looking for a reliable repeatable method

We measured 18 points on the face of a building that had some regular structure that suited our requirements. The face of the building was at a range of approximately 95 metres from the measurement site. The ranges actually spanned from approximately 92 metres to 96 metres over a horizontal extent of approximately 16 metres. The face of the building was not normal to the line of sight so there was deliberate perspective introduced. The control was a series of surveyed points. The surveying was done by a professionally trained surveyor using a standard theodolite.

The results are quite conclusive. When the system does the matching we achieve a standard deviation in the difference between the positions measured by the two methods of 2.5 centimetres. The standard deviation in the worst dimension (always the range for any triangulation measurement when the angular resolution is sensitive enough) was then compared for measurements obtained using both methods (this can only be done this way because of the natural spatial scatter of the data). The standard deviation for the theodolite based measurements was 1.5 centimetres and for the photogrammetry measurement it was 2 centimetres. The increase in the standard deviation for the difference data indicates the existence of a slight systematic bias or more correctly differences in systematic bias between the two measurement methods. Close examination of the data show a slightly worse systematic bias for the Sirovision data than for the theodolite based data.

The standard deviation of this data is actually slightly better than indicated since the range from the sensor varies over the height of the building and no correction has been applied for this.

Overall the Sirovision data shows scatter of about 0.5 centimetres more than the theodolite based measurements and is consistently within the predicted accuracy / precision. The accuracy / precision of the system is approaching 1 part in 10,000 for this set-up.

These results are consistent with other tests that have validated the theoretical models.

*Measurement Of The Orientation Of A Plane*

The determination of the orientation of a plane in space involves the use of a number of point measurements and errors in point measurements therefore accumulate unless an appropriate method of analysis is used. The prediction of measurement precision for planes assumes that a tool such as Sirojoint will be used and that the tool uses some

statistical processing to reduce the error in measuring orientation.

The simplest measurement of the orientation of a plane is achieved by determining the position of three points on the plane. If the plane has a given chord length and is perpendicular to the line of sight of the measurement system the average errors in orientation are, to a first approximation:

$$\tan^{-1}\left(\frac{2 \cdot range\_precision}{chord\_length}\right) \qquad (2)$$

For a chord length of one metre and a range precision of 2 cm this is 2.3 degrees.

When a number of measurement points are available a more accurate estimate is achieved by mathematically solving for the orientation using all the available points. The improvement in precision is difficult to estimate but is of the order of the square root of the number of points used. Therefore, if using Sirojoint with 25 points on the plane (this is less than the minimum recommended) the expected precision will be around 0.5 degrees.

*Orientation Accuracy*
Estimation or validation of the 'accuracy' of orientation measurement is fraught with difficulty.

The biggest problem in comparing measurements made by a geologist and measurements made using Sirovision is the fact that you will effectively be comparing apples with oranges. A geologist / geotechnical engineer makes a measurement (subject to human error) of their best guess of the orientation of the joint. Sirovision does a mathematical fit to all the data defining the joint in the 3D image.

## IMPLICATIONS

Remote sensing methods provide data that differs from that collected using 'conventional' area or scan line mapping as used in practice for mapping discontinuities. What does the development of these methods imply?

The use of remote sensing for mapping the surface structure of a rock mass raises a number of issues:

- How does data gathered from conventional line mapping or window mapping compare with data gathered by remote sensing techniques?
- Are any biases in the data evident?
- Do we get less scatter in our results? i.e. can families of joints be more precisely defined?
- What do we lose by mapping with these techniques and how do we compensate for that?

One potential 'loss' is knowledge of the surface texture of discontinuities; for example, is the surface rough or smooth etc. Where the surface of the rock mass can be imaged, these data can be easily integrated with the data acquired by a 3D imaging system.

Perhaps of more interest are the questions of:

- What more data can we acquire using remote sensing?
- What better applications can we develop using remotely sensed data?

In many cases the requirements of safety and the physical inaccessibility mean that, unless 3D imaging is used no data would be gathered. Therefore the use of 3D imaging, in conjunction with other techniques where possible or appropriate, will always deliver more, and arguably 'better', data than conventional mapping techniques.

## ISSUES IN APPLICATION

*Planning*
Planning a mapping task is always an essential prerequisite for successful field work. The measurement accuracy that can be achieved with a remote sensing system is not intuitive. Planning a mapping task that will use 3D imaging requires a fundamentally different approach to planning a manual mapping task. The Sirovision® software provides a comprehensive set of tools to predict measurement performance for a range of scenarios.

*Cost*
The cost of professional standard digital cameras has decreased dramatically and cameras with greater than 10 million pixel resolution are available for a few thousand dollars (US). More importantly the processing time required to create 3D images has decreased dramatically. This means that the cost of acquisition of 3D data has dropped considerably. To ensure that the cost of mapping remains commensurate with the cost of 3D data acquisition computer based methods of measurement have been developed. These will be soon augmented by automated measurement techniques.

*Additional Benefits*

Digital imaging brings with it the ability to share data quickly and effectively. The distribution of data in the form of physical images can be replaced by electronic distribution and visualisation of data allowing multiple users to access data quickly and easily. One application of Sirovision® that is currently being pursued is the electronic transfer of data to a central office where specialists can assist mine personnel at a number of different sites reducing the overheads of transporting valuable staff to widely separated sites.

The digital records created when the structure of a rock mass is mapped can be stored in a format that records all the mapping detail thus enabling staff to review the results of mapping even after a structure may have been removed by mining. This capability provides a 'long term memory' of structure and rock conditions thus supporting reverse engineering or back analysis when required.

Digital records of structure combined with 3D images of extended areas of mines can be communicated across systems such as the Internet quickly and cheaply. The development of interactive, web base visualisation technology such as the Virtual Mine developed by the C.S.I.R.O. (Australia) Division of Exploration & Mining.

## MEASURING ORIENTATION IS ONLY THE STARTING POINT

While remote sensing techniques can enable a user to measure the orientation of an exposed surface safely and accurately these methodologies do not provide a complete solution to the measurement of rock mass structure. In fact, application of remote sensing technologies without due consideration of the sampling bias that they introduce can lead to erroneous conclusions about the distribution of joint sets. Effective use of remote sensing technologies requires correction for the sampling bias that they introduce and current correction techniques are not applicable.

The role of statistical estimators in the determination of rock mass structure may be underestimated at the current stage of development of remote structural mapping technologies. Traditional mapping methodologies introduce a statistical bias that is well known and understood. The nature of the statistical bias introduced by remote mapping methodologies is not well understood and the tools required to correct for the sampling bias do not exist therefore interpretation of the results requires considerable care.

CSIRO Exploration and Mining and the Julius Kruttschnitt Mineral Research Centre (JKMRC) have commenced a program of research and development of the mathematical methods required to characterise and correct for the statistical bias introduced by remote sensing technologies when mapping rock mass structure.

## CONCLUSION

Remote sensing for the measurement of the position and orientation of discontinuity surfaces in rock masses is becoming a routine method of mapping rock mass structure. The technology allows geologist and geotechnical engineers to gather data over larger areas of faces. At best an unaided geologist can only map the bottom 2 metres of a steep face if safety considerations allow approach to the face. At worst access to faces in mine sites for mapping purposes is being increasingly prohibited for safety reasons. Remote sensing allows mapping of structure at distances in excess of three or four hundred metres.

The use of remote sensing allows personnel to exercise quality control over the data in the comfort of an office rather than under sometimes-extreme field conditions thus resulting in improved quality. Digital records of the data (2D and 3D images as well as mapping records) allow full traceability of the mapping process. Since a user can gather and analyse a large volume of data using 3D imaging it is easier to identify and discard suspect data and to gather statistically significant data.

The use of these technologies introduces a range of new applications however users must also be aware of the limitations of the technologies and the implications of issues such as the sampling bias introduced by the measurement technology.

## REFERENCES


1. S.D. Priest *Discontinuity Analysis For Rock Engineering* Chapman and Hall 1993
2. Besl P.J., Active Optical Range Imaging Sensors *Machine Vision and Applications*, 1988, Vol 1, 127-152
3. Grobler H.P., Guest A.R., Poropat G.V., Photogrammetry for Structural Mapping in Mining presented to SANIRE September 2003

4. Krosley, L. K. and Shaffner, P. T., Digital Ground-based Photogrammetry for Measuring Discontinuity Orientations in Steep Rock Exposures *Proceedings of the ARMA Golden Rock Conference*, Denver, Colorado June 17-19 2006.

# Summary Paper on the Morrison Field Exercise

Tonon, F.
*University of Texas, Austin, TX, USA*
Kottenstette, J.T.
*U.S. Bureau of Reclamation, Denver, CO, USA*

Copyright 2006, ARMA, American Rock Mechanics Association

This paper was prepared for presentation at the workshop: "Laser and Photogrammetric Methods for Rock Face Characterization" organized by F. Tonon and J. Kottenstette, held in Golden, Colorado, June 17-18, 2006.

This paper was selected for presentation by F. Tonon and J.T. Kottenstette following review of information contained in an abstract submitted earlier by the author(s). Contents of the paper, as presented, have not been reviewed by F. Tonon and J. Kottenstette, and are subject to correction by the author(s). The material, as presented, does not necessarily reflect any position of USRMS, ARMA, their officers, or members. Electronic reproduction, distribution, or storage of any part of this paper for commercial purposes without the written consent of ARMA is prohibited. Permission to reproduce in print is restricted to an abstract of not more than 300 words; illustrations may not be copied. The abstract must contain conspicuous acknowledgement of where and by whom the paper was presented.

**ABSTRACT:** This paper presents a comparison of rock mass data provided to the authors by 3G Measurement and AdamTech. Data were collected during the field exercise carried out on June 17th, 2006 at an outcrop near Morrison, CO. It is found that both systems lead to very similar results in terms of: digital terrain models (DTMs), fracture clustering and orientations, trace lengths, and roughness. Fracture spacing showed more variability because of the waviness of the fractures, which were not planar. The obtained results indicate that digital photogrammetry yields reliable and reproducible results when applied to rock mass characterization. Digital photogrammetry is a mature enough technology that can be used with confidence by the industry.

## INTRODUCTION

Only two out of four Presenters (AdamTech and 3G) provided us with the data obtained during the field exercise carried out at Morrison, CO, on June 17th, 2006. The following information is contained in the Presenters' papers:

- Type of camera/scanner, year it was manufactured.
- Lens, focal lengths, aperture, baseline/(distance to face).
- For all images taken: camera/scanner position and external orientation.
- For scanners: planimetric accuracy and depth accuracy at all available face distances, including distances used in the field exercise.
- For cameras: pixel size, planimetric accuracy, and depth accuracy for a single pair.
- Method and software used to merge images/scans, to obtain the DTM and the draped DTM.
- For the given constraints (3 at the bottom, and 2 at the top of the outcrop, or 3 scans): workflow and time used to acquire data.
- For the given constraints (3+2 pictures or 3 scans): workflow and time used to generate draped DTM including any calibration (camera or scanner).

## SITE GEOLOGY

The test site is located about 20 miles southwest of Denver, Colorado, in the Idaho Springs Formation, which is a blocky, Precambrian gneiss, about 1,700 million years old. The Idaho Springs Formation consists of sedimentary rocks that were subject to high grade metamorphism that obliterated the original structures and textures of the rock. High pressures and temperatures transformed the original sedimentary rocks to hornblende and granitic gneiss. These rocks were uplifted about 65 million years ago along the Golden Fault Zone, a high angle reverse fault zone, during the Laramide Orogeny which formed the Rocky Mountains. This faulting also steeply tilted the unconformably overlying Paleozoic sedimentary rocks to the east, resulting in the Dakota Hogback, Dinosaur Ridge, and other hogback landforms.

The gneiss is strongly jointed by several sets of joints. A manual structural investigation indicated that predominant joint sets include a high angle set that dips to the south and two moderately dipping

sets that dip northeast and northwest. The test site face is nearly bisected by a hornblende gneiss dike which was probably emplaced along an existing fracture. The dike is sheared along the southern contact as evidenced by a zone of soft, decomposed gneiss.

## COMPARISON OF FIELD EXERCISE RESULTS

*Surveyed points*

As shown in Figure 1, a total of 21 points on the outcrop surface (which measures about 50 m wide by 20 m high) were surveyed before the field exercise. The first comparison was aimed at checking whether these points were close to the Digital Terrain Models (DTMs) produced by the Presenters.

The Presenters provided comparisons on six targeted control points; all other control points were removed before the exercise. These points were used to provide the global coordinate system. The Federal Highway Administration (FHWA) established the survey control at this site. These State Plane Coordinates, CO Central Zone 502, were derived from an adjustment with Star*Net software. Coordinates for points #2001 and #2002 are GPS solutions using NOAA's OPUS software. #2001 was held in the Star*Net adjustment as it showed to be the best of the OPUS solutions. The basis of bearing used to locate the 4000-series points on the rock was from 2001 to 2002. Table 1 provides the standard deviations for the control point survey.

Of the set of 21 control points, only 12 were used to provide an independent test with the aim of determining how close the Presenters' DTM surfaces matched the surveyed values. These 12 points were not marked by targets during the photo sessions and as such could not be measured directly as they were not visible in the images. To test how close the surfaces came to these points, the surface point data needed to be imported into a common CAD system, and the data rotated such that the normal to a vertical plane containing points 4001 and 4006 became the new *z*-coordinate. The rotated survey values were draped to each rotated surface and the differences calculated. Table 2 shows this result.

Although these 12 points do not provide a comprehensive comparison, the surfaces contain several hundred thousand points. Because only two Presenters provided DTM surfaces, we could only determine how close these two surfaces are to each other. Had we received more data sets, it would have become clearer which data set provided the best solution. Indeed, our original intent was to compare several surfaces to these points, then select the closest on, and finally compare the rest of the surfaces to this one. An important difference between these surfaces is the density that was used to produce them: AdamTech used three times as many points as 3G. The denser the surface the closer it will match the actual ground. The level of density that is provided in the data set should be a function of the measurements required. The choice of data point density was left to the Presenters.

*DTM comparison*

The "isopac method" was used to compare these surfaces. An isopac is a surface that is created by subtracting the *z*-coordinate values for the same *x*- and *y*-coordinate values on two surfaces. This can only be done if the surfaces are created in the same software package. Surfaces that have overhangs in the *z*-direction are not suitable for this method. Since the surfaces at the site presented overhangs, we defined an axis of rotation that would minimize the overhangs. The 3-D point data were imported into the CAD software Microstation, and rotated to reduce overhangs. The point data needed to be trimmed to a common area. Figure 2 shows these data before and after they were trimmed. These points were surfaced with a triangular mesh maintaining the original points. These surfaces were rendered as a visual check. New high-density grids were created. These new points were surfaced and rendered as a visual check. Figures 3 and 4 show these rendered surfaces. Figure 5 is an isopac map of the re-grided surfaces. The color key provides the difference in the *z*-coordinate (Delta-Z) values for each color on the map.

The isopac map in Figure 5 indicates that, for over 90% of the points, the *z*-coordinate values differed less than 3 cm (0.1 ft). This result is in line with AdamTech differences in Table 1, and is much better than the 3G results in Table 1. It indicates that, on a large population of data points, both the AdamTech and the 3G programs provided high quality results and that the larger deviations in Table 1 are caused either by vegetation or bad camera angle.

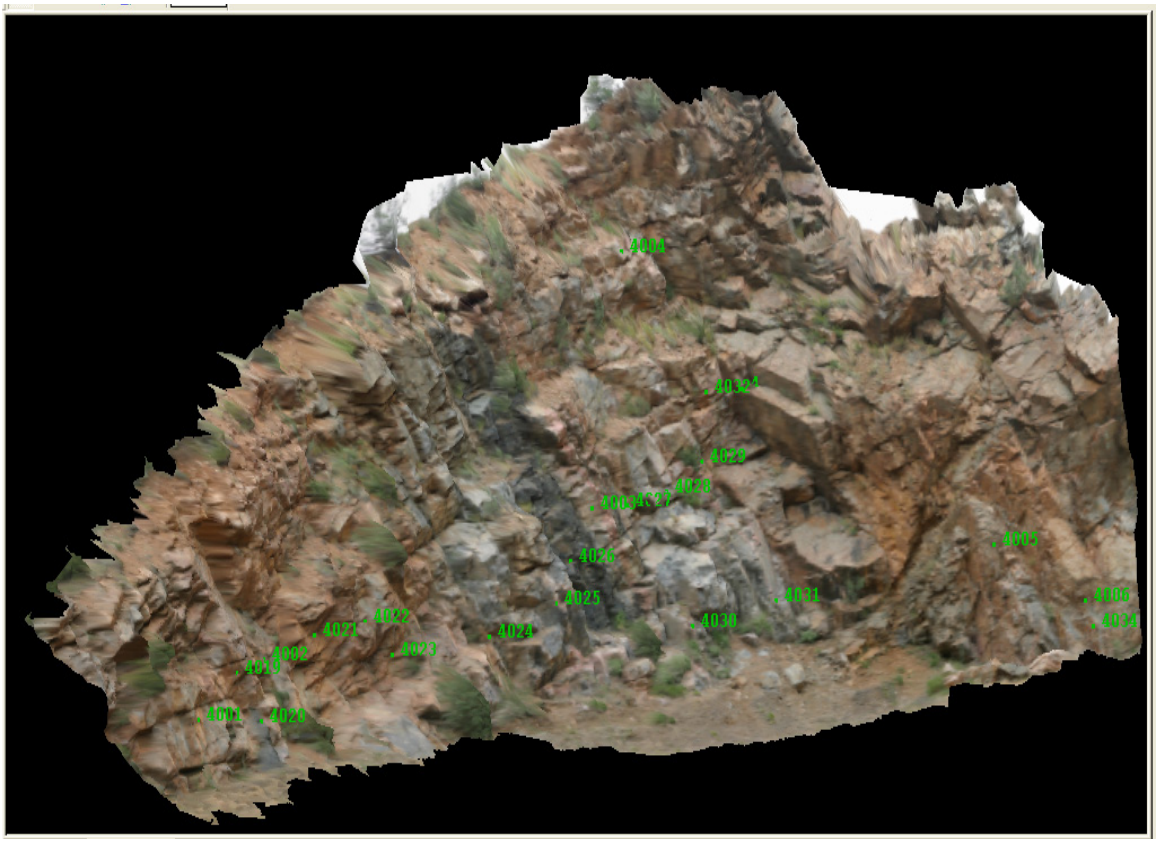


**Figure 1.** Control Points on Rock Face (this picture was generated by J.T. Kottenstette using 3DM Analyst).

**Table 1.** Standard deviation of the control point coordinates.

| Station | N-cm-(Y) | N-cm-(X) | N-cm-(Z) |
|---|---|---|---|
| 2001 | 0 | 0 | 0 |
| 2002 | 0.051298 | 0.03764 | 0.048707 |
| 4001 | 0.162336 | 0.18578 | 0.131064 |
| 4002 | 0.165842 | 0.18538 | 0.132283 |
| 4003 | 0.174224 | 0.18209 | 0.134569 |
| 4004 | 0.183215 | 0.18568 | 0.141488 |
| 4005 | 0.171602 | 0.17011 | 0.129662 |
| 4006 | 0.173431 | 0.16868 | 0.129479 |
| 4019 | 0.23052 | 0.26118 | 0.184252 |
| 4020 | 0.229667 | 0.26048 | 0.183733 |
| 4021 | 0.235001 | 0.2603 | 0.185715 |
| 4022 | 0.235793 | 0.2592 | 0.185806 |
| 4023 | 0.237195 | 0.25908 | 0.185989 |
| 4024 | 0.237774 | 0.25649 | 0.185562 |
| 4025 | 0.23814 | 0.25448 | 0.185288 |
| 4026 | 0.243108 | 0.25631 | 0.187513 |
| 4027 | 0.247101 | 0.25658 | 0.18922 |
| 4028 | 0.24829 | 0.25612 | 0.189494 |
| 4029 | 0.251795 | 0.25722 | 0.19111 |
| 4030 | 0.318912 | 0.37917 | 0.259994 |
| 4031 | 0.245913 | 0.25164 | 0.186416 |
| 4032 | 0.252618 | 0.25737 | 0.192512 |
| 4033 | 0.253441 | 0.25704 | 0.192573 |

**Table 2.** Delta-Z values for the 12 draped control points (these targets were removed before the Morrison exercise).

| Point ID | Delta-Z (cm) ADAM Tech | Delta-Z (cm) 3G Measurement |
|---|---|---|
| 4019 | 0.57 | 2.36 |
| 4020 | 6.00 | 29.10 |
| 4021 | 3.04 | 2.90 |
| 4022 | 3.32 | 3.13 |
| 4023 | 5.08 | 8.03 |
| 4024 | 2.18 | 21.02 |
| 4025 | 2.74 | 3.24 |
| 4026 | 3.17 | 1.49 |
| 4030 | 0.87 | 3.09 |
| 4031 | 0.80 | 8.26 |
| 4032 | 5.29 | 11.41 |
| 4033 | 0.01 | 4.12 |
| | | |
| Average | 2.76 | 8.18 |
| MAX | 6.00 | 29.10 |
| MIN | 0.01 | 1.49 |
| Standard Deviation | 1.98 | 8.59 |

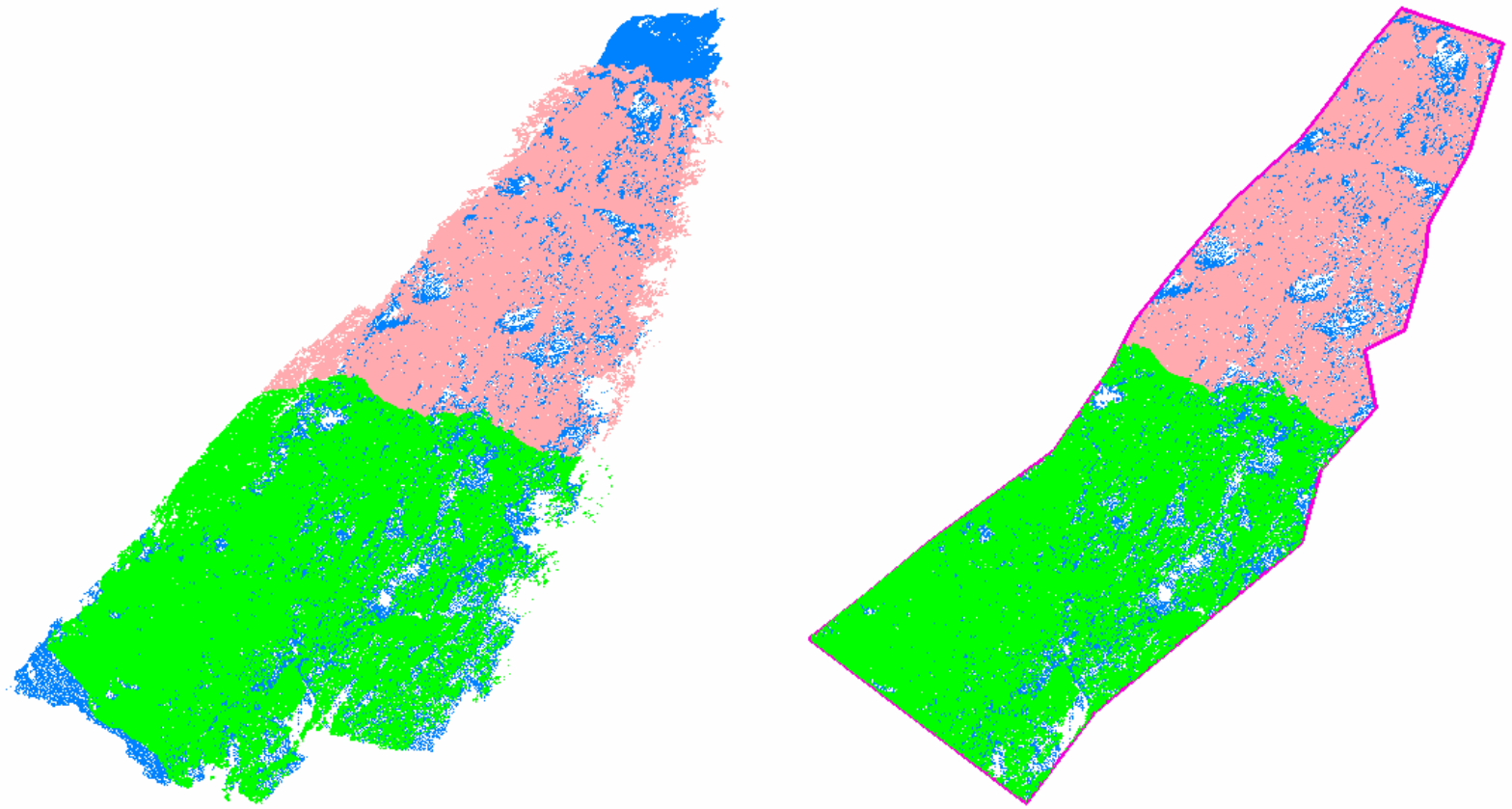

**(a)** **(b)**

**Figure 2**. – Rotated point cloud data: (a) not trimmed; (b) trimmed. Blue are 3G data points, and green and pink are AdamTech data points.
.

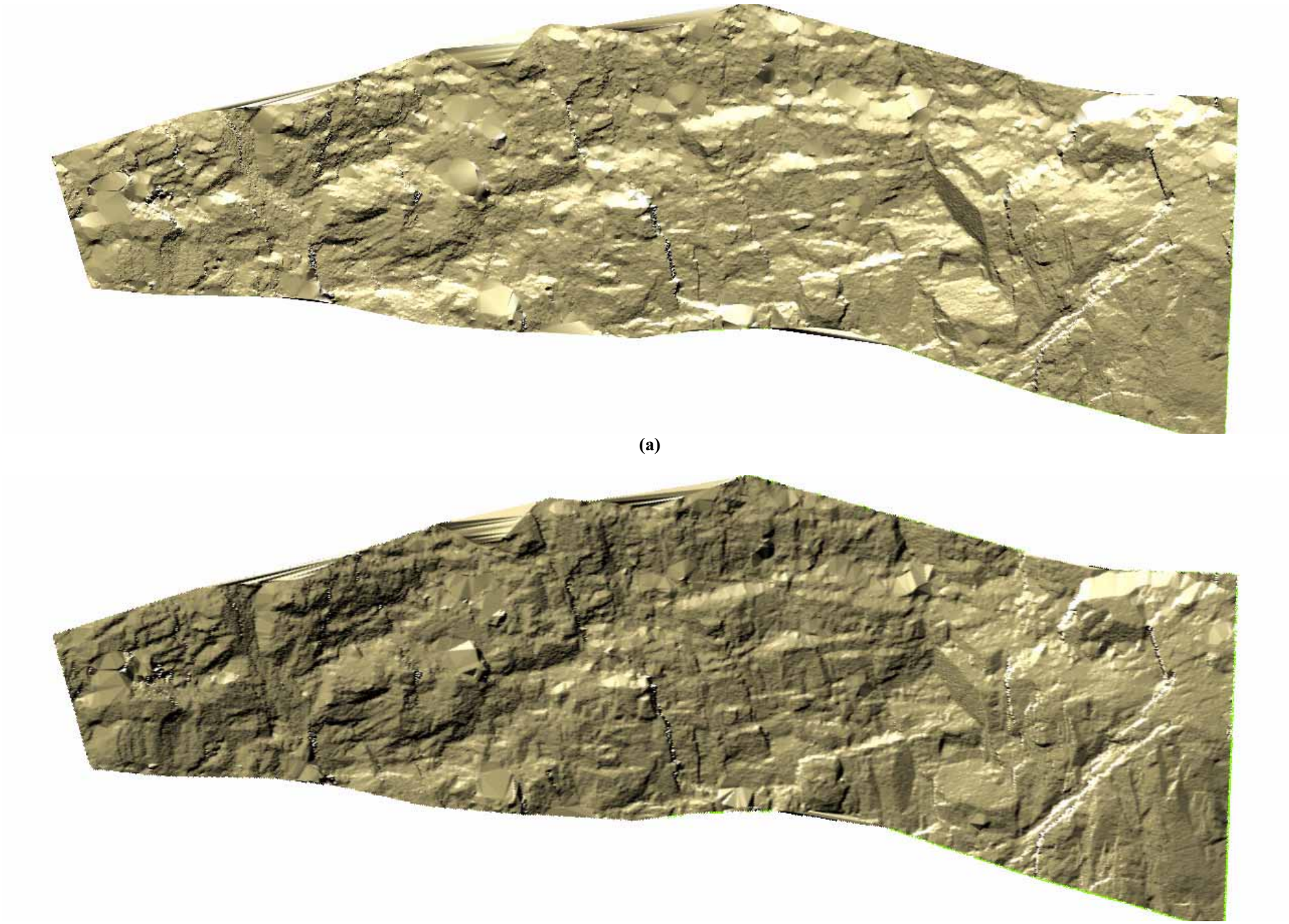

**(a)**

**(b)**

**Figure 3.** AdamTech points: (a) rotated, trimmed and rendered points; (b) re-gridded and rendered points.

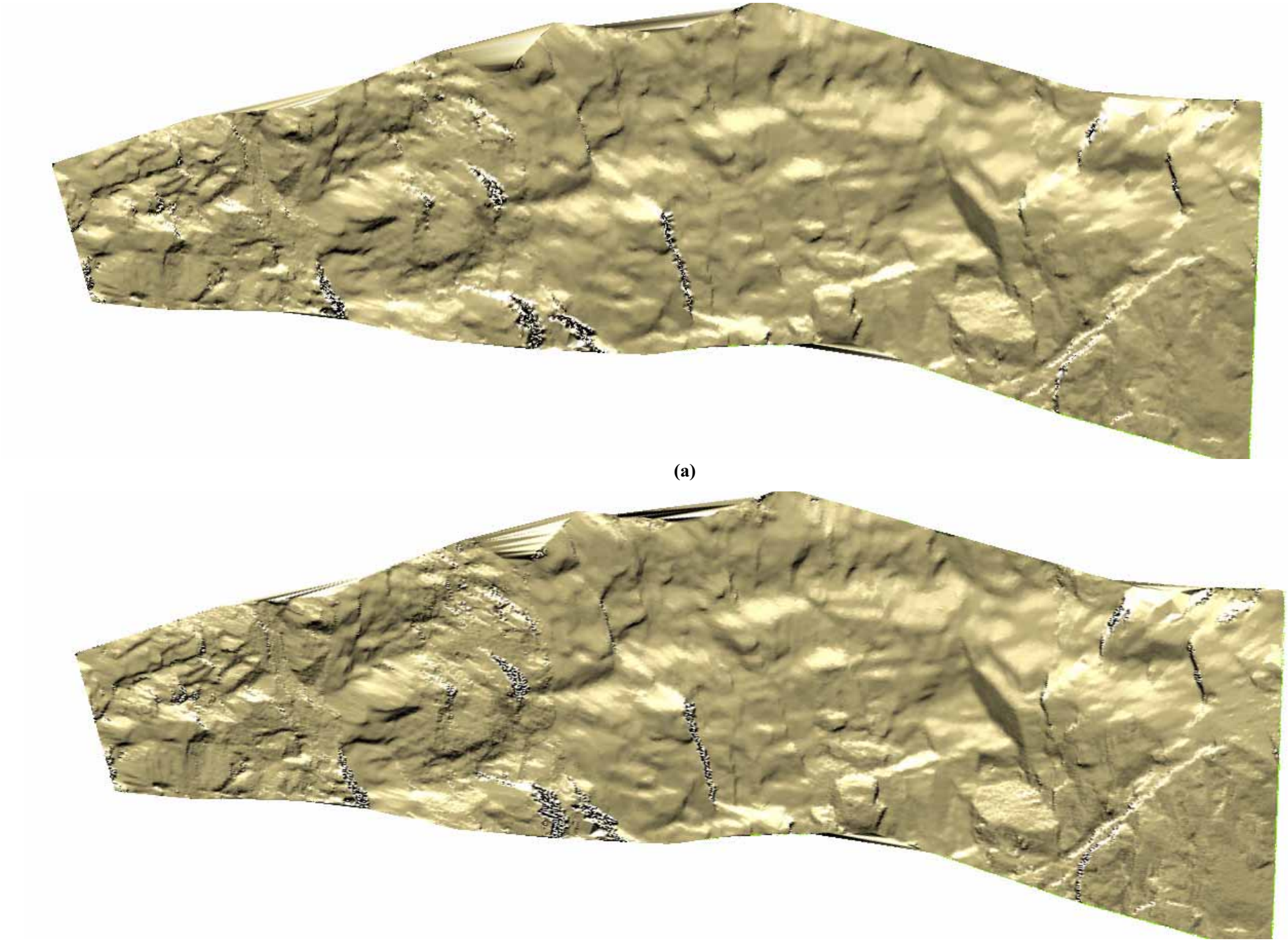

**(a)**

**(b)**

**Figure 4.** 3G points: (a) rotated, trimmed and rendered points; (b) re-gridded and rendered points.

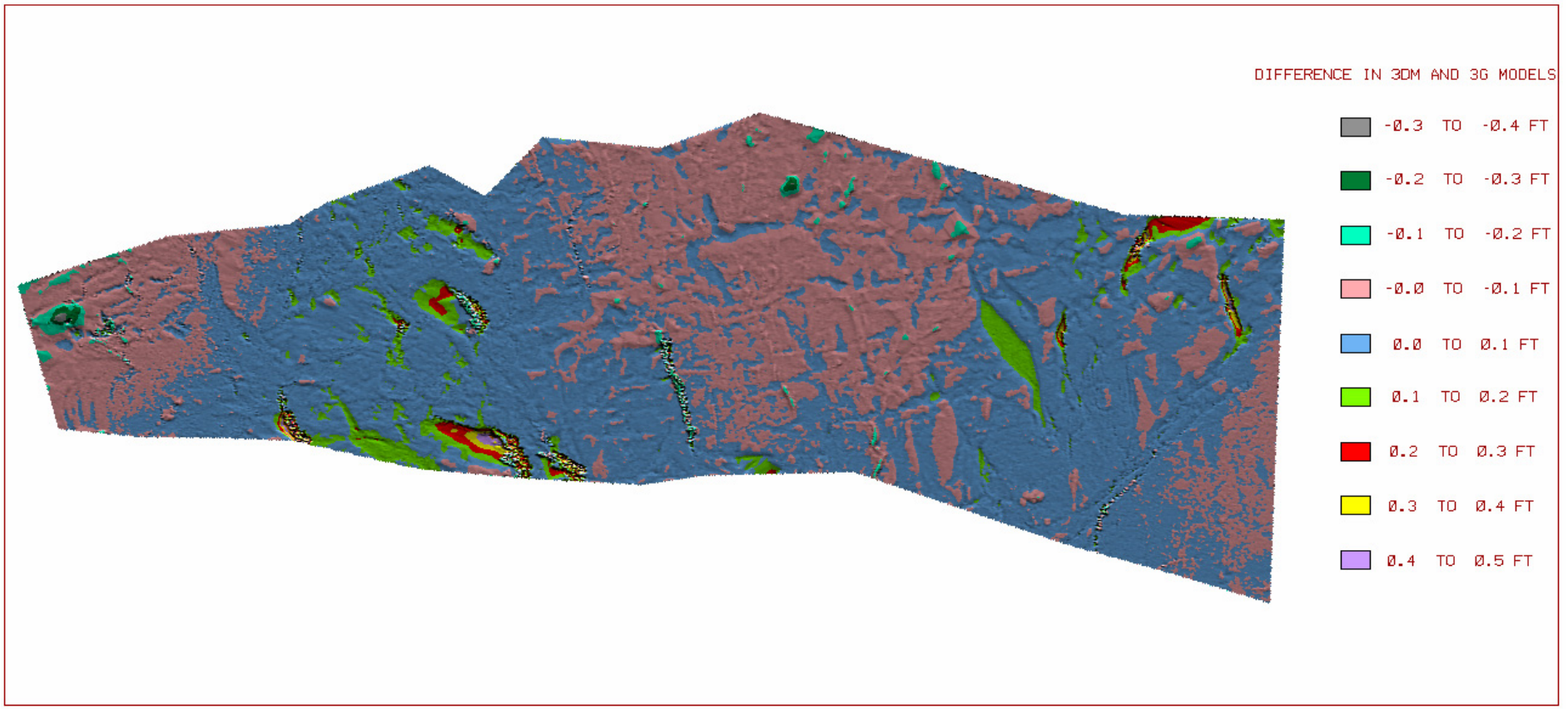


**Figure 5.** Isopac map of the differences in rotated *z*-coordinate values for the re-gridded surfaces: for over 90% of the points, the *z*-coordinate values differ less than 3 cm (0.1 ft).

Figure 5 shows that the isopac areas with the largest differences in the *z*-coordinate values are primarily a result of vegetation or bad camera angle. Indeed, the 3G rendered surfaces in Figure 4 have dark patches in the same locations as the isopac areas with the large Delta-Z values in Figure 5. This is most likely caused by a bad camera angle for these areas in the 3G models. These surfaces could be corrected by taking the images from a better location such that the camera view direction is not nearly parallel to the rock surface. Recall that, however, Presenters had very tight constraints on the number of photographs they could take (3 at the bottom, and 2 at the top of the outcrop). The sharpness of the rendered surfaces is likely caused by the level of density in the original point data. The AdamTech data is much denser than the 3G data: in the trimmed data set used for the isopac, AdamTech had 564,675 points, and 3G had 151,600 points. This is not due to a limitation in the 3G system, which can handle virtually any number of points: structural data and roughness were determined using 658,000 points.

The appropriate level of density depends on the measurement objectives. Reasonable topography can de derived from data with significantly less dense point clouds than is required for detailed roughness measurements or orientation measurements of small features

*Orientation of specific features*

Presenters were asked to provide the authors with the orientation (Dip Dir/Dir) of a total of 158 fractures: 80 of them were visible as traces, while the remaining 78 were visible as faces.

These features are highlighted in Figures 6a and 6b.

Presenters encountered several challenges in obtaining their fracture quantities:

1) Figures 6a and 6b were captured from a higher vantage point than was available to the Presenters, and some of the marked faces were actually parallel to or even sloping slightly away from the vantage points Presenters took their images from.
2) Some of the fractures were very far from being planar. In most cases Presenters tried to pick them up exactly as delimited on Figures 6a and 6b, even if that meant the surface itself ended up being quite ondulating.
3) Some features were too small, too close to a straight line, or hidden behind vegetation.

As a result, Presenters may have:

1) Split a single feature in Figures 6a and 6b into two or more features; or,
2) Identified a face in Figure 6b only as a trace in their DTM.

*Pole plot on a stereonet*

Figures 7 through 9 show the two stereographic plots (lower hemisphere, upper focal point) of the trace poles, face poles, and trace and face poles, respectively. These plots were obtained using the Dips computer program of Rocscience, and no bias correction was used. To allow for a meaningful comparison, the same number of contour levels was used throughout.

Based on these plots, a total of six fracture sets were identified by the authors; however, not all six fracture sets appear on all plots. Figure 7 plots the four fracture sets identified by using trace poles: for each fracture set, the same window was overlaid on the two stereonets of Figure 7. All fracture sets are similarly represented except for Set 1, which is underrepresented in AdamTech data. Set 3 has two modes in Figure 7a, which are not so clearly distinguishable in Figure 7b.

Table 3 gives the mean orientations calculated using AdamTech and 3G trace data. All dip direction and dip angles are within a 3 degree interval, which is considered to be an excellent result.

The same procedure was repeated for the stereonets of the face poles in Figure 8. A total of four fracture sets are represented in Figure 8, namely fracture sets 1, 2, 5, and 6. Fracture sets 3 and 4 thus appear only in the trace poles of Figure 7. In Figure 8a, AdamTech data contours reach higher densities for fracture sets 1, 2, and 6 than 3G data contours in Figure 8b. Mean dip direction and dip angles given in Table 4 differ by no more than 3 degrees, except for the dip direction of set 2 and the dip angle of set 5, which differ by 5 degrees. Set 6 is sensibly vertical, and thus its dip direction is defined up to a 180° shift. Overall, this is considered to be a very good result.

**Figure 6a.** Traces.

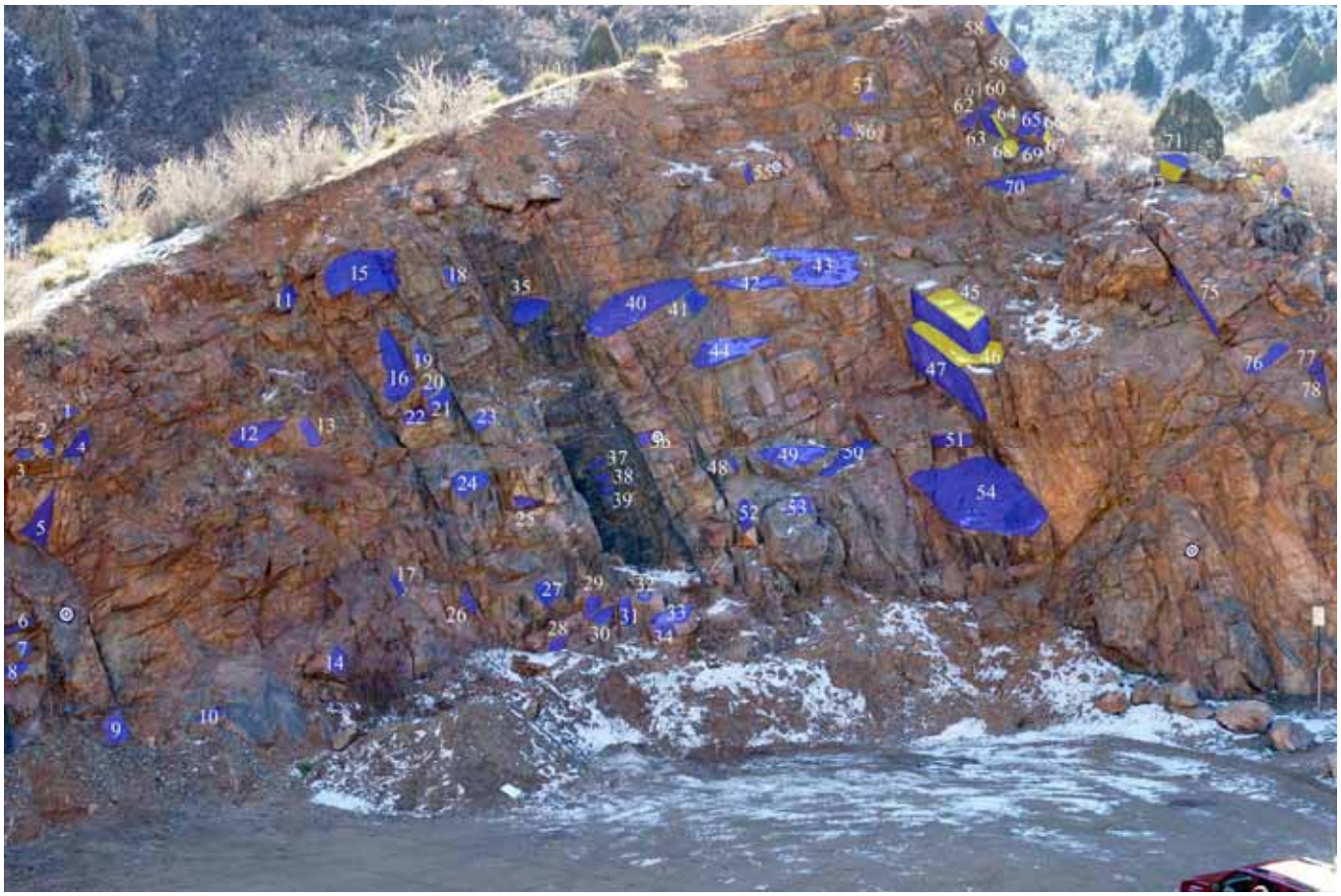

**Figure 6b.** Faces.

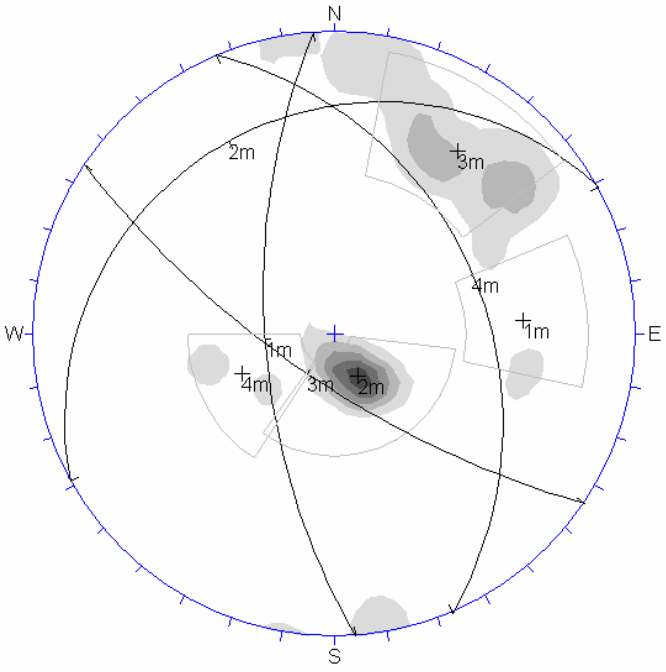


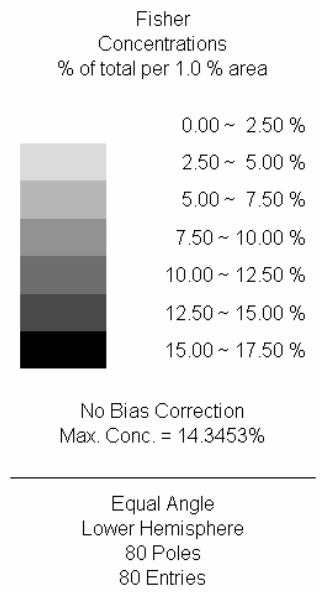


**(a)**

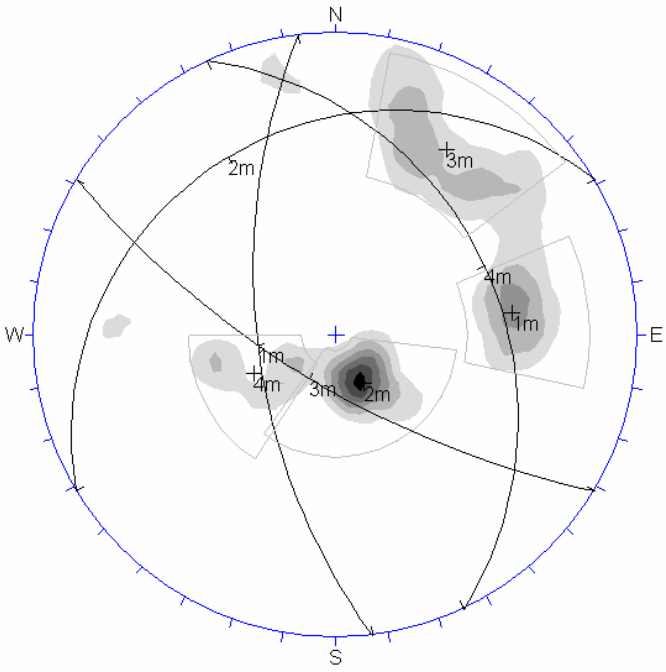


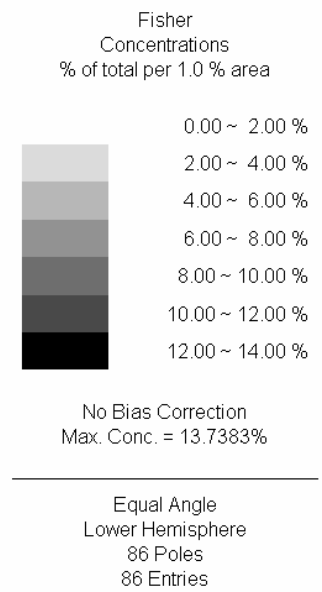


**(b)**

**Figure 7.** Contouring of equal angle, lower hemisphere stereographic projection of the poles: trace planes. (a) AdamTech data; (b) 3G data.

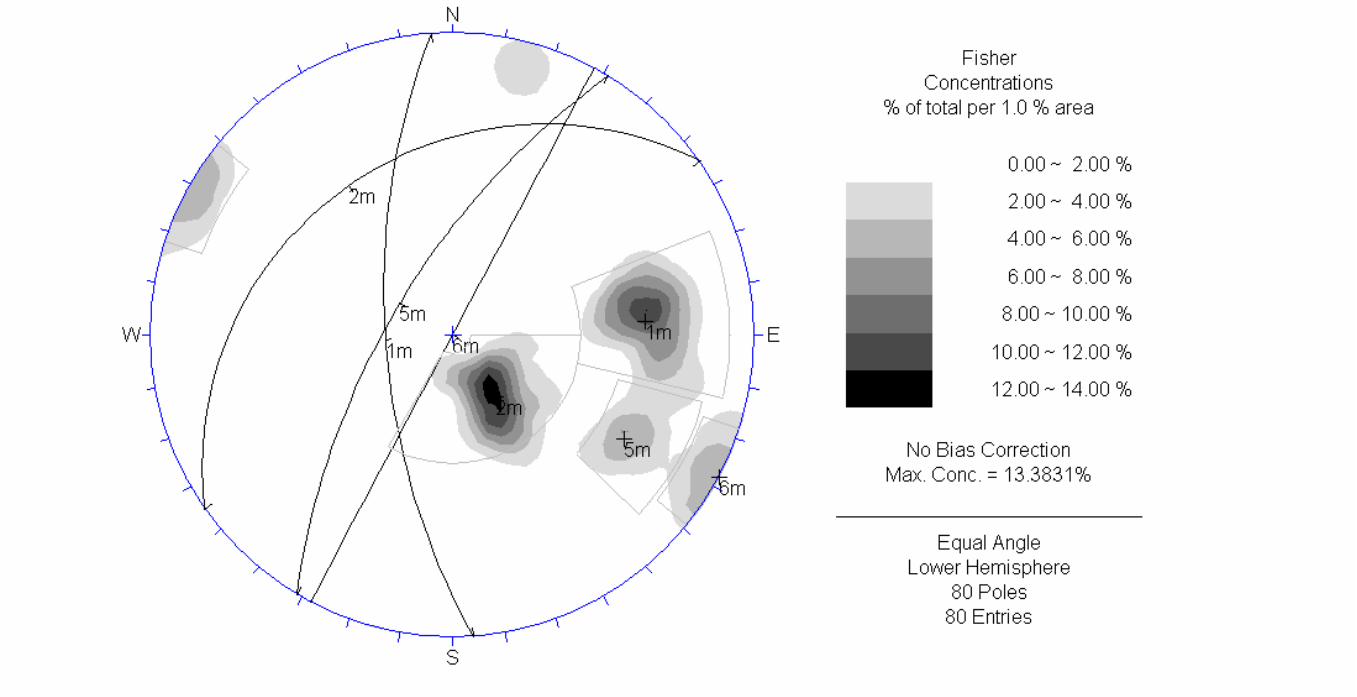


**(a)**

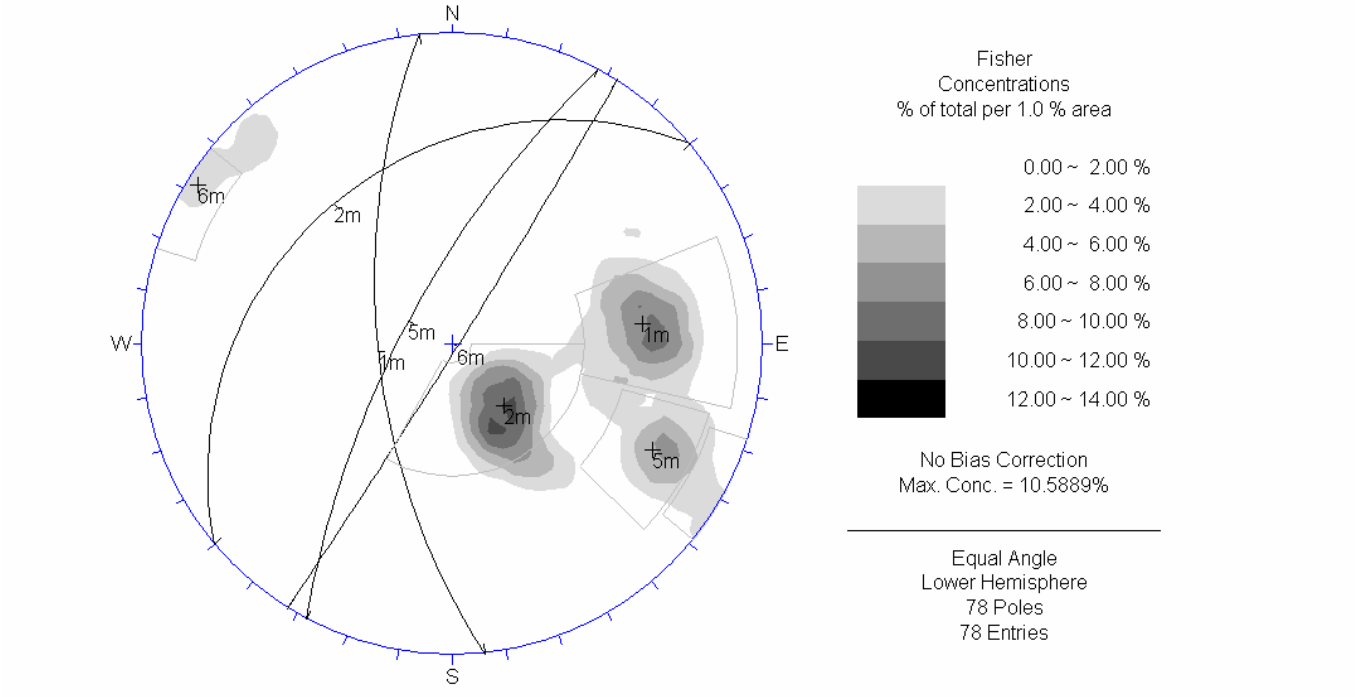


**(b)**

**Figure 8.** Contouring of equal angle, lower hemisphere stereographic projection of the poles: face planes. (a) AdamTech data; (b) 3G data.

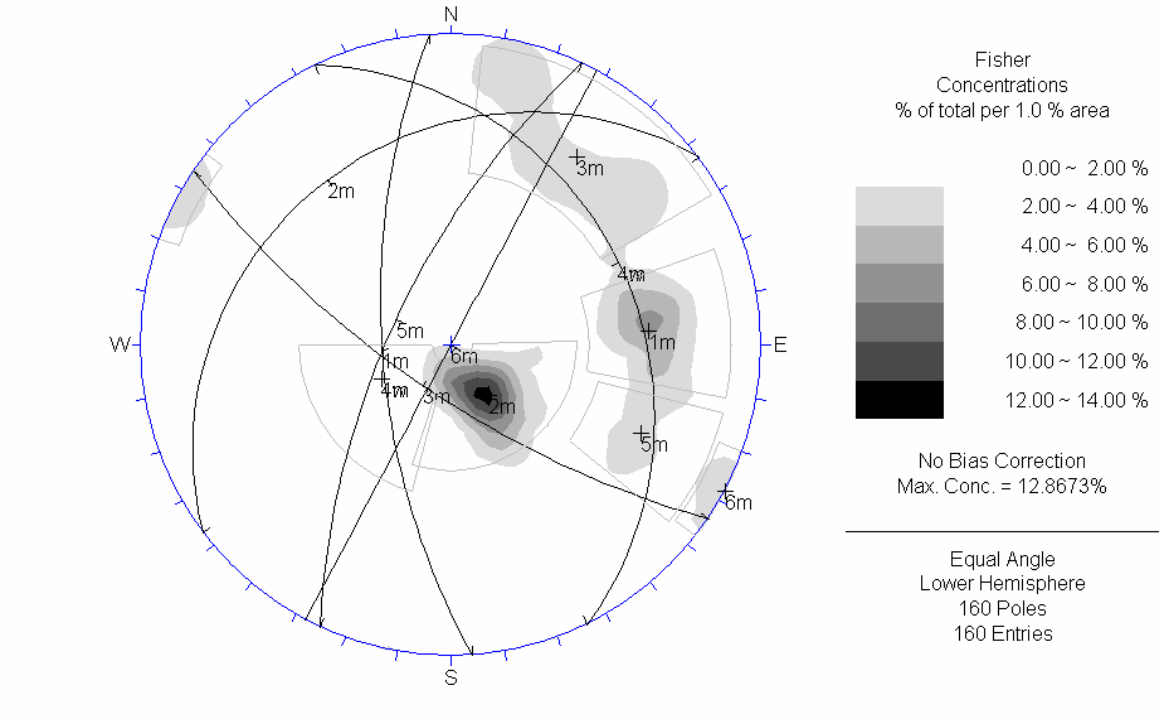


**(a)**

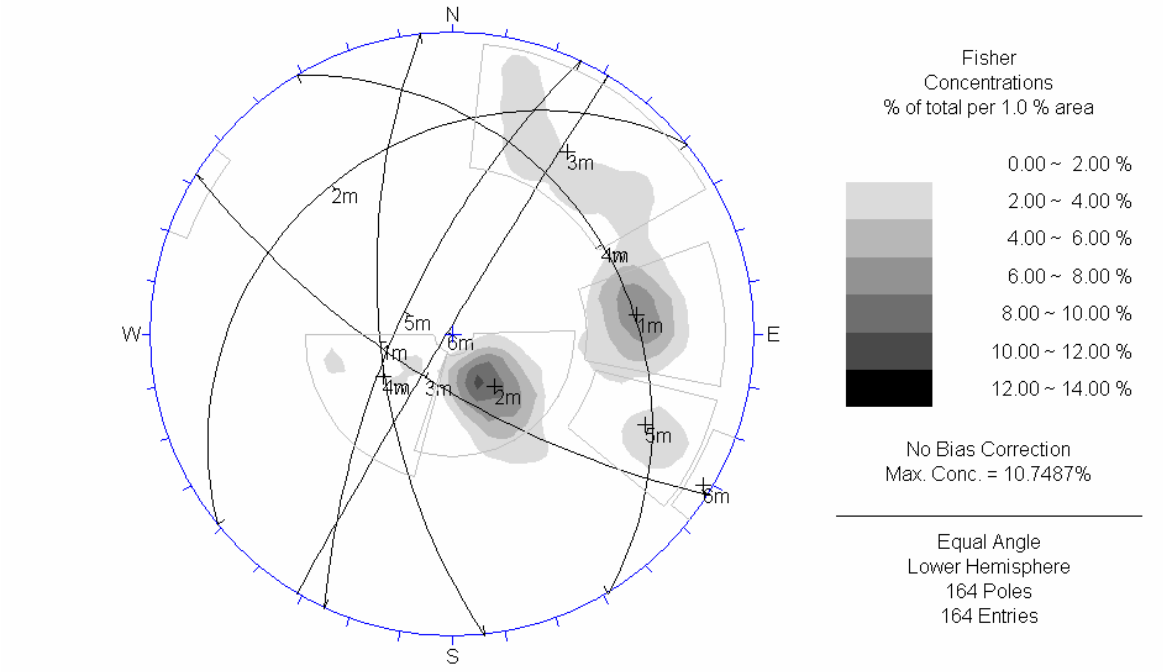


**(b)**

**Figure 9.** Contouring of equal angle, lower hemisphere stereographic projection of the poles: trace and face planes. (a) AdamTech data; (b) 3G data.

**Table 3.** Dip direction/dip for the fracture sets in Figure 3.

| | Set 1 | Set 2 | Set 3 | Set 4 |
|---|---|---|---|---|
| AdamTech | 266/64 | 331/18 | 214/72 | 67/36 |
| 3G | 263/61 | 329/21 | 211/71 | 65/33 |

**Table 4.** Dip direction/dip for the fracture sets in Figure 4.

| | Set 1 | Set 2 | Set 5 | Set 6 |
|---|---|---|---|---|
| AdamTech | 266/65 | 325/27 | 301/67 | 298/90 |
| 3G | 264/63 | 320/29 | 298/72 | 122/88 |

**Table 5.** Dip direction/dip for the fracture sets in Figure 5.

| | Set 1 | Set 2 | Set 3 | Set 4 | Set 5 | Set 6 |
|---|---|---|---|---|---|---|
| AdamTech | 265/65 | 323/23 | 214/72 | 64/28 | 295/68 | 298/90 |
| 3G | 264/63 | 321/25 | 212/71 | 59/30 | 295/69 | 121/89* |

* = only one data point in window.

Figure 9 illustrates the results for trace and face poles combined. Sets 1, 2, 3, and 5 have densities higher than 2% in both plots. Set 4 appears in Figure 9b (3G data), but not when using AdamTech data (Figure 9a). On the other hand, Set 6 appears in Figure 9a (AdamTech), but not when using 3G data (Figure 5a). Set 5 is well defined in Figure 9b (3G data), whereas it shows as a continuation to Set 1 in Figure 9a (AdamTech data). Mean dip direction and dip angles given in Table 5 differ by no more than 2 degrees, except for the dip directions of Set 2, which differ by 3 degrees. As for Set 6, only one point is included in the chosen window for 3G data.

As a conclusion, when considering both traces and faces, both AdamTech and 3G data allowed the most frequent four fracture sets to be identified. For these fracture sets, both systems yielded the same mean orientations.

*Joint spacing*

Presenters were asked to identify the joint set with the largest number of orientation measurements. For this set of measurements, they calculated the mean orientation, they put a 5° cone around the mean orientation, and they recalculated the mean orientation, M, using only the poles that fell in the 5° cone.

AdamTech found the nearly horizontal features (Set 2) to be the most numerous. Using a 5° cone, 12 features with a mean orientation of 329/22 were located. Expanding the cone to 10°, 28 features were obtained with a mean orientation of 328.3/22.5. If a weighted mean for the set orientation was used (giving larger structures more influence on the orientation of the set), 9 features fell within the 5° cone, giving a mean orientation of 328/21, and 30 features fell within 10° of this mean.

3G also found the nearly horizontal features (Set 2) to be the most numerous. Using a 5° cone, 4 features with a mean orientation of 323.2/24.7 were located. Expanding the cone to 10°, 25 features were obtained with mean orientation equal to 327.3/22.7. One can thus conclude that orientation measurements are extremely reliable and that the difference in mean orientations is an order of magnitude smaller than the accuracy of a single compass reading as suggested by ISRM [1].

Finally, 3G and AdamTech calculated the spacing for all features whose pole fell in a 10° cone around the second mean orientation, M. These features are shown in Figures 10a and 10b. Distance was measured between any two consecutive planes along a line parallel to M and through the target to the left of feature 56 and above feature 33 in Figure 6a.

Table 6 gives the mean, median, and standard deviation of the spacing measurements. The mean spacing differs by 60%, the median differs by 30%, and the standard deviation differs by 300%. It is believed that the discrepancies in these results are due to the subjectivity in attaching the mean plane attitude to features, which were not planar.

*Trace lengths*

Presenters calculated the length of the traces whose pole fell in the 10° cone around the mean orientation, M, calculated above.

Table 7 gives the mean, median, and standard deviation of the trace length measurements. The means differed by 10%, the medians coincided, and the standard deviations differed by 20%. These excellent results display much less variability than observed in manual scanline exercises.

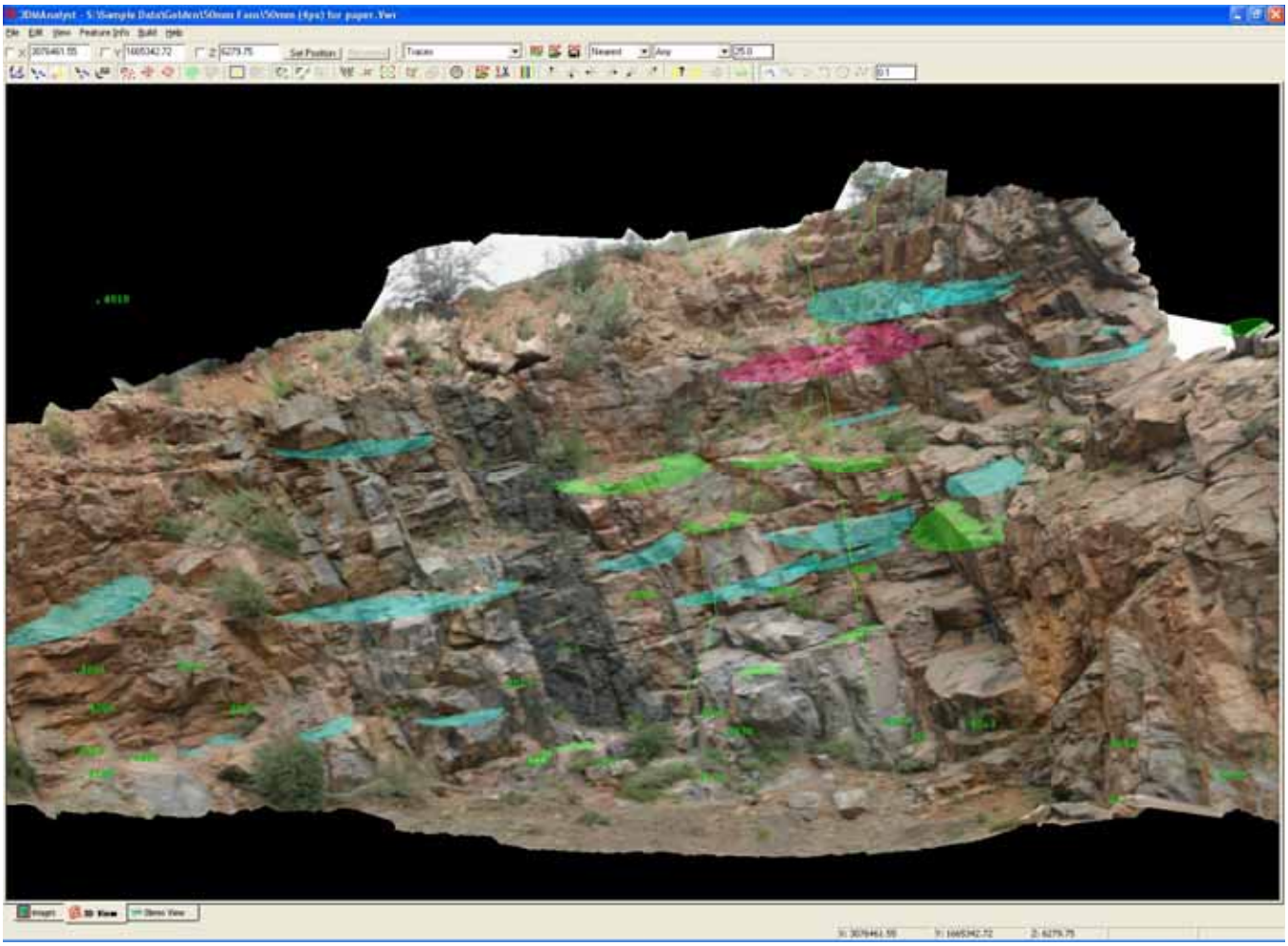

**Figure 10a.** AdamTech traces and faces used to determine spacing and trace length.

**Figure 10b.** 3G traces and faces used to determine spacing and trace length.

**Table 6.** Mean, median, and standard deviation of the spacing measurements (in meters).

| | Mean | Median | StDev |
|---|---|---|---|
| AdamTech | 1.00 | 1.01 | 0.58 |
| 3G | 1.59 | 1.33 | 1.46 |

**Table 7.** Mean, median, and standard deviation of the trace length measurements (in meters).

| | Mean | Median | StDev |
|---|---|---|---|
| AdamTech | 3.44 | 2.99 | 1.49 |
| 3G | 3.13 | 2.99 | 1.80 |

*Roughness*

The face used for roughness determination is identified in Figure 6b by no. 54. During the field exercise, Presenters were not told to pay special attention to this feature, and no detailed picture was taken with the purpose of determining roughness. The purpose of the present section is to quantify roughness reliability from data obtained for general rock mass characterization.

Presenters calculated a reference plane by interpolating or approximating their point cloud for that face; the methods used are described in their papers. Subsequently, presenters cut their face DTMs along a vertical plane through the face dip direction, thus obtaining a piecewise linear profile. Consider a local coordinate system in which $x$ is on the reference plane, parallel to the dip direction and positive downwards, and $y$ is orthogonal to the reference plane and positive upwards. Presenters provided the ($x$, $y$) coordinates of the vertices of the piecewise linear profile as well as the accuracy in the $x$- and $y$-directions.

AdamTech and 3G used two slightly different vertical cutting planes, called planes 1 and 2, respectively, in this text. We asked AdamTech and 3G to provide us with profiles through both planes. They are depicted in Figures 11a and 11b.

AdamTech estimated the depth accuracy to be about 15 mm, and the planimetric accuracy to be about 3 mm. 3G's estimated accuracy is about 9 mm. Because that face is nearly pointing directly at the cameras, the expected accuracy in the $y$-direction is close to the planimetric accuracy, while the expected accuracy in the $x$-direction is close to the depth accuracy.

In Figure 11a, AdamTech provided two profiles constructed using pictures taken with 38 mm and 50 mm lens, respectively: they are nearly indistinguishable one from the other, which indicates that the final roughness profile is insensitive to the lens used. In particular, the maximum discrepancy between them is 15 mm, with the RMS being 3 mm. This value is much lower than the expected RMS of 18 mm, which is based on the assumption that accuracy is equal to 0.5 pixels, as normally used for planning.

Comparison of AdamTech with 3G profiles in Figures 11a and 11b reveals that, for the most part, profiles differ by less than the claimed accuracy. This indicates that the results are fairly insensitive to the system adopted for obtaining the DTMs. In particular, 3G's profile in Figure 11a appears to more compressed in the dip direction than AdamTech's.

## CONCLUSIONS

The following conclusions can be drawn from the comparison of DTMs and of the fracture data produced by AdamTech and 3G:

1) On a large population of data points, both the AdamTech and the 3G programs provided high quality DTM results, with deviations of a maximum of 3 cm from the actual rock surface.
2) When the rock face presents an overhang, pictures/scans should be taken from many different angles to ensure that no surface is parallel to all pictures/scans. This is especially valid if the rock face is temporary (e.g., staged excavation) or if regaining access to the face is difficult and costly (e.g., remote areas, difficult weather conditions, snow blankets, ice sheets, etc.).
3) Guidelines on point density are still unavailable, and should be problem-specific because they must be tailored to the information being sought.
4) When considering both traces and faces, both AdamTech and 3G data allowed the four most frequent fracture sets to be identified. For these fracture sets, both systems yielded the same mean orientations.
5) Both systems found that the nearly horizontal fracture set was the most

represented, and determined its mean orientation to within 2°.

6) For the most represented fracture set, mean joint spacing differed by 60%, and larger discrepancy affected the standard deviation.
7) Trace lengths of the most represented fracture showed a very good match, with their means within a 10% difference, and their standard deviations within a 20% difference.
8) Heights of roughness profiles differed by a maximum of 1 cm, except for one location, where they differed by 4 cm. The maximum roughness height was 9 cm. These results pertain to a general rock mass characterization, and not to specific photographs taken for determining roughness profiles of fractures.

Presenters encountered major challenges: given features were identified on pictures taken from different vantage angles than available to Presenters; some fractures were not planar; and some fractures were quite small, or close to a straight line, or hidden behind vegetation.

Despite these major challenges, the obtained results indicate that digital photogrammetry yields reliable and reproducible results when applied to rock mass characterization. Digital photogrammetry is thus a mature enough technology that can be used with confidence in the profession provided care is taken to follow the guidelines provided by the Presenters in their papers and by the authors in the introductory paper to this report.

REFERENCES

1. ISRM, *Suggested methods for the quantitative description of discontinuities in rock masses.* Int. J. Rock Mech. Min. Sci. & Geomech. Abstr, 1978. **15**: p. 319-368.

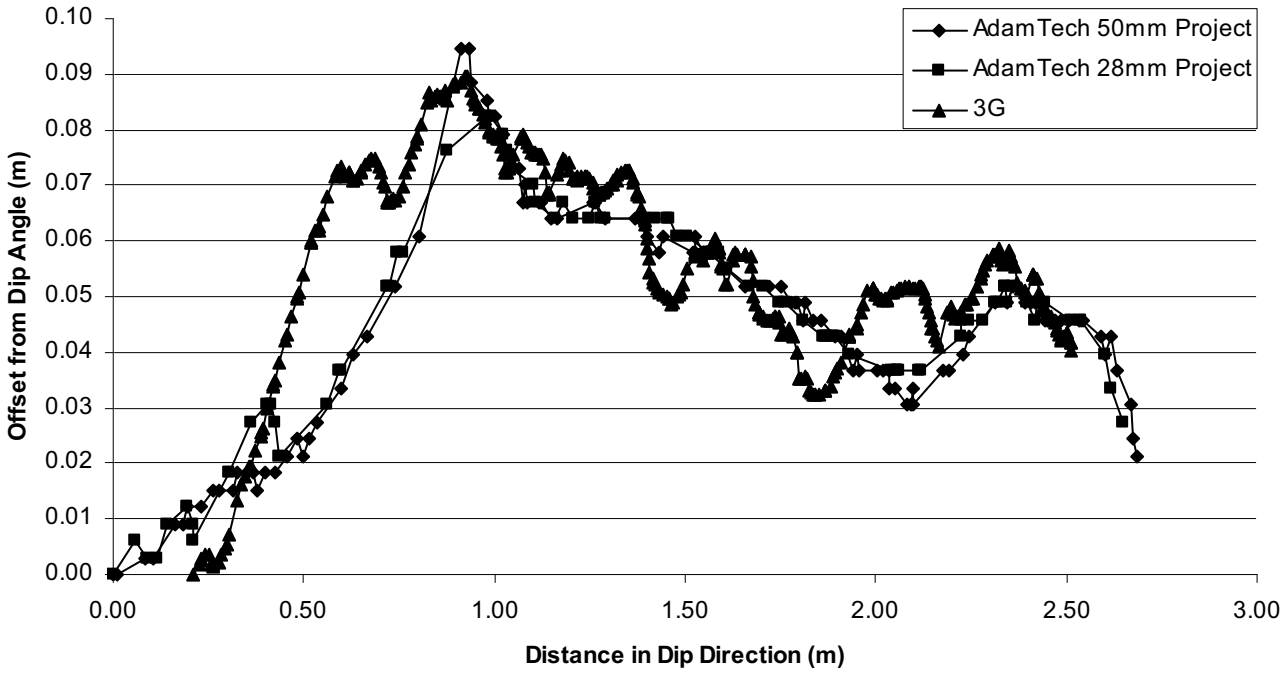


**Figure 11a.** Roughness profile for face 54 along plane 1.

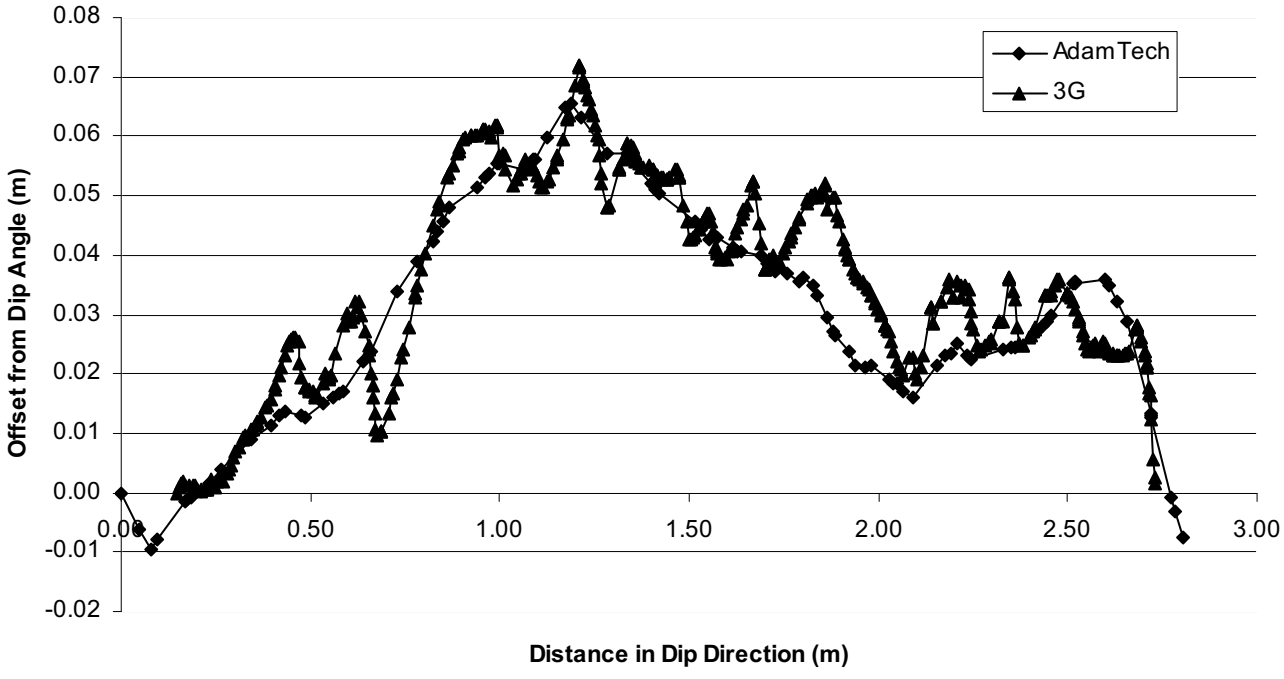


**Figure 11b.** Roughness profile for face 54 along plane 2.

# SUPPORTING PAPERS

# Advanced techniques for geo structural surveys in modelling fractured rock masses: application to two Alpine sites

Voyat, I.

*Politecnico di Torino – Dipartimento di Ingegneria Strutturale e Geotecnica – Corso Duca degli Abruzzi 24, Torino, Italy*

Roncella, R. and Forlani, G. and Ferrero, A.M.

*Università degli Studi di Parma – Dipartimento di Ingegneria Civile, Ambiente e Territorio e Architettura, Parco Area delle Scienze 181/a, Parma, Italy*

Copyright 2006, ARMA, American Rock Mechanics Association

This paper was prepared for presentation at the workshop: "Laser and Photogrammetric Methods for Rock Face Characterization" organized by F. Tonon and J. Kottenstette, held in Golden, Colorado, June 17-18, 2006.

This paper was selected for presentation by F. Tonon and J.T. Kottenstette following review of information contained in an abstract submitted earlier by the author(s). Contents of the paper, as presented, have not been reviewed by F. Tonon and J. Kottenstette, and are subject to correction by the author(s). The material, as presented, does not necessarily reflect any position of USRMS, ARMA, their officers, or members. Electronic reproduction, distribution, or storage of any part of this paper for commercial purposes without the written consent of ARMA is prohibited. Permission to reproduce in print is restricted to an abstract of not more than 300 words; illustrations may not be copied. The abstract must contain conspicuous acknowledgement of where and by whom the paper was presented.

**ABSTRACT:** The study of the mechanical behavior of fractured rock masses should always be based on accurate rock surveys of the geological structure. Traditionally surveys are performed manually by using compass and directly accessing the rock mass: this is often dangerous or difficult; the samples size is therefore small, i.e. not optimal to characterize the rock mass completely. In this paper, alternative techniques will be discussed. Using photogrammetry or a laser scanner, a dense point cloud is collected on the rock surface. Discontinuity orientation and position on the rock face are computed extracting semi-automatically plane surfaces from the point cloud with robust estimators. The implementation of the method in a software program allows, through a user interface, the identification of single planes or the selection of macro-areas with automatic segmentation of several planes. Segmentation results are organized in order to be directly used for the deterministic reconstructions of the rock masses and the study of the rock mass stability conditions with the key block method and the Distinct Element Method in a 3 dimensional field. The method has been validated through the comparison with traditional surveys in two different pilot sites (Arnad, North West Italy and Le Trappistes, Swiss).

## INTRODUCTION

The study of the stability condition of a rock mass is usually based on a geo structural survey of the discontinuities. Surveys are devoted to a systematic and quantitative description of rock discontinuities and can be executed on natural or artificial (excavations, boreholes, etc.) rock faces.

Traditionally surveys are performed with a geological compass, measuring directly dip and dip direction on the rock face. In several cases, this can be difficult because rock masses:

- cannot be easily accessed, or the size of rock faces is so large that the data acquisition may be long and expensive when done manually;
- are so heavily fractured and not supported that it can be dangerous to climb the slope or even stand at its base.

Sometimes the on-site interpretation of the data is not easy; a better understanding of the rock structure can be achieved later, when the data have been properly organized and compared; alternative surveying methods may also allow additional measurements without going back to the field.

Traditional surveys are carried out on scan-lines or, in a more detailed way, through observation windows (figure 1). Nevertheless, in several cases, they cannot highlight key fracture aspects that are needed to per-form stability analysis.

In particular, failure to acknowledge the relationship between discontinuity sets (in terms of joint hierarchy and different kind of joint

terminations) can strongly influence the rock mass mechanical behavior.

In order to set up a 3D geometrical model of the rock mass, both its topography and its geo-structure are necessary. As shown in [1, 2] both types of information may be provided using alternative surveying technologies, such as stereo photogrammetry and laser scanning. The former can be executed with an off-the-shelf digital high resolution camera, taking images from different standpoints; the latter with a medium to long range terrestrial laser scanner, possibly joining several scans from different stations; both supply a dense 3D point cloud.

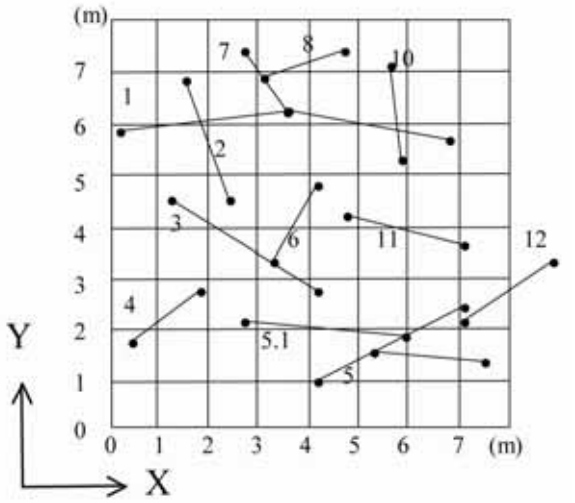


Fig. 1. Data acquisition through observation window.

From the acquired point cloud, the slope topography can be reconstructed and information on discontinuities (position, orientation, spacing, persistence) as well as joint hierarchy, can be extracted. Building a 3D mesh (e.g. by spatial Delaunay triangulation) is not required: the procedure can be performed directly on the unstructured point cloud, limiting post-procesing time.

Assume we have a sufficient number of suitably distributed points measured on a discontinuity plane and determined in a mapping frame (North, East, Elevation): the gravity centre of the points will give the location of the plane; fitting a plane to the set of points, the coefficients of the plane equation will provide the components of the vector normal to the plane; the dip and dip direction of the discontinuity plane can be recovered with simple computations. Repeating this procedure for the whole rock structure, a spatial database, containing discontinuities location and orientation, can be populated. Discontinuities spacing and densities can be evaluated by clustering planes with similar orientation and by analyzing their spatial distribution.

Overall, more information can be collected with respect to traditional surveys: a larger number of measured values, distributed all over the slope, including those not directly accessible, are easily extracted. Besides, the overall process relies more on objective information and it is therefore less prone to subjective evaluations and judgments. Finally, the availability of 3D point cloud data as well as image information allows for a more efficient analysis of the slope: measurements may be taken at any time, without returning to the field.

To mark a real improvement upon traditional survey techniques, an alternative system should not require access to the rock face and should be able to recover dip and dip direction on every main or significant discontinuity with an accuracy matching at least the one of the compass. Overall costs should be smaller than those of a comparable traditional survey.

In this paper, we review both technologies (photogrammetry and laser scanning), discussing their pro and cons along with the results achieved in two sites in the Alps, where reference data provided by a direct survey allowed a comparison between the traditional and the proposed survey methodology.

In section 1 photogrammetry and laser scanning are briefly introduced, highlighting the main issues in their application to this kind of survey; in section 2 different algorithms and approaches to point cloud segmentation in plane surfaces are presented. In section 3 the results achieved on the pilot sites will be discussed. Finally, after some concluding remarks, the ongoing activities and perspectives will be presented.

## COLLECTING A DENSE POINT CLOUD ON ROCK FACES

Since the 3D analysis of the rock mass surface is basically performed using a point cloud, different technologies may be applied to obtain the required 3D data: in the past some work have been presented using total stations [3], but nowadays the most

appealing techniques seems to be stereo photogrammetry and laser scanning.

*Photogrammetry*

Photogrammetry is a well established technique delivering 3D coordinates of points with predictable accuracy from stereo or multiple images.

Photogrammetry is based on the collinearity principle, namely the alignment on a straight line of object point, lens centre (the camera perspective centre) and image point. Building on this principle, any photogrammetric survey is executed in a three-step procedure, which reverses the image formation process: camera calibration, image orientation and restitution. Camera calibration allows one to convert the pixel coordinates of an image point into the direction of the ray in image space, i.e. with respect to a camera-fixed reference system. Image orientation yields the position in the mapping frame and the orientation (attitude angles) of the camera body at each station. This provides one with the projection centre and allows one to compute, for each image point, the direction of the ray in object space. Restitution derives object point coordinates by spatial intersection of two or more homologous rays (i.e. the projecting rays corresponding to the same object point), together with evaluation of their accuracy.

The accuracy of the object coordinates depends on a number of factors, which must be accounted for in the survey design. When applying photogrammetry to the determination of discontinuity parameters, one has also to deal with a number of issues and operational choices, specific to the task. Without going too much in detail, these are now addressed.

The accuracy of dip and dip direction will mainly depend on two factors: the ratio between the point accuracy and average distance between points, and the roughness of the actual rock surface. Obviously, wide flat surfaces can be determined very well also with points of relatively poor accuracy, provided they are taken apart from each other; if planes are very small or elongated, points must be closely spaced to ensure that at least some fall in each plane; in such cases, however, even small uncertainties may lead to errors of several degrees in dip and dip direction. Camera stations and camera focal length must be chosen to ensure appropriate image resolution on the object; depending on site characteristics, terrestrial or aerial (from helicopter or from airplane) photogrammetry may be used.

Object point accuracy depends on the accuracy of calibration, image orientation and restitution. While calibration is a periodic laboratory operation, the technique and the accuracy of image orientation depends on project characteristics. The exterior orientation parameters (the position of the projection centre and the rotations from image system to object system) may be determined indirectly, measuring the image coordinates of object points with known coordinates (GCP or Ground Control Points) or directly by coupling a GPS (Global Positioning System) receiver and an IMU (Inertial Measurement Unit) to the camera [4, 5].

When a block of several images is necessary to cover the object, orientation can be performed simultaneously on the whole block, allowing for a very significant reduction in the number of GCPs, with no accuracy loss.

Assume the camera to be well calibrated and the image orientation to be accurate. The accuracy of point determination improves:

- the closer the angles between homologous rays to 90° (in a stereo pairs, this depends on the ratio of the distance between the two camera stations with respect to the camera-to-object distance);
- the larger the image scale (ratio between camera focal length and camera-to-object distance);
- the better the accuracy of the measurement on the images (with digital images, in the order of 0.1÷1 pixel).

The orientation and the restitution may be executed either manually by an operator or automatically, using image correlation techniques. The first option exploits the ability of the operator to select the minimum number of points necessary for a reliable identification of the plane; the latter exploits the capabilities of matching algorithms to compute up to several thousand points per minute, but has to deal later on with outliers removal and identification of planes within the point cloud obtained. Nowadays, the development of highly

efficient correlation algorithms allows for the automation of many photogrammetric tasks and the extraction of a huge number of points (from several hundred thousand up to millions) on the object surface [6, 7, 8].

*Laser Scanning*

LIDAR (LIght Detection And Ranging) data are a primary data source for DTM (Digital Terrain Model) generation; laser scanners can be operated either from ground, as a stand-alone system, or in airborne systems (in the latter case integrated with a navigation system). The main components of a LIDAR system are a laser telemeter and a scanning mechanism, normally made of one or two rotating mirrors. A pulse emitted from the laser source is reflected by the object surface and its echo is captured by the optics; measuring the time-of-flight, the sensor-to-object distance is computed. Terrestrial and aerial laser scanners differ in the way the distance information is combined to provide the target position.

Terrestrial lasers are equipped with two mirrors mounted on two orthogonal axes; when the instrument is leveled, the synchronized rotation provides scanning in azimuth and zenith; the polar coordinates of the target are then converted to a local cartesian frame with origin in the instrument centre. Most of the times the instrument is leveled, with z-axis vertical and x-axis in arbitrary direction. There are a number of systems available, suited to different applications. In the context of point clouds generation of rock faces, operating ranges are from 100 to 800 *m* and more, with measurement accuracies of the distance in the range 0.5÷3 *cm* and scanning speed from 2000 to 12000 pts/*s* (www.leica-geosystems.com, www.optech.com, www.riegl.com, www.trimble.com, accessed March 6, 2006).

Angular scanning resolutions are in the order of 100 mrad and allow for a very high sampling density on the object in relatively short acquisition times, resulting in millions of points that can be measured on the object surface.

Since coordinates refer to an instrumental system, targets are set on reference points to compute a spatial transformation from instrument to object frame. Likewise, if several scans have to be joined to complete the DTM of a large area or to avoid occlusions, registration of the scans in a common reference system must be performed. To this aim, two main techniques are available: accurate and reliable results are obtained using point-based registration while less accurate results are obtained by surface matching techniques (such as ICP, Iterative Closest Point [9]). In the first case several methods can be applied, either using different analytical approaches (conformal, procrustean, etc.) and simple pair wise registration or simultaneous registration; the common points are usually high reflectivity targets (possibly spherically shaped) well distributed on the scan area, which can be detected very precisely in the point cloud. In the second case, no common target points are needed, since the algorithms use the (triangulated) surfaces of overlapping scans to find the transformation parameters best fitting in the common area.

Airborne laser scanners determine the ground position of points with an accuracy of 5÷15 *cm* in elevation and 15÷50 *cm* in horizontal, depending on flight height and surface characteristics. The main components of an airborne LIDAR system are a scanning laser telemeter, which measures the sensor-to-ground distance, and a GPS receiver integrated with an IMU. The sensor position and attitude is interpolated at the time each pulse is emitted, so that the 3D coordinates of each echo received back from a single pulse are computed. The system may be operated from helicopters or aircrafts. Combination of a forward movement and scanning across flight direction by an oscillating mirror results in a swath of terrain being sampled. The point density can be adjusted to the order of 10 pt/$m^2$ for high accuracy DTMs, although it is normally 0.3÷1 pt/$m^2$ in DTM production. Although improving fast in hardware performance, airborne laser scanning does not represent yet, in our opinion, a suitable alternative to photogrammetry or terrestrial laser scanning: its dependence on the GPS/IMU accuracy will prevent the system to reach overall accuracies on the ground better than 10÷20 cm, an accuracy level perhaps acceptable in the survey of large rock faces. It should not be underestimated that the system relies heavily on GPS: flying in narrow valleys, where GPS constellation is unfavorable, may lead to rather inaccurate results.

*Rock analysis: which technology?*

An exhaustive comparison of pros and cons of both techniques is beyond the scope of this paper and should be deferred to a later time, when a

significant sample of results from test sites with different characteristics will be available; some remarks can be made, though.

At a first glance, laser scanning is more attractive than photogrammetry, since it does not require stereoscopy, it is faster and it obtains the object geometry in a straightforward manner. On the other hand, laser scanning may run into problems when several scans are necessary and, because of the steepness of the terrain combined perhaps with a dense forest with high trees at the bottom of the wall, stations must be set rather apart from each other and from the wall. In such cases, guaranteeing sufficient resolution on the object, good registration of scans and coverage of all relevant viewing directions may be difficult, although hardware and software performance are improving by the day. Interpretation of the point cloud acquired by laser may be hard without co-registered images, which are indeed now offered by almost all manufacturers.

Photogrammetry is in principle more flexible, since image scale can easily be adapted to the need; occlusions or big walls are not a problem, if an helicopter and a large format camera is available. On the other hand, while photogrammetry must be at least stereo, laser does not, and so is less prone to occlusions; shadows do not affect measurement accuracy nor do large perspective differences due to object curvature. In terms of total surveying time (acquisition, processing, editing and revision) laser scanning should be faster than photogrammetry, even if automatic procedures in orientation and/or restitution [10, 11] make the gap rather small.

As stressed by several authors [12, 13] the two approaches offer complementary assets and their combined use is highly recommended. As far as accuracy is concerned, both laser scanning and photogrammetry fulfill and even exceed the requirements (0.5÷2 *cm*); photogrammetry is more flexible since its accuracy depends mainly on image scale and can be adapted to the survey features. Laser scanning is better when the area to be investigated is large and point cloud density has to be very high: most of the hardware currently on the market has high angular resolution (30÷300 μ*rad*) and wide field of view (in most cases almost 360° in both azimuth and zenith) compared to photogrammetry (using focal lengths in between 35÷80 *mm* and common digital sensors, 300÷700 μ*rad* correspond to 15°÷35° angle of view).

As far as ease of use is concerned, in rock slopes survey the site is hardly accessible: while laser scanner hardware is usually heavy (25÷30 *kg*) and power hungry, only a digital camera with a light tripod is required to perform a photogrammetric survey.

Finally, despite the on-going reduction of hardware cost, laser scanning is at least 10 times more expensive with respect to photogrammetric instrumentation and software.

## SEGMENTATION OF POINT CLOUDS

Once the point cloud is available, irrespective of the production technology adopted, it must be segmented to single out the discontinuity planes of the rock slope: the point dataset has to be divided into groups, each made of points belonging to a single plane.

The generic equation of a 3D plane is:

$$aX + bY + cZ + d = AX^T = 0 \qquad (1)$$

where $X$ represents the homogeneous coordinates of a point on the plane determined by the four (linearly dependent) parameters $a$, $b$, $c$, $d$. The over-determined estimation of the plane parameters may be stated as the residual minimization of the problem

$$\left\| XA^T \right\| = \min, \qquad subject\ to \left\| A \right\| = 1 \qquad (2)$$

which may be solved through a least squares approach using the Singular Value Decomposition [14].

The Dip and Dip Direction can be easily determined [3] from the parameters $a$, $b$, $c$ and $d$, while the center of mass of the point set used in the estimation provides the position of the discontinuity.

Although the solution arising from Eq. (2) is statistically optimal (in terms of Maximum Likelihood Estimation), the procedure outlined does not include any mechanism to identify and reject outliers in the observations set. Since the whole dataset will contain data belonging to several planes as well as proper outliers (e.g. points on vegetation, etc.) it should be broken in sub-sets before any least squares technique is applied. Otherwise, large estimation errors in the parameters may arise even with a small percentage of outliers.

To overcome this limitation, a robust approach, based on Ransac procedure [15, 16], has been developed [10, 17]: Ransac is a widely applied algorithm in image analysis and cartography capable to cope with outlier percentages close to 100%. The basic idea of the method is to initially identify the model (in our case: a plane) with the minimum number of data required (in our case: 3 points) and try to widen the set of data coherent with it.

A minimum subset of points is randomly sampled from the point cloud, defining a plane; the coefficients of the plane are computed by Eq. (2) and the distance between each point of the set and the selected plane is computed: if it is less than a threshold, the point is included in the consensus set of the plane, otherwise it is considered as an outlier.

The process is repeated for a given number of times: the N iterations required to obtain (with a certain probability p) that at least one of the subsets is outlier-free, assuming ε = percentage of outlier, is straightforwardly computed as [15]:

$$N = \frac{\log(1-p)}{\log\left(1-(1-\varepsilon)^{s}\right)} \tag{3}$$

where $s$ is the minimal subset size (i.e. for plane estimation s = 3). The outlier percentage is usually unknown, but can be evaluated as:

$$\varepsilon = 1 - \frac{1}{N_p} = \frac{N_p - 1}{N_p} \tag{4}$$

where $N_p$ represents the number of planes expected to be extracted onto the rock surface. It can be verified that, if more than 10 planes have to be extracted the outlier percentage quickly gets close to 100%.

When the maximum consensus set is chosen for a given plane, its points are used to estimate by least squares the final coefficients of the plane, to get an optimal estimate.

If more than one functional model has to be considered in the dataset (i.e. if more than one discontinuity plane is included in the dataset) the Ransac algorithm may be reiterated until all points have been linked to a plane: once a plane has been extracted, its consensus set is removed from the original set, to allow the determination of other planes. In principle, this will lead to the hierarchical segmentation of the whole dataset, from the largest to the smallest plane, where the ranking depends on the cardinality of the maximum consensus sets.

The use of the Ransac segmentation algorithm on the whole point cloud is not computationally feasible since, with too many functional models (i.e. different planes) in the dataset, the iterations required are too many, as shown in Table 1. Unless different strategies are implemented to reduce the problem complexity (see [17]), an automatic segmentation of the whole rock surface is unfeasible, and semi-automatic extraction of planar patches is required.

Each extracted plane is classified in terms of goodness of fit (mean square error), cardinality, location of the gravity centre and finally dip and dip direction. The interactive selection of point cloud subsets to be processed by the Ransac segmentation algorithm is greatly facilitated if the 3D coordinates can be linked to images of the rock surface.

If the point cloud was generated by photogrammetry, this is straightforward, since all images used to produce it are obviously consistent (oriented) with respect to the same reference frame. If a laser scanner was used instead, images can be acquired on site and oriented with a space resection, by identifying image points with point cloud features and using their coordinates as GCP; this is not always easy and does not lead to accurate registration, but might suffice the purpose in most cases; better results might be achieved using targets

Table 1. Number of Ransac iterations, Eq. (3); assuming ε = percentage of outlier, and accepting probability $p$ to obtain at least one (minimal) outlier-free subset, obtained by.

| iteration | | outlier percentage ε | | | | |
|---|---|---|---|---|---|---|
| | | 50.0% | 90.0% | 95.0% | 99.0% | 99.5% |
| probability $p$ | 99% | 34 | 4603 | 36.839 | 4.605.168 | 36.841.359 |
| | 95% | 22 | 2994 | 23.964 | 2.995.731 | 23.965.857 |
| | 90% | 17 | 2301 | 18.420 | 2.302.584 | 18.420.680 |
| | 80% | 12 | 1609 | 12.875 | 1.609.437 | 12.875.502 |

visible in both the point cloud and the image, but this is not always feasible; as already pointed out in § 1.2, most laser systems are now equipped with a camera whose orientation and position with respect to the instrumental reference system is calibrated, so that image registration is straightforward.

Using a previously oriented image, the point cloud is back-projected onto the image frame, allowing for queries on point coordinates as well as other geometric information.

*Interactive extraction of planar surfaces.*

A software called ESP has been developed to query the point cloud data directly on an oriented image of the slope. Through an interactive GUI (Graphical User Interface) the user draws a polyline on the image, bounding an area enclosing the discontinuities; the corresponding points are selected and sent to the Ransac routine where planes are identified. The user can specify different values for the Ransac threshold, depending on the level of discretization in the representation of the rock face discontinuities: to obtain a meaningful segmentation, values in the range from 10 to 20 *cm* are commonly used. Outlier percentage and iteration number are adaptively computed as described in [10, 17].

By dividing the rock face into different areas with roughly the same orientation and letting the algorithm to execute a detailed segmentation we obtained, without significant computational effort, results very close to the reference data.

## ON-SITE TECHNIQUES COMPARISONS

In this section the application of photogrammetry and laser scanning in two different surveys is described, showing the results obtained in the discontinuity identification.

*Application of the photogrammetric method*

The photogrammetric method has been applied to a pilot site at the Corma di Machaby (Figure 2), a large gneiss structure about 1000 m wide and 400 m high located near Arnad (Valle d'Aosta, North West Italy). The surveyed area is approximately 100 m wide and 70 m high.
The site geology is characterized by light brown gneiss alternating with metabasitic lens parallel to the schistose (Sc) planes.

At the slope base, several detached blocks have been observed and measured.

A geostructural survey has been performed by means of traditional methods in order to compare and validate the results obtained with the photogrammetric method. Both horizontal scan-lines at the base of the slope and vertical scan-lines in different slope areas have been executed.

Overall, the reference survey has identified and measured about 190 discontinuities, leading to the identification of 5 principal sets and 3 minor ones. A summary of their characteristics (in addition to dip and dip direction, also trace length and spacing were measured) is shown in Table 2.

Figure 2. The Corma of Machaby test site.

Table 2. Traditional survey results.

| *Family* | | Orientation (deg) | | Trace Length (m) | | Spacing (m) | |
|---|---|---|---|---|---|---|---|
| | | *Dip* | *DD* | *Min* | *Max* | *Min* | *Max* |
| Principal | Scv1 | 75 | 140 | 20–40 | 100 | 0.5–5 | 10 |
| | Scv2 J6 | 75 | 195 | 20–30 | 80 | 0.5–5 | 10 |
| | J1 | 78 | 238 | 30–50 | 80 | 4–6 | 8 |
| | J2 | 10 | 50 | 4–10 | 15 | 0.5–5 | 10 |
| | J7 | 35 | 295 | 5–20 | 30–50 | 0.5–2 | 10 |
| Secondary | J3 | 40 | 250 | 4–6 | -- | 0.5–1 | -- |
| | J4 | 35 | 25 | 4–7 | 10 | -- | -- |
| | J5 | 55 | 160 | 6–8 | 15 | 2–4 | -- |

The photogrammetrical survey was performed by a digital camera Nikon D100 (resolution = 3000 x 2000 pixels, pixel size = 7.8 $\mu m$) with a 18 *mm* lens. The mean ground resolution of the images is about 3 cm. Five images in normal stereo configuration were used.

To georeference the photogrammetric block, a reflectorless theodolite was used to determine a set of 35 ground control and check points on the rock face from two GPS stations. Six of them were used as ground control points for the model orientation.

The image orientation and the generation of the point cloud was performed using the software Virtuozo from SupreSoft. While image orientation requires the manual identification of tie points and ground control points, Virtuozo uses image correlation algorithms to automatically estimate the points on the object surface. Using 4 stereo-models, a point cloud of 1.5 million of points with an average spacing of 5 *cm* was obtained. The mean accuracy of the measured points is in the range 2÷3 *cm*, verified using the available check points.

*Measurement of dip and dip direction with ESP*

Interactive determination of discontinuities was performed using the program ESP; applying the method to the same slope section but using different images, a series of preliminary tests were executed, in order to verify the software consistence.

Several tests have also been performed to find out a range of values for the distance threshold in Ransac, as pointed out in § 2.1, to get a stable and correct segmentation of the 3D points dataset.

Ransac capability to perform a consistent and accurate slope segmentation regardless of outlier percentage in the dataset (i.e. considering regions with just one orientation vs. regions containing several planes) was thoroughly investigated. First small portions (called micro-areas in the following, see figure 3.a.) of the point cloud, corresponding to a single plane, were selected and 177 planes were extracted. Then, larger portions of the point cloud (called macro-areas, see figure 3.b.), consisting of more than one plane, have been processed and 111 planes were identified. While the size of a micro-area is basically the same as the corresponding plane (usually from less than 1 $m^2$ to 10 $m^2$) macro-areas were selected encompassing a number of planes from 3 to 10.

Note that even in micro-areas, were the point cloud selection roughly correspond to a single discontinuity plane, Ransac is required to filter out those point not actually lying on the plane.

Both sets of planes were projected on a stereographic net by using the software Dips (by M. S. Diederichs and E. Hoek - Rock Engineering Group, Department of Civil Engineering - University of Toronto) and a statistic analysis was performed.

The comparison between the obtained stereonet, depicted in Figure 4, shows that the analysis performed by RANSAC on micro and on macro zones are in good agreement. This means that large areas can be selected without loss of information, since the algorithm will still identify, if not exactly the same planes, at least those defining the main families of discontinuities. Therefore, the work required to contour slope areas can be limited to macro-regions.

As a matter of fact, discontinuities identified on micro-areas show larger dispersions around the mean orientation values for each family. On the other hand too large macro-areas can sometimes result in the loss of minor joint systems.

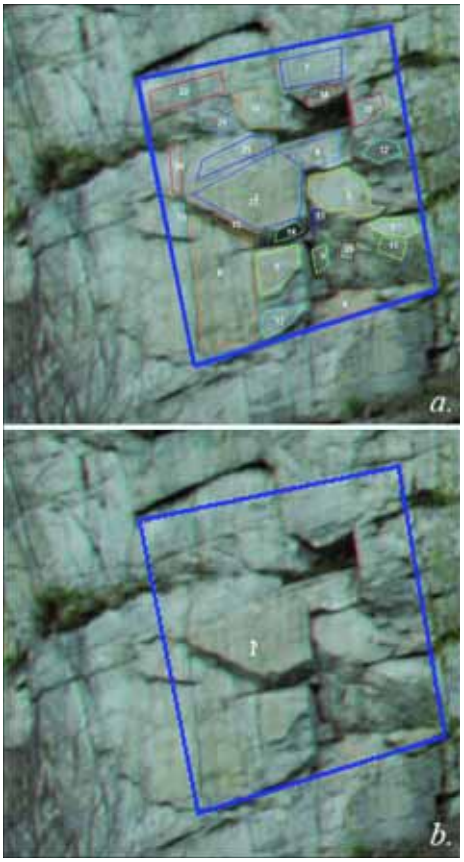


Figure 3. Subdivision of the rock surface in micro-areas (*a.*) and in macro-areas (*b.*).

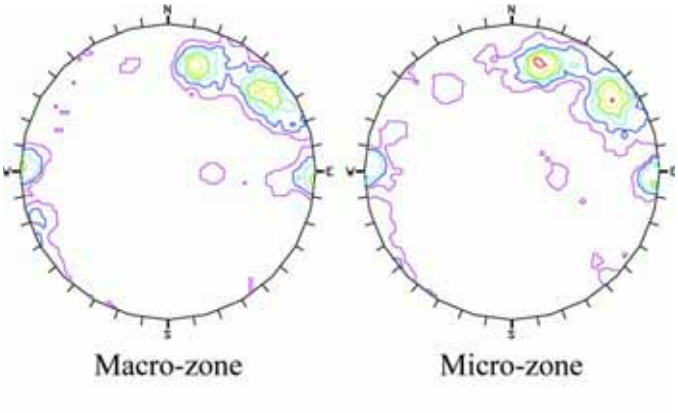


Fig. 4. Stereonet comparison between micro-zones and macro-zones selection.

Finally a comparison between traditional compass survey and photogrammetrical results has been carried out (Table 3 and Figure 5).

Table 3. Discontinuity joint set orientation obtained with traditional and photogrammetrical method.

| *Families* | Traditional survey | | ESP | |
|---|---|---|---|---|
| | *Dip* | *DD* | *Dip* | *DD* |
| **SCv1** | 75 | 140 | 78 | 143 |
| **J6-Scv2** | 75 | 195 | 73 | 200 |
| **J1** | 78 | 238 | 81 | 238 |
| **J2** | 10 | 50 | * | * |
| **J7** | 36 | 295 | 39 | 283 |
| **J8** | * | * | 89 | 271 |

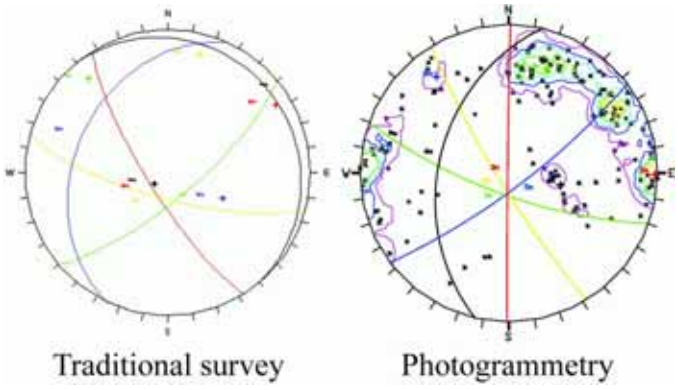


Figure 5. Discontinuity joint set orientation obtained with traditional and photogrammetrical method.

Figure 5 shows that all discontinuity families identified are in good agreement, apart from family J2. This is a sub horizontal family that cannot be captured by the images, since they were taken at the base of the slope, with camera stations nearly on the same horizontal plane: this is a poor geometry for the determination of points lying on horizontal planes, affected by occlusion or high perspective distortion. On the other hand sub-vertical Set J8 was identified by the photogrammetric restitution whilst it was neglected by the traditional survey, since it was confused with joint set J1 that has similar orientation. Joint set J8 plays an important role in the slope stability condition, since it determines the formation, together with J6, of the characteristic columnar structure in the right side of the slope.

A geometric reconstruction of the rock mass has been carried out by applying the code RESOBLOCK [18, 19].

Joint data have been implemented in the model: in a deterministic way on the slope surface where their position could be defined, and in a statistical way within the rock mass. Finally a model (Figure 6) composed of 1952 blocks representing a volume of 50x70x50 *m* has been set up.

Stability analysis has been carried out by the limit equilibrium method (LEM) running the code BSA (Block Stability Analysis) that is a part of the code Resoblok. A rock matrix unit weight of 27 $kN/m^3$ and a friction angle of 40° and 55° representing the peak and residual strength value of the discontinuity shear strength have been considered. The friction angle has been determined by direct shear tests performed in laboratory on natural discontinuities.

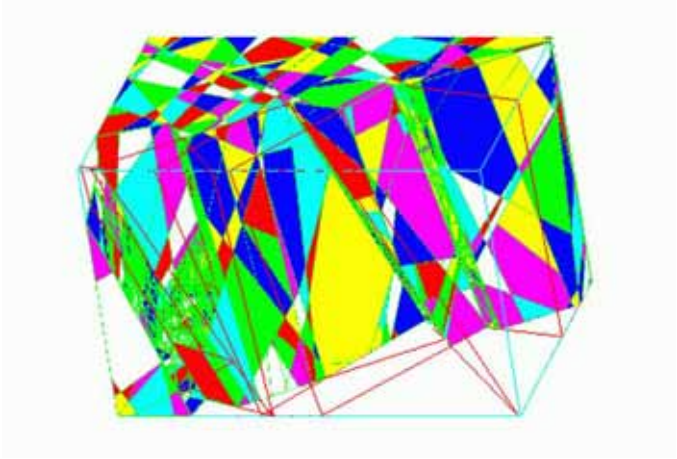

Figure 6. Blocks representing the geometrical reconstruction of Arnad pilot site by Resoblock application.

The slope appear stable for peak values of the friction angle, whilst both planar sliding and tridimensional sliding on joint set J1 e SCv1 and joint set J6 e J8 occurred for residual values. The kind of the kinematism identified by the stability analysis is in good correspondence with in situ observations.

The analysis results showed that the rock slope is in stable condition when shear peak values are available along the discontinuity planes, but when shear strength drops to residual values, several instability phenomena occur. This fact is confirmed by several blocks observed at the base of the slope. The global volume of blocks surveyed and measured at the base of the slope is about 4000 $m^3$ . This volume is of the same order of magnitude of the global volume of blocks computed by BSA.

Finally, on the basis of the same geometric model, a 3DEC (Itasca Consulting Inc., Minneapolis) model was set up (Figure 7), and the rock mass displacement were simulated. The DEM model showed the occurrence of the same kind of kinematisms identified by LEM and verified by in situ surveys.

However the results obtained with 3DEC needed a much longer computation time with comparison with the BSA results and in many cases convergence could not be reached without manually deleting falling blocks. Consequently, since the main aim of the modeling work was to determine the possible global volume involved in the instability, LEM analysis are suggested for future applications.

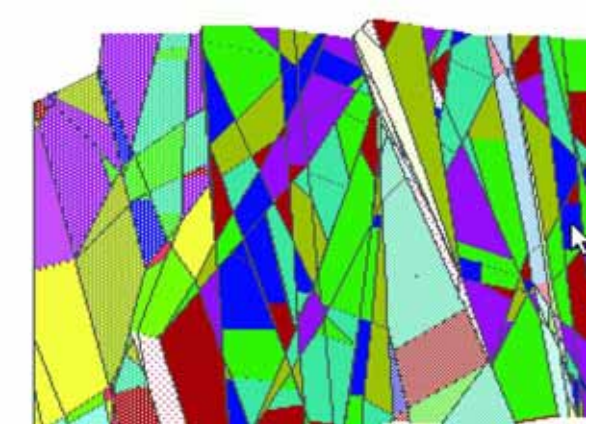

Figure 7. 3DEC model.

Figure 8. The “Falaise des Trappistes” test site.

*Application of laser scanner methodology*

The laser scanning technology has been applied at a rock slope denominate “Falaise des Trappistes” in the Valais region in Switzerland (figure 8.).

The area surveyed is about 100 m wide and 35 *m* high. Laser scanner measurements have been performed by the surveying group of the Politecnico di Torino, Department of Earth resources and land management, with a RIEGL LMS-Z420. Measurements have been made by 3 different positions in order to minimize occlusions. Digital images have also been taken by a digital camera Nikon D1X fixed to the laser scanner device. The survey was georeferenced in the mapping frame through 4 GPS stations.

Discontinuity planes have been extracted with a software (denominated LSR2004) specifically set up by the research group of the Politecnico of Torino, to obtain a 3D digital model of the slope.

The program allows one to read the coordinates of each point visible on the slope, to carry out virtual scanlines to determine discontinuity spacing, to select part of the image corresponding to a plane. In the last case the program computes the plane equation and its dip and dip direction by least squares.

About 200 planes were detected on the rock face. Comparison with traditional compass survey shows a good agreement (Table 4). Eight sets were identified (Figure 9) with the compass; six were identified by using with the laser survey. One of the missing families is sub horizontal and, consequently, it cannot be identified because the laser scanner station was located at the base of the slope. The second one is not visible on the part of

the slope that has been measured. Other scans on the East part of the slope should be considered to this aim.

Figure 9. Main discontinuity families in the Falaise des Trappistes.

Table 4. Discontinuity joint set orientation obtained with traditional and laser scanner method.

| *Families* | **Traditional survey** | | **LSR2004** | |
|---|---|---|---|---|
| | *Dip* | *DD* | *Dip* | *DD* |
| **S1** | 60-75 | 135-150 | 66 | 143 |
| **J1** | 40-65 | 45-65 | 76 | 46 |
| **J2** | 65-90 | 180-185 | 86 | 185 |
| **J3** | 60-85 | 320-350 | 90 | 160 |
| **J4** | 40-70 | 240-260 | 58 | 237 |
| **J5** | 70-85 | 90-105 | 76 | 78 |
| **J6** | 20-35 | 10-20 | - | - |
| **J7** | 45 | 5 | - | - |

## CONCLUDING REMARKS

It has been shown that both photogrammetric techniques and laser scanning can be applied to the geostructural survey of rock faces.

Both methods couple the surveyed point cloud with images of the slope; by an interactive software specifically developed, discontinuities can be identified and their dip, dip direction and position in the space computed.

In comparison with the traditional survey method, they provide a much larger wealth of information that remains available once back in the office. Additional measurements can be performed if deemed necessary, or previous ones can be checked; data can be collected and compared at different times for a quantitative evaluation of the rock slope stability condition. Survey of very large rock faces or of slopes not easily accessible is also allowed.

Comparison with measurements obtained by a traditional survey shows a good agreement, apart from the identification of horizontal planes due to the fact that all images were taken at the same level.

Finally, the proposed technique also enable the set up of rock mass 3D modeling for discontinuous approach. Both LEM and DEM model have been set up, showing as a deterministic reconstruction of the rock mass, like the one obtained by interfacing the survey results with the code Resoblock, can give a useful tool for understanding the rock mass mechanical behavior.

## REFERENCES


1. Harrison, J. P. and T. R. Reid. 2000. A semi-automated methodology for discontinuity trace detection in digital images of rock mass exposures. *International Journal of Rock Mechanics & Mining Sciences*. 37:1073–1089.
2. Kemeny, J., J. Monte, J. Handy and S. Thiam. 2003. The use of digital imaging and laser scanning technologies in rock engineering. In *Int. Symp. On the fusion Technology of Geosystem engineering, Rock engineering and Geophysical exploration, Seoul, Korea, 18-19 November*.
3. Feng, Q., P. Sjogren, O. Stephansson and L. Jing. 2001. Measuring fracture orientation at exposed rock faces by using a non-reflector total station. *Engineering Geology*. 59:133-146.
4. Vallet J., J. Skaloud, O. Koelbl and B. Merminod. 2000. Development of a Helicopter-based integrated system for avalanche and hazard management. In *IASPRS, 33(B2): 565-572, Amsterdam, Netherland.*
5. Forlani G. and L. Pinto. 1994. Experiences of combined block adjustment with GPS data. In *IASPRS, 30(3/1):219-226, Monaco, Germany*.
6. Grün A. and E. P. Baltsavias. 1988. Geometrically Constrained Multiphoto Matching. *PERS*, 54(5):663-671.
7. D'Apuzzo, N. 2003. *Surface Measurement and Tracking of Human Body Parts from Multi Station*

*Video Sequences*. Ph. D. thesis, Institute of Geodesy and Photogrammetry, ETH Zurich, Switzerland, Mitteilungen No. 81.

8. Grün A., F. Remondino and L. Zhang. 2003. Modeling and visualization of the Great Buddha statue in Bamiyan, Afghanistan. In *IAPRS, 34(5/W10), Tarasp-Vulpera, Switzerland*.

9. Besl P.J. and N.D. McKay. 1992. A method for registration of 3-D shapes. In *IEEE Transactions on Pattern Analysis and Machine Intelligence*, 14(2). February.

10. Roncella R., G. Forlani and F. Remondino. 2005. Photogrammetry for geological applications: automatic retrieval of discontinuity orientation in rock slopes. In *Videometrics IX – Eletronic Imaging – IS&T/SPIE 17th Annual Simposium,* pp. 17-27.

11. Remondino F. , A. Guarnieri and A. Vettore. 2005. 3D Modeling of Close-Range Objects: Photogrammetry or Laser Scanning? In *Videometrics IX – Eletronic Imaging – IS&T/SPIE 17th Annual Simposium,*pp. 216-225.

12. Beraldin, J. A. 2004. Integration of Laser Scanning and Close-Range Photogrammetry - The Last Decade and Beyond. In *IAPRS, 35(7), Istanbul, Turkey*.

13. Habib A., M. Ghanma and M. Tait. 2004. Integration of LIDAR and Photogrammetry for Close Range Applications. In *IAPRS, 35(5), Istanbul, Turkey*.

14. Golub, G. H. and C. F. Van Loan. 1989. *Matrix Computations*. 2nd ed. Baltimore, MD: The John Hopkins University Press.

15. Fischler M. and R. Bolles. 1981. Random sample consensus: a paradigm for model fitting with application to image analysis and automated cartography. In *Commun. Assoc. Comp. Mach.*, 24(3):81-95.

16. Torr P. H. S. and D. W. Murray. 1997. The Development and Comparison of Robust Methods for Estimating the Fundamental Matrix. *Internation Journal of Computer Vision*, 1-33, Kluwer Academic Publishers Boston.

17. Roncella R., G. Forlani. 2005. Extraction of Planar Patches from Point Clouds to Retrive Dip and Dip Direction of Rock Discontinuities. In *IASPRS 36(3W19): 162-167, Laser Scanning 2005, Enschede, Netherland*.

18. D. Hèliot D. 1988. Generating a Blocky Rock Mass. *Int. J. Rock Mech. Sci.& Geomech. Abstr.* 25(3):127-138.

19. Hèliot D. 1988. *Conception et Réalisation d'un Outil Intégré de Modélisation des massifs Rocheux Fracturés en Blocs*. Ph.D. Thesis, Institut National Polytechnique de Lorraine.

# The use of LiDAR to overcome rock slope hazard data collection challenges at Afternoon Creek, Washington

Stroth, A. and Eberhardt, E.
*Geological Engineering/EOS, University of British Columbia, Vancouver, Canada*

Copyright 2006, ARMA, American Rock Mechanics Association

This paper was prepared for presentation at the workshop: "Laser and Photogrammetric Methods for Rock Face Characterization" organized by F. Tonon and J. Kottenstette, held in Golden, Colorado, June 17-18, 2006.

This paper was selected for presentation by F. Tonon and J.T. Kottenstette following review of information contained in an abstract submitted earlier by the author(s). Contents of the paper, as presented, have not been reviewed by F. Tonon and J. Kottenstette, and are subject to correction by the author(s). The material, as presented, does not necessarily reflect any position of USRMS, ARMA, their officers, or members. Electronic reproduction, distribution, or storage of any part of this paper for commercial purposes without the written consent of ARMA is prohibited. Permission to reproduce in print is restricted to an abstract of not more than 300 words; illustrations may not be copied. The abstract must contain conspicuous acknowledgement of where and by whom the paper was presented.

**ABSTRACT:** Obtaining a thorough and accurate rock slope characterization data set can be very costly or impossible when the critical slope exposures are inaccessible or hazardous. To overcome these challenges a terrestrial-based LiDAR scanner was used to collect a 3-D point cloud model of one such slope near Newhalem, Washington, from which initiated the 2003 Afternoon Creek rockslide. This paper reports on the methodology and analysis techniques used to collect the 3-D point clouds, and extract the orientation, spacing, and persistence of important discontinuity sets. It includes a discussion of the benefits and limitations of these methods, as well as practical recommendations based on this case study.

## INTRODUCTION

Accurate rockslide characterization is difficult, in part, because of the large degree of uncertainty regarding the spatial and physical properties of the unstable rock mass, including, but not limited to, the geometry and interconnectivity of controlling discontinuities, and mechanical properties of the discontinuities and rock mass. This uncertainty can be reduced (although not eliminated) by a thorough and accurate site investigation and data collection program. The traditional data collection program for a hazardous rock slope typically involves discontinuity orientation measurements through scan-line survey and outcrop mapping. However, obtaining a thorough and accurate data set can be costly or impossible, especially when the critical slope exposure is steep, high, hazardous, or in other ways inaccessible.

To overcome these challenges, a terrestrial-based, Light Detection And Ranging (LiDAR) scanner was used to collect discontinuity and rock mass characterization data on a steep, inaccessible, hazardous rock slope, at the site of a recent rockslide near Newhalem, Washington. The November 9, 2003 Afternoon Creek rockslide involved a volume of approximately 750,000 $m^3$, a portion of which fell more than 600 meters in elevation down a steep slope onto Washington State Route 20 (SR 20), an important route through the North Cascade Mountains. The slope continues to threaten SR20 due to potentially unstable material at the top ridge formed by the earlier event. The slope is large, and exceptionally steep. Access to the unstable zone is extremely limited, requiring workers to be dropped at the top by helicopter and then use ropes to rappel down, and maneuver around the main failure escarpment.

LiDAR scans were performed, with an Optech ILRIS-3D laser scanner, from several vantage points ranging from 100-m to 1,000-m distance to the slope face. The result of each laser scan is a three-dimensional point cloud of the scanned surface from which discontinuity orientation,

persistence, and spacing data were extracted. This paper reports on the methodology and analysis techniques employed to characterize the structural patterns of the Afternoon Creek rock slope, using the results of a terrestrial-based LiDAR survey. It includes a discussion of the benefits and limitations of these methods, and practical recommendations based on the case study.

## BACKGROUND

On November 9, 2003, the Afternoon Creek rockslide occurred near Newhalem, Washington [1]. Most of the rock avalanche debris (approximately 750,000 $m^3$) traveled more than 300 meters in elevation down a steep slope and landed in the narrow, steep-walled Afternoon Creek valley. The leading edge of the material flowed approximately 500 meters in horizontal distance from the center of the source area, but did not reach the nearby Washington State Route 20 highway. The dry, very-coarse granular slide deposit is composed of orthogneiss boulders ranging in size from 1-m to 25-m in diameter. The source area for the failure lies at the top of a steep ridge. This topographic control allowed lesser amounts (<10%) of the debris to travel down the back side of the ridge into Falls Creek and Falls Creek Chute. This debris traveled more than 600-m in elevation down a steep slope and landed on SR 20, an important route through the North Cascade Mountains. Portions of the roadway and guardrail were destroyed and boulders up to 4-m in diameter were deposited on the road. The Afternoon Creek slope continues to threaten SR 20 due to potentially unstable material at the top ridge (Fig. 1).

Analysis of the Afternoon Creek rockslide is in progress at the University of British Columbia. The primary tools for the analysis are discontinuum-based numerical modeling codes, e.g. UDEC and 3DEC [2], and the dynamic runout simulation code DAN3D [3]. The objectives of the analysis are to: (1) advance the current understanding of the operative slope deformation and failure mechanisms; and (2) investigate how slope deformation and failure mechanisms relate to runout path, distance, and velocity. The geometry of the topography and discontinuities, including orientation, spacing, and persistence, is a required component of the numerical modeling input.


Fig. 1 Afternoon Creek rockslide above SR 20 near Newhalem, WA. Photograph provided by John Scurlock.

Several traditional methods for characterizing the discontinuity pattern were considered including a scan line and window surveys in the failure zone; however these methods were quickly deemed insufficient as access to important areas near the top of the slope was limited by the steepness of the slope and the hazard of rock falls in the working area (Fig. 2). One alternative would have been to transport workers to the top of the failure zone by helicopter, and then have them use ropes to rappel down, and maneuver around the main failure escarpment. Drawbacks to this alternative were the associated costs (both in terms of money and time), and the risk of injury posed to workers. Therefore a second alternative involving terrestrial based LiDAR was explored and adopted.

## METHODS

LiDAR represents a key technological development that improves our capacity to collect reliable rock mass and landslide data [4-7]. Several researchers have been exploring and developing 3-D laser mapping methodologies specifically for rock mass characterization and discontinuity analysis [8-10]. Three-dimensional 'point clouds' and digital images of the scanned sections of the Afternoon Creek rock slope were captured with an Optech ILRIS-3D laser

Fig. 2 Photograph of the Afternoon Creek rock slope from Afternoon Creek (August, 2005).

scanner. The point clouds were visualized, and discontinuity description data extracted using Split-FX™ beta version 1.0, developed by Split Engineering LLC.

*Terrestrial LiDAR Scanning*

A total of 21 terrestrial LiDAR scans of the Afternoon Creek and Falls Creek Chute slopes were attempted. These scans were completed from five different stations in the Afternoon Creek deposit zone, and from two stations on the slope south of the Skagit River (Table 1; Fig. 3). Several of these scans involved repeat surveys of the same area but at different distances and resolutions in order to test the limits of the instrument and compare the quality of the resulting 3-D point cloud.

For each scan, the LiDAR scanning unit was positioned on a tripod, leveled (perpendicular to the line of sight), and aimed at the desired location on the slope. The plunge and trend of the instrument's line-of-site was then measured. This information was used in the data reduction phase of analysis to orient the point cloud with respect to true North. The scanner was connected to a laptop via a wireless connection. Using the controller software, the digital camera settings of the instrument were adjusted for the present lighting conditions, and the region to be scanned was selected. The point cloud resolution was set by adjusting the 'spot-spacing', which is a parameter that defines the scan density. A small spot-spacing provides high resolution, while a large spot-spacing provides low resolution. Point cloud data is collected by the instrument at a rate of 2,000 points per second [11], allowing a typical scene of a few million data points to be captured in 10 – 20 minutes.

For useful, high quality point clouds, the strike-line of the target area should be approximately perpendicular to the line-of-sight of the scanner, and the target should be within the maximum operating range of the instrument. The relative quality of each scan, shown in table 1, describes the usefulness of the point cloud. 'Good' quality point clouds exhibit complete point coverage of the target area with sufficient resolution for data analysis. A 'very poor' quality point cloud means that few spot reflections were received by the instrument; therefore the resolution of the resulting point cloud is so coarse that no useful joint orientation data can be extracted. Very poor quality point clouds typically resulted from scans used to test the limitations of the instrument, when the station to target distance exceeded 1000 m.

Ideally, the entire failure scarp and other areas of interest would have been scanned at a similar resolution from several angles with considerable overlap; this would have enabled the different point clouds to be joined, creating a single 3-D model of the entire slope. A single, continuous point cloud would have made the data processing and analysis simpler, and more objective. However, in this case, overlapping data from all portions of the failure scarp was not collected because access was limited to the narrow Afternoon Creek channel.

Good quality point clouds for the failure scarp were collected from Stations 2, 6, and 7; however Stations 6 and 7 were too close to the failure scarp to allow for the entire zone to be captured, and therefore the resulting point clouds do not overlap. The Station 6 and 7 scans do however provide data for shadowed portions of the point cloud from the Station 2 scan. Another limitation imposed by the narrow confines of the Afternoon Creek channel was that the scanner was steeply inclined when

directed towards the base of the failure scarp; 'false' summits in the failure scarp created a complete shadow of the upper portions of the failure zone. This shadow could have been removed by performing a scan midway up the valley wall opposite the failure scarp; however no safe access path or setup point could be found.

Table 1 LiDAR scans attempted.

| survey station/ scan | target | spot spacing | approx. distance* (m) | approx. resolution (cm) | relative quality |
|---|---|---|---|---|---|
| 1/1 | failure scarp | 7 | 600 | 11 | moderate |
| 1/2 | lower slope | 20 | 300 | 16 | good |
| 2/1 | failure scarp | 8 | 500 | 11 | good |
| 2/2 | failure scarp | 15 | 500 | 20 | moderate |
| 2/3 | failure scarp | 30 | 500 | 40 | moderate |
| 3/1 | scanline 1 | 60 | 60 | 10 | moderate |
| 3/2 | scanline 1 | 20 | 60 | 3 | good |
| 3/3 | scanline 1 | 20 | 50 | 3 | good |
| 3/4 | scanline 1 | 20 | 50 | 3 | good |
| 4/1 | failure scarp | 10 | 1000 | 27 | very poor |
| 4/2 | Falls Creek runout path | 10 | 300 - 1000 | 8 - 27 | poor |
| 5/1 | failure scarp | 10 | 1000 | 27 | very poor |
| 5/2 | lower slope | 10 | 500 | 13 | good |
| 5/3 | Falls Creek runout path | 10 | 750 | 20 | moderate |
| 5/4 | range test | 10 | > 1200 | 32 | very poor |
| 5/5 | range test | 10 | > 1500 | 40 | no data |
| 6/1 | failure scarp - zone 3 | 16 | 250 | 11 | good |
| 7/1 | failure scarp - zone B, zone 3 | 20 | 150 | 8 | good |
| 7/2 | failure scarp - zone 3 | 20 | 100 | 5 | good |

*This is the estimated line-of-sight distance from the scanner station to the center of the target.

*Laser Scanning Data Processing*

Split-FX™ software, developed by Split Engineering LLC, was used to orient and visualize the 3-D point clouds, and extract the orientation, spacing, and persistence of dominant discontinuity sets. Ideally, overlapping point clouds would have been merged into a single, comprehensive point cloud of the entire slope using a program such as PolyWorks®, developed by InnovMETRIC Software Inc. However since the collected point clouds did not have sufficient overlap, each scan's point cloud was analyzed separately. Nine scans of various portions of the failure scarp were completed; however only four scans were considered to be of sufficient quality to be incorporated into the analysis: 2/1, 6/1, 7/1, 7/2 (see Table 1).

The remaining five scans were not used because they were either 'very poor' quality or coarser resolution copies of one of the included scans. Each of the four point clouds was processed and analyzed in the same way using the following procedure (Fig. 4):


Fig. 3 Terrestrial LiDAR scanning stations.

(i) Orient the point cloud. Input the true bearing of the scanner's line of sight and components of tilt (as measured in the field at the time of scanning).

(ii) Edit the point cloud. Remove points that are not related to joint orientation (e.g. reflections from vegetation, talus, soil-cover, etc.).

(iii) Create a mesh. The Split-FX™ software drapes a polygonal surface mesh over the point cloud. The analyst decides the mesh grid size, which controls the size of the cells, the number of points per cell, and the precision of the polygonal surface model [12].

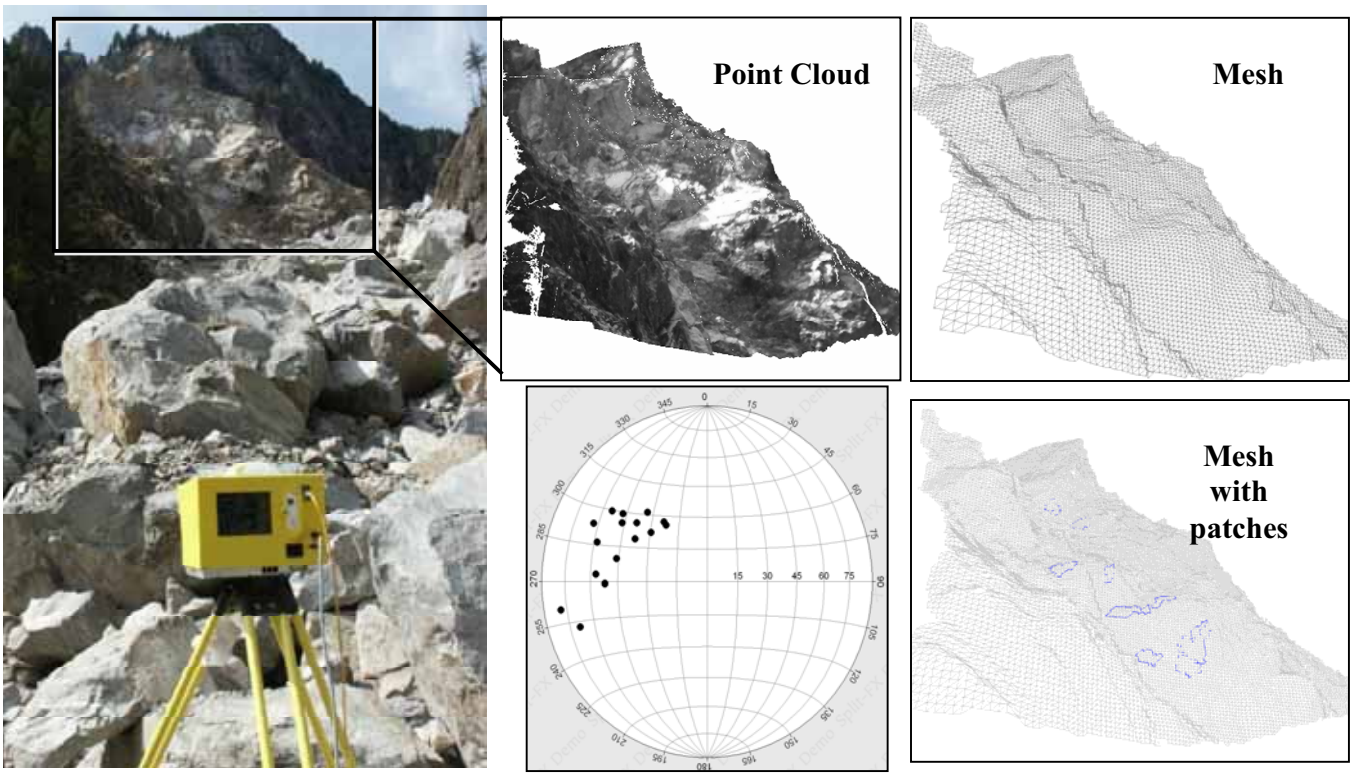


Fig. 4 Point cloud processing procedure.

(iv) Automatic patch generation. Patches are planes fit to the discontinuity surfaces present in the point cloud. Patches are found first by grouping neighboring mesh triangles together based on the similarity of their vector normals, and then by using least squares to fit a plane through the points bounded by the grouped triangles [12]. User controls include the *minimum patch size* and *maximum neighbor angle,* which is the tolerance used to group neighboring mesh triangles.

(v) Edit patches. The analyst visually inspects the patches and deletes erroneous patches and adds missing patches, if necessary.

(vi) Stereonet Analysis. The patch orientation, size, and roughness are recorded by the software. These can be exported to any stereonet analysis package or analyzed with the Split-FX™ stereonet software.

A bias is introduced to the final data set through discontinuity surfaces that are small relative to the point spacing and mesh size; these will not be sampled by the method described above. This biasing is unavoidable, although the influence of the small, unsampled discontinuities can still be accounted for by the designation of rock mass quality.

*Laser Scanning Data Analysis*

To determine the influence of the mesh density and patch control parameters on the processing accuracy, with respect to the true joint surfaces measured, a qualitative parametric study was conducted. The mesh density recommended by the software manual yields approximately 30 points per mesh grid cell. The results of the parametric study showed that this was a valid point density for the Afternoon Creek slope. A coarser mesh density missed capturing important (small) features of the rock slope, whereas a finer mesh did not add any features of significance to the data set. Also the finer mesh resulted in more patches that were smaller in size, that in turn were more difficult to visually inspect.

The minimum patch size parameter is used to filter out small patches that are difficult to visually inspect and which add significant noise to the stereonets. This parameter was typically set to a value between 10 and 40 grid cells per patch. The maximum neighbor angle determines which grid cells are included in the patch. This parameter was typically set to a value between 4º and 8º. A value less than 4º typically yielded very few patches, and

excluded surfaces in the point cloud that were obvious joint surfaces. A value greater that 8º typically yielded numerous erroneous patches that were removed during visual inspection. When a relatively fine mesh density was used the minimum patch size and maximum neighbor angle were typically set to the upper end of the described ranges.

*i. Discontinuity Orientation*

Each joint set was defined by its orientation. The pole to each patch was automatically plotted on a stereonet. Joint sets were visually identified and then defined on the stereonet. The visual identification of the sets was verified by contouring the poles, and by highlighting all of the patches within a set and then visually inspecting the patches on the point cloud image. The selection of joint sets was repeated and compared for a range of minimum patch sizes and maximum neighbor angles.

Two joint sets were found (designated sets A and B). The average dip direction/dip angle of joint set A is 116/51 with standard deviation 10/9 (Fig. 5). Planar sliding is a kinematically feasible failure mode for this joint set, and is proposed as the primary failure mechanism in the November, 2003 slope failure. The automatically generated patches of joint set A are plotted as poles in figure 5 with the pole size proportional to the patch area. Joint set A patches typically have a large surface area (Fig. 5), indicating that these joints are highly persistent and relatively smooth.

The average dip direction/dip angle of joint set B is 57/61 with standard deviation 9/8 (Fig. 5). These discontinuity surfaces provide the lateral release necessary for planar sliding on joint set A. Failure of wedges formed by joint set A and B is also kinematically feasible. In terms of persistence, the automatically generated patches were typically small. However, when the maximum neighbor angle was increased to 10º during automatic patch generation, the joint set B patches were found to be as persistent as those for joint set A. Visual inspection confirmed that the patch size determined by the automatic procedure was artificially small due to the rough and undulating texture of these surfaces, and in fact, the joints were highly persistent.

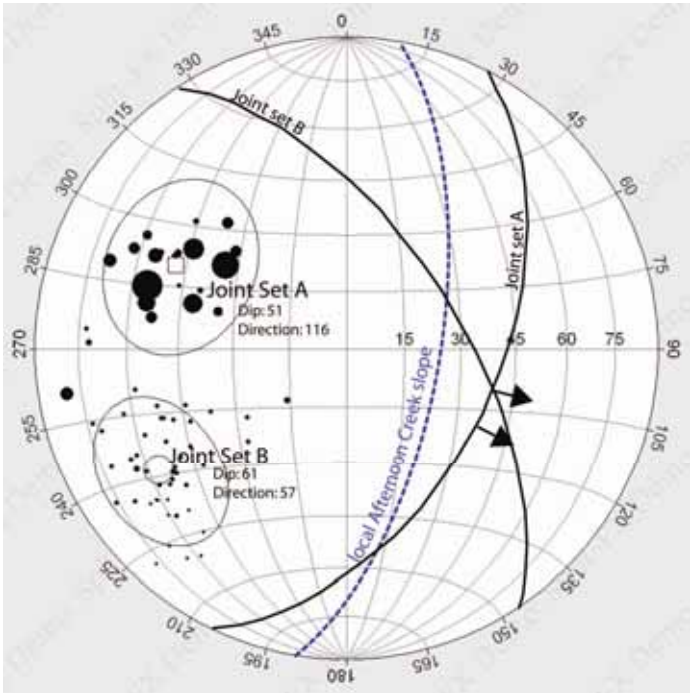


Fig. 5 Equal area, lower hemisphere stereographic projection of automatically generated patches (minimum size = 20, maximum neighbor angle = 6º) in point clouds 2/1, 6/1, 7/1, 7/2. Pole size is scaled to patch area. Joint set orientation is the average orientation of poles included in the set.

*ii. Discontinuity Set Spacing*

The average spacing of joints within a set was estimated by inserting a "virtual scan line" of known length into the point cloud approximately normal to the joint set, and counting the number of joints belonging to the set that crossed the line. Split-FX$^{TM}$ was used for the entire procedure. In detail, the procedure involved the following:

**(i)** Isolate patches belonging to the same joint set. This involves an initial grouping based on the stereonet analysis and pole plot contouring, and then visually inspecting and deleting all patches that do not belong to the joint set of interest.

**(ii)** Record the average orientation of the joint set in terms of its unit normal vector, *n*.

**(iii)** Insert the scan line. The scan line should be contained within parts of the cloud that are highly populated with points. Select a point on the slope at the beginning and end of the scan line; these two points define the line. Orient the scan line so that it is approximately perpendicular to the joint set.

(iv) Record the unit vector in the direction of the scanline, *l*; and the length of the scanline, L.

(v) Orient the point cloud so that the entire scan line is visible. Select all patches (i.e., joint planes) that intersect the scan line.

(vi) Count the number of patches (N) that intersect the scan line.

(vii) The average true spacing (s) can be approximated with eq. 1, where θ is the angle between the vectors *l* and *n*:

$$s = \frac{L * \cos\ \theta}{N}\ ; \qquad (1)$$

Where,

$$l \bullet n = |l||n| * \cos\theta\ . \qquad (2)$$

The average spacing of joint sets A and B was estimated using this virtual scanline technique. Six scan lines were considered, for which the average spacing of joint set A ranged from 4 to 7 meters. The average spacing of joint set B was estimated with six additional virtual scan lines. Joint set B spacing was considered at two different scales based on distinctions made with respect to persistence (see next section). Within set B, several joints were observed to be highly persistent (on the scale of the entire rock slope). The average spacing for these joints ranged from 12 to 15 meters. The spacing of the less persistent planes within set B was found to range from 3 to 5 meters. The highly persistent, widely spaced plane B zones appear to be more important in terms of the overall slope stability.

*iii. Discontinuity Persistence*

No feature is currently present within Split-FX™ to automatically calculate persistence. As such, the following three methods were considered for estimating the average persistence of joints within each set: (1) measure trace length on oblique photographs; (2) measure the maximum dimension of exposed planes in the 3-D point cloud; (3) relate the persistence to area of patches in the 3-D point cloud. Each method involved measuring all of the visible discontinuities in the point cloud that meet some size and orientation criteria, and then assuming that the average persistence is equal to the mean of the measurements.

The first method was to identify representative discontinuities for the different joint sets in digital photographs taken of the slope, and then calculate their trace lengths. The scale of the rock slope in the photograph is a function of the distance between the rock slope and the camera lense. However, it was difficult to keep track of these distances/scales. Photographs of the Afternoon Creek slope have a widely varying scale because the slope is composed of numerous benches and near-vertical faces and because many of the photographs were taken at an oblique angle to the slope. Where possible, the scale was estimated by the height of trees. However trees do not exist within the main failure scarp. Split-FX™ has a function that estimates trace length based on a user defined scale. The program assumes that the photographed rock face is a single continuous slope. Photographs of the Afternoon Creek slope generally do not meet this assumption. In some cases, photographs of smaller portions of the slope do meet this assumption; however the smaller frame of reference means that many of the discontinuity traces are truncated. Overall, this method was able to provide an estimate of discontinuity trace length, but the accuracy of those estimates is suspect.

The second and third methods applied were based on the dimensions of exposed planes in the 3-D point clouds. Cracks in an otherwise flat rock face can not be seen in most point clouds. Therefore joint traces that are obvious in photographs are invisible in the point cloud. The term "*exposed persistence*" was adopted in recognition that the joint may be more persistent than that suggested by the plane exposed/visible on the slope face. In this sense, the exposed persistence can be treated as an estimate of the minimum persistence, or lower bound of the average persistence for each particular joint set.

'Method 2' involved the direct measurement of the exposed persistence. The average exposed persistence was assumed to be the mean of the measurements. Accurate measurement of the joint dimensions is made possible by selecting points on the surface of the discontinuity and then calculating the distance between them. This method is similar to 'Method 1' in that it requires good geological engineering judgment when selecting, and measuring relevant discontinuity surfaces; however distance measurements on the point cloud are far

more accurate than persistence measurements made on the photographs.

'Method 3' was an attempt to partially automate the procedure for estimating exposed persistence. The implied assumption is that there is a relationship between the area of the exposed discontinuity plane and the exposed persistence of the discontinuity. In the Afternoon Creek point clouds, the patches (i.e., the discontinuity planes) appear to be rectangular in shape; therefore the relationship between area and exposed persistence ('*ep*') is based on a subjective estimate of the aspect ratio (*A*) of most of the patches. The area of the patch is equal to the aspect ratio times the square of the minimum dimension (*x*) (Fig. 6). Given the aspect ratio and area of the patch, the minimum dimension (*x*) is found with Equation 3. An estimate of the exposed persistence is easily calculated using Equation 4.

$$x = \sqrt{\frac{Area}{A}} \tag{3}$$

$$ep = \sqrt{x^2 + (Ax)^2} \tag{4}$$

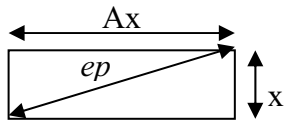


Fig. 6 Schematic, annotated patch.

Problems with 'Method 3' are that it requires the patches to be rectangular in shape, and the aspect ratio to be accurately estimated for all of the patches. Additionally, the patches must completely cover the exposed joint surfaces in the point cloud, a condition that is not often met by the automatic patch generator. This necessitates that the patches be manually adjusted, a procedure that requires considerable time and effort.

In summary, based on these experiences, it was found that it was easier to directly measure the *exposed persistence* using 'Method 2'. 'Method 1' was ineffective in measuring the persistence of joint set B as set B strikes parallel with the rock face and therefore did not form prominent traces in the photographs. Table 2 is a comparison of the mean persistence/exposed persistence and standard deviation obtained by the three methods for the Afternoon Creek rock slope.

Table 2 Estimates of persistence and exposed persistence for joint sets A and B in the Afternoon Creek slope.

| Joint sets | | mean persistence (meters) | mean *exposed persistence* (meters) | standard deviation (meters) |
|---|---|---|---|---|
| **A** | Method 1 | 28 | n/a | 14 |
| | Method 2 | n/a | 42 | 28 |
| | Method 3 | n/a | 34 | 17 |
| **B** | Method 1 | ** | n/a | ** |
| | Method 2 | n/a | 84 | 20 |
| | Method 3 | n/a | 50 | 15 |

** Trace of joint undetectable as the joint set strikes sub-parallel to the rock face/photographs.

*Data Use in Slope Instability Analysis*

Two-dimensional and three-dimensional distinct element numerical models were the primary tools used in the back analysis of the November, 2003 rockslide at Afternoon Creek. Since it was impractical to collect all of the data necessary to replicate the slope with the numerical models, they were used to perform parametric studies to better understand the physical properties of the slope, and the failure mechanism. Accurate estimates of discontinuity set orientation, spacing, and persistence helped to constrain the models, and the interpretation of the failure mechanism.

The average orientation and spacing of the two joint sets were important parameters for all numerical models. The average orientation and spacing were incorporated in baseline models. The orientation of the sets was varied to one standard deviation during parametric studies. The spacing of each joint set was increased during many of the parametric studies to reduce the total number of discrete blocks. The shape of the blocks was maintained during these studies by increasing the spacing of both joint sets by an equivalent amount. The joint set persistence was not explicitly used in the UDEC

and 3DEC analyses because fully persistent discontinuities were used to create a network of discrete blocks before each simulation began. However an understanding of the persistence of critical discontinuities (with respect to the size of the slope) was important for interpreting the results of the simple, idealized models.

The UDEC (Fig. 7) and 3DEC models suggested that the failure mechanism of the November, 2003 rockslide was planar sliding on joint set A discontinuities. Joint set B provided rear and lateral release for sliding. Tensile failure of the rock mass provided rear release for sliding, and caused disintegration of the failure volume.

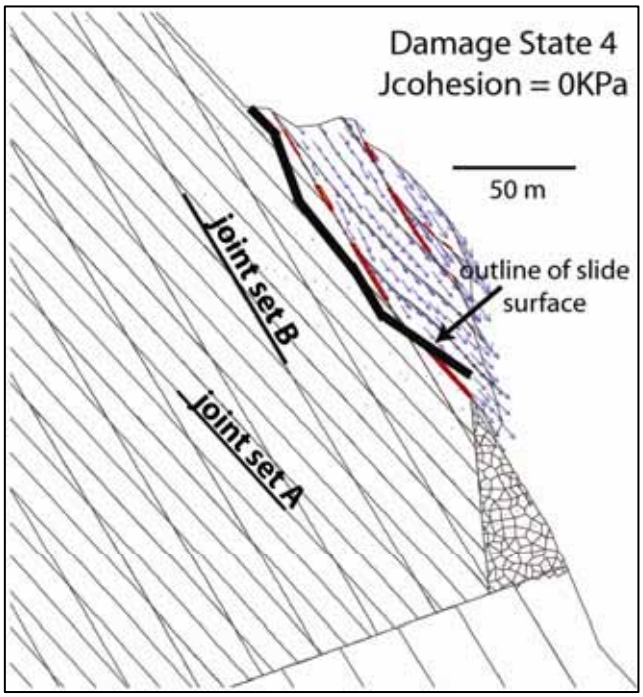


Fig. 7 Example UDEC model of the Afternoon Creek slope showing joint sets A and B.

## DISCUSSION AND CONCLUSIONS

A chief purpose of this paper is to provide practical recommendations in relation to collecting and processing terrestrial LiDAR data. The following comments describe the benefits and limitations of LiDAR as a tool for rock mass and discontinuity characterization, as experienced through this case study.

### *Benefits*

**(i)** *The only feasible method*: When the rock slope of interest is inaccessible or dangerous, remote sensing methods provide the only feasible means to collect rock mass and discontinuity data. This was the case for the Afternoon Creek rock slope, for which the orientation of key joint sets was obtained through LiDAR point cloud analysis. It was more accurate to measure joint spacing and persistence from point clouds than single, oblique photographs.

**(ii)** *Time savings*: A complete data set can be collected and processed significantly quicker with the LiDAR survey and point cloud analysis as opposed to traditional scan-line and window surveys. A typical scan of the Afternoon Creek slope, including setup, took less than 60 minutes. A simple analysis of the point cloud also took less than 60 minutes. A full mapping survey of the slope, consisting of several scanlines, generally takes an entire day. Additional time would then be required to manually process and plot the data.

**(iii)** *Complete, objective, reproducible data set*: A LiDAR survey creates a digital 3-D model of the target. This model is a complete data record that can be revisited months or years later. Questions about the geometry of the slope surface, long after the field work has been completed, can be answered by inspection of the digital point cloud rather than requiring an additional site visit.

**(iv)** *Automation of analysis procedures*: Some of the point cloud analysis steps, such as recognizing joint planes, calculating orientations, and calculating exposed persistence, can be fully or partially completed automatically by the analysis software. These automated procedures save time and can find joint surfaces that would otherwise be overlooked by the analyst. The potential exists to automate other aspects of the analysis as well. It should be stressed though that the automatic procedures should only be used as tools; they can not replace the judgment or expertise of the analyst. Each step involving an automated procedure should be carefully inspected and modified as necessary.

### *Limitations*

**(i)** *Survey locations:* Survey stations must be positioned at a suitable distance from the target, and the line-of-sight between the survey station and target must be unobstructed. The effective range of the Optech ILRIS-3D scanner for the case study presented above was about 600-m; however we suspect that useable data can be collected from distances of up to 800-m if scans are attempted at the highest possible resolution, and the atmosphere between the scanner and target is clear. This

maximum range also depends on the target reflectivity; the relationship is described by Optech [11]. Also it is important that the survey stations are not too close to the target. This was a problem for many of the scans where the close proximity of the instrument to the rock face, as forced by the narrow confines of Afternoon Creek, did not allow the point clouds to overlap, and therefore a single slope model could not be formed.

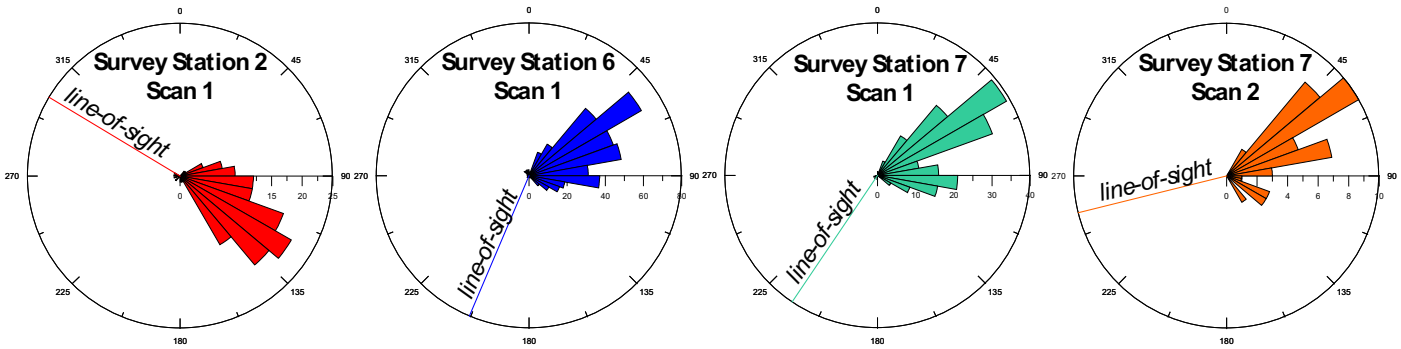


Fig. 8 Histograms of dip direction vs. frequency for four scans of the failure scarp showing a bias in the orientation of automatically generated patches. Joint planes that strike perpendicular to the scanner position tend to reflect more laser strikes. Line-of-sight of the scanner is superimposed over the histogram.

**(ii)** *LiDAR scanning can not replace actual observation of a rock slope:* A 3-D point cloud is useful for making orientation and distance measurements; however it can not be used to describe the rock strength, roughness, weathering characteristics, seepage conditions, or infilling/aperture of joints. Manual field observations are required in addition to LiDAR scanning to adequately characterize a rock mass.

**(iii)** *Sample Bias*: Discontinuities which do not form sufficiently large exposed surfaces are not sampled with the LiDAR methods used in this study. This may include highly-persistent, important cracks that would easily be recognized and sampled with traditional techniques, however are invisible in the LiDAR point cloud. Exposed surfaces that are small relative to the point spacing and mesh size are not sampled.

Additionally, surfaces that strike sub-parallel to the line-of-sight of the scanner tend to reflect few laser strikes; therefore joint sets that strike parallel are poorly sampled, while sets that strike perpendicular are well sampled, introducing a bias to the final data. This point is illustrated by Figure 8, showing rose diagrams of automatically-generated patches found in four different point clouds of the failure scarp. Joint set A surfaces were preferentially recognized in the scan from survey station 2 because this joint set was orthogonal to the scanner line-of-sight. Joint set B surfaces were preferentially recognized in the scans from survey stations 6 and 7. This bias can be removed by scanning the target from all possible angles and analyzing all of the scans (either individually or by aligning the scans into a single point cloud).

*Recommendations*

**(i)** *Accurately measure the orientation of the LiDAR scanner for each survey*: For point cloud analysis, the orientation of surfaces in the point cloud is based on the line-of-sight and tilt of the scanner. Any error in the recorded scanner orientation will be projected to all of the joint orientation measurements derived from the point cloud.

**(ii)** *Check the digital photograph quality*: The Optech ILRIS-3D scanner records a digital photograph with the point cloud. The included camera does not automatically adjust to optimum settings for photograph quality. The photographs are important for visualization of the rock slope, as well as for estimating joint persistence and spacing.

**(iii)** *Consider the weight and bulk of the instrument when designing a LiDAR survey*: The Optech ILRIS-3D laser scanner can be carried by one person on foot; although due to its weight and bulk, carrying the scanner across rough terrain (e.g. bouldery, rock avalanche debris) can be very challenging as was the case with the Afternoon Creek rock slope survey. In such cases, it may

require two people and longer setup times to move equipment and perform the survey.

**(iv)** *Consider the weather when designing a LiDAR survey*: Clouds, fog, smoke, or haze in the air between the instrument and the survey target do affect the results of the survey. This effect depends on the survey distance, and density of the cloud. During the Afternoon Creek survey, only one survey was completed during a period of light rain; however as the setup point was only 100-m from the rock face, little to no affect was detected in the survey results.

**(v)** *The area of interest should be scanned from several different angles*: The laser scanner is a line-of-sight instrument, meaning that the position of the first object in the laser's path is recorded. Therefore small (and large) variations in topography, and vegetation create shadows – i.e. areas where no data is collected - in the resulting point cloud. Additionally, surfaces that strike sub-parallel to the line-of-sight of the scanner tend to serve as poor reflectors; therefore joint sets that strike parallel are poorly sampled, while sets that strike perpendicular are well sampled introducing a bias to the final data (Fig. 8). The area of interest should be scanned from several different angles to remove this bias and to collect data that would otherwise be masked by shadows.

**(vi)** *Overlapping point clouds should be aligned to form a single model of the slope*: The data analysis phase of the investigation is simplified and more comprehensive when a single model of the entire slope is used. Joint surfaces are truncated at the boundary of each point cloud scan. The number of truncated discontinuity surfaces can be minimized by aligning overlapping point clouds. Estimates of discontinuity persistence and spacing are most accurate when the entire rock slope is considered. Note that several scans from different angles are required to align overlapping point clouds.

**(vii)** *Inspect and edit the automatic discontinuity characterization results*: Automatic routines for identifying joint surfaces and estimating persistence are quick, objective, repeatable and capable of finding joint surfaces that otherwise are not obvious; however they can not replace the expertise of a trained engineer or geologist. The 'patches' that are automatically generated by programs like SplitFX$^{TM}$ must be inspected and edited as necessary. Some patches may need to be altered, others will need to deleted or added.

REFERENCES


1. Stroth, A., Burk, R.L., and Eberhardt, E. 2006. The Afternoon Creek rockslide near Newhalem, Washington. *Landslides*. Online First.
2. Itasca, *UDEC: User's Guide (Version 3.1)*. 2000, Minneapolis: Itasca Consulting Group.
3. McDougall, S. and Hungr, O. 2004. A model for the analysis of rapid landslide motion across three-dimensional terrain. *Canadian Geotechnical Journal*. 41: p. 1084-1097.
4. Alba, M., et al. Feasibility and problems of TLS in modeling rock faces for hazard mapping. in *ISPRS WG III/3, III/4, V/3 Workshop "Laser scanning 2005"*. 2005. Enschede, the Netherlands.
5. Pringle, J., Gardiner, A., and westerman, R. 2004. Virtual geological outcrops - fieldwork and analysis made less exhaustive. *Geology Today*. 20(2): p. 67 - 72.
6. Rowlands, K.A., Jones, L.D., and Whitworth, M. 2003. Landslide Laser Scanning: a new look at an old problem. *Quarterly Journal of Engineering Geology and Hydrogeology*. 36: p. 155-157.
7. Rosser, N.J., et al. Terrestrial laser scanning for quantitative rockfall hazard assessment. in *International Conference on Landslide Risk Management*. 2005. Vancouver, Canada: Balkema.
8. Kemeny, J., et al. Automatic discontinuity Characterization of rock faces usign 3D laser scanners and digital imaging. in *Gulf Rocks 2004 (ARMA 2004 Rock Mechanics Symposium and the 6th NARMS)*. 2004. Houston, TX.
9. Monte, J., *Rock mass characterization using laser scanning and digital imaging data collection techniques*. 2004, University of Arizona.
10. Slob, S., et al. A method for automated discontinuity analysis of rock slopes with 3D laser scanning. in *Transportation Research Board (TRB) 84th Annual*

*Meeting*. 2005. Washington, D.C.: A.A. Balkema.

11. Optech, *ILRIS-3D sales brochure*. 2002.

12. Split_Engineering, *Split-FX User's Manual; Beta version 1.0*. 2005, Split Engineering LLC. p. www.spliteng.com.